

PREPARATION OF HIGH PERFORMANCE ACRYLONITRILE
COPOLYMERS

A THESIS SUBMITTED TO
THE GRADUATE SCHOOL OF NATURAL AND APPLIED SCIENCES
OF
MIDDLE EAST TECHNICAL UNIVERSITY

BY

BENĞİ ARAN

IN PARTIAL FULFILLMENT OF THE REQUIREMENTS
FOR
THE DEGREE OF DOCTOR OF PHILOSOPHY
IN
POLYMER SCIENCE AND TECHNOLOGY

DECEMBER 2009

Approval of the thesis:

**PREPARATION OF HIGH PERFORMANCE ACRYLONITRILE
COPOLYMERS**

submitted by **BENGI ARAN** in partial fulfillment of the requirements for the degree of **Doctor of Philosophy in Polymer Science and Technology Department, Middle East Technical University** by,

Prof. Dr. Canan Özgen _____
Dean, Graduate School of **Natural and Applied Sciences**

Prof. Dr. Cevdet Kaynak _____
Head of Department, **Metallurgical and Materials Engineering Dept.**

Prof. Dr. Ali Usanmaz _____
Supervisor, **Chemistry Dept., METU**

Asst. Prof. Dr. Mehmet Sankır _____
Co-Supervisor, **Nanotechnology and Membrane Science Laboratory, TOBB-ETU**

Examining Committee Members:

Prof. Dr. Duygu Kısakürek _____
Chemistry Dept., METU

Prof. Dr. Ali Usanmaz _____
Chemistry Dept., METU

Prof. Dr. Cevdet Kaynak _____
Metallurgical and Materials Engineering Dept., METU

Prof. Dr. H. İbrahim Ünal _____
Chemistry Dept., Gazi University

Prof. Dr. Zuhale Küçükayvaz _____
Chemistry Dept., METU

Date: 21.12.2009

I hereby declare that all information in this document has been obtained and presented in accordance with academic rules and ethical conduct. I also declare that, as required by these rules and conduct, I have fully cited and referenced all material and results that are not original to this work.

Name, Last name: Bengi ARAN

Signature:

ABSTRACT

PREPARATION OF HIGH PERFORMANCE ACRYLONITRILE COPOLYMERS

Aran, Bengi

Ph.D., Department of Polymer Science and Technology

Supervisor: Prof. Dr. Ali Usanmaz, METU

Co-Supervisor: Asst. Prof. Dr. Mehmet Sankır, TOBB ETU

December 2009, 141 pages

Acrylonitrile based engineering random copolymers were prepared via one step emulsion polymerization using ammonium persulfate (initiator), 1-dodecanthiol (chain transfer agent) and DOWFAX 8390 (surfactant) in the presence of water at approximately 65 °C. Three copolymer compositions were studied for novel polyacrylonitrile, (PAN)-polyhydroxyethyl acrylate (PHEA), PAN-polybutyl acrylate (PBA), novel PAN-polyt-butyl acrylate (PtBA), PAN-polyethyl acrylate (PEA) and PAN-polymethyl acrylate (PMA) with acrylate content varying from 8, 12 and 16 molar percent. Infrared spectroscopy, proton and carbon NMR were successfully utilized to confirm the chemical structure of copolymers. In order to determine the comonomer compositions in the copolymer structure, proton nuclear magnetic resonance, ¹H NMR studies were carried out. Thermal (TGA, DSC) and mechanical properties of homo and copolymers were also investigated. Intrinsic viscosity (IV) measurements in dimethyl formamide (DMF) solution revealed that the molecular weight of the copolymers were quite enough to form ductile films.

In this study, hydrogels and their copolymers of acrylonitrile (PAN-PHEA) were also studied. Some properties of the free standing copolymer films such as; swelling behaviors and densities were evaluated. It was also demonstrated that the nanocomposites of these copolymers could be utilized in filtration technology. Hence, novel PAN(88)-co-PMA(12) and polyaniline (PANI) nanocomposites were prepared at various PANI loadings to remove toxic chromium(VI) solution from water. Chemical structure, swelling and fracture morphology of the nanocomposites membranes were studied. It was observed that PANI had a great impact on the chromium removal. Permeate flux and rejection of chromium(VI) were demonstrated for various pHs and chromium(VI) concentrations. Finally, influences of comonomer composition on the thermal properties of the copolymers were investigated to input their structure property relation.

Keywords: Acrylonitrile, Acrylate, Emulsion Polymerization, Removal of Chromium ion, Desalination, Swelling Degree

ÖZ

YÜKSEK PERFORMANSLI AKRİLONİTRİL KOPOLİMERLERİNİN HAZIRLANMASI

Aran, Bengi

Doktora, Polimer Bilimi ve Teknolojisi Bölümü

Tez Yöneticisi: Prof. Dr. Ali Usanmaz, METU

Yard. Tez Yöneticisi : Yard. Doç. Dr. Mehmet Sankır,

TOBB ETU

Aralık 2009, 141 sayfa

Akrilonitril tabanlı mühendislik rasgele kopolimerleri tek adımlı emülsiyon polimerizasyon tekniği ile, amonyum persülfat (başlatıcı), 1-dodekantiyol (zincir transfer maddesi) ve DOWFAX 8390 (surfactant) kullanarak yaklaşık 65 °C lik su ortamında hazırlandı. Özgün poliakrilonitril (PAN)-polihidroksietil akrilat (PHEA), PAN- polibütil akrilat (PBA), özgün PAN- poli-t-bütil akrilat (PtBA), PAN-polyetil akrilat (PEA) ve PAN- polimetil akrilat (PMA) kopolimerlerinin 8, 12 ve 16 molar yüzdelerinde olmak üzere 3 farklı oranda kompozisyonları çalışıldı. Kopolimerlerin kimyasal yapılarını doğrulamak için FTIR ve ¹³C-NMR karakterizasyon metodları uygulandı. Kopolimerlere dahil olan her bir komonomerin miktarını belirleyebilmek için ¹H NMR tekniği kullanıldı. Kopolimer kompozisyonundan etkilenen termal (DSC ve TGA) ve mekanik özellikler incelendi. Mekanik özellikleri inceleyebilmek için gerekli olan filmlerin anamaddesi olan kopolimerlerinin IV ölçümler yapıldı ve film yapımı için molekül ağırlıklarının yeterli olduğu saptandı. Bu sayede bu filmlerin mekanik özellikleri incelenebildi.

Bu çalışmada, hidrojeller ve onların kopolimerleri ayrıca çalışıldı ve PAN/PHEA kopolimerinin şişme davranışları ve filmlerinin yoğunlukları da değerlendirildi. Bu çalışmada elde edilen kopolimerin filtrasyon teknolojisinde kullanılabileceği öngörüldü. Değişik miktarlarda PANI içeren özgün PAN(88)-co-PMA(12) ve polianilin (PANI) nanokompozitleri krom (VI) çözeltisini sudan ayırmak için hazırlandı. Nanokompozit membranların kimyasal yapıları, swelling davranışları ve kesit morfolojileride incelendi. PANI'nın kromun uzaklaştırılmasında büyük etkisi olduğu gözlemlendi. Süzüntü suyunun akışı ve membranın krom tutuşu çalışıldı. Son olarak, kopolimer kompozisyonunun camsı geçiş sıcaklığına (T_g) olan etkisinin yanı sıra, kopolimer yapımında kullanılan komonomer çeşidinin T_g ye olan etkisi ve ayrıca komonomer çeşidinin mekanik özelliklere olan etkisi çalışıldı.

Anahtar Kelimeler: Akrilonitril, Akrlat, Emülsiyon Polimerizasyonu, Krom İyonunun Uzaklaştırılması, Tuz Uzaklaştırma, Şişme Derecesi

to my grandmother, Şehnaz Hisarcıklı
my mother, Saadet Aran
my brother, Burç Aran
my beloved father, late Yalçın Aran

ACKNOWLEDGEMENTS

I would like to express my gratitude to my supervisor Prof. Dr. Ali Usanmaz for his guidance, encouragement, and support throughout the research. He supplied all opportunities in his laboratory and always had confidence in me. He always has a practical and a positive attitude and this approach will be a model in my future life.

I would like to thank my co-advisor Assoc. Prof. Dr. Mehmet Sankır because he introduced me to acrylonitrile copolymers and helped me to design and realize the experimental setup. This thesis would have been less complete without the experimental contributions of him. He is not only provided an academic insight when I needed, but he also cared about my well being on a personal level.

I wish to acknowledge the PhD committee members, Prof. Dr. H. Ibrahim Ünal and Prof. Dr. Cevdet Kaynak for their valuable suggestions and constructive criticism.

I would like to express my special thanks to Assoc. Prof. Dr. Nurdan D. Sankır for her valuable suggestions and comments and always having a smiling face.

My sincere appreciation goes to Dr. Elif Vargün for her valuable comments and also her friendship not only through out the past eight years, but also a friendship which will continue in the future. I can never thank her enough.

Furthermore, I would like to thank my dearest friend, Elif Kemeröz, not only for helping me all the time in thermal analysis, she also always listened to me even when I got crazy, or when I started to talk nonstop. I can never repay her.

I would like to express my appreciations to METU Central Laboratory specialist Dr. Selda Keskin. She always showed great patience to me during characterization

experiments. Also, I would like to thank to Dr. Eda Ayşe Aksoy and Leyla Molu for their moral support and friendship.

My sincere appreciation goes to my labmates Bahadır Doğan, Tamer Tezel and Selçuk Bozkır for their help and understanding and for being lunch-mate during the past two years.

TUBITAK is gratefully acknowledged for the financial support via grant no 108T099.

I owe a very special thanks to my fiancé Mehmet Ömerbeyoğlu for being by my side during the hard times and for endless support and of course for his patience in waiting me for the past three years to get married.

Finally, I would like to dedicate this dissertation to my loving family, my mother, my brother, my grandmother and my father. I love them with my all heart, always.

TABLE OF CONTENTS

ABSTRACT.....	iv
ÖZ.....	vi
ACKNOWLEDGEMENTS.....	ix
TABLE OF CONTENTS.....	xi
LIST OF TABLES.....	xv
LIST OF FIGURES	xvii
ABBREVIATIONS.....	xxi
CHAPTERS	
1. INTRODUCTION.....	1
1.1 Free Radicalic Polymerization	1
1.2 Polymerization Processes	2
1.2.1. Bulk Polymerization.....	2
1.2.2. Solution Polymerization.....	2
1.2.3 Suspension Polymerization	3
1.3. Emulsion Polymerization	3
1.3.1 Emulsion Polymerization Process.....	6
1.3.2 Harkins-Smith-Ewart Mechanism.....	9
1.3.3. Quantitative Aspects	10
1.4 Literature Review of Emulsion Copolymerization of PAN.....	12
1.4.1 Polyhydroxyethyl acrylate Copolymers	13
1.4.2 Polybutylacrylate Copolymers	13
1.4.3 Polyethylacrylate Copolymers	14
1.4.4 Polytertiarybutyl acrylate Copolymers	15
1.4.5 Polymethylacrylate Copolymers	15
1.5 Membrane Technology and Advantages.....	16
1.5.1 Historical Background of Membrane Technology.....	16
1.5.2 Membrane Technology	17
1.5.3 Membrane Definition and Classifications.....	18

1.5.4 Basic Principles of Membranes	20
1.5.5 Membrane Separation Processes	24
1.5.6 Membrane Fouling	29
1.5.7 Composite Membranes.....	29
1.6 The Aim of this study	32
2. EXPERIMENTAL.....	33
2.1 Acrylonitrile Copolymers Synthesis	33
2.1.1 Materials used for Homopolymer and Copolymer Synthesis	33
2.1.2 Method for Homopolymer and Copolymer Synthesis	34
2.1.3 Film preparation for Mechanical Tests and Water Uptake Measurements	35
2.1.4 Nanocomposite Membrane Preparation	36
2.2 Polymer Characterization Methods.....	36
2.2.1 Fourier Transform Infrared Spectroscopy (FTIR)	36
2.2.2 Nuclear Magnetic Resonance Spectroscopy (NMR)	37
2.2.3 Differential Scanning Calorimetry (DSC).....	37
2.2.4 Thermogravimetric Analysis (TGA).....	37
2.2.5 Mechanical Tests.....	41
2.2.6 Viscosity Measurements	41
2.2.7 Scanning Electron Microscopy (SEM)	42
2.2.8 Sheet Resistivity Measurements.....	42
2.2.9 Water flux and Cr(VI) Removal Tests of Membranes	42
3. RESULTS AND DISCUSSION.....	45
3.1 Polyacrylonitrile-Polyhydroxyethyl acrylate Copolymers.....	45
3.1.1 Fourier Transform Infrared Spectroscopy (FTIR) Results.....	46
3.1.2 Nuclear Magnetic Resonance Spectroscopy (NMR) Results.....	48
3.1.3 Differential Scanning Calorimetry (DSC) Results.....	51
3.1.4 Thermogravimetric Analysis (TGA) Results	53
3.1.5 Mechanical Test Results.....	55
3.1.6 Swelling Behaviour Analysis of PAN-PHEA copolymers	58

3.2 Polyacrylonitrile-Polybutylacrylate Copolymers	60
3.2.1 Fourier Transform Infrared Spectroscopy (FTIR) Results.....	61
3.2.2 Nuclear Magnetic Resonance Spectroscopy (NMR) Results.....	63
3.2.3 Differential Scanning Calorimetry (DSC) Results.....	66
3.2.4 Thermogravimetric Analysis (TGA) Results	67
3.2.5 Mechanical Test Results.....	70
3.3 Polyacrylonitrile-Polytertbutylacrylate Copolymers.....	71
3.3.1 Fourier Transform Infrared Spectroscopy (FTIR) Results.....	72
3.3.2 Nuclear Magnetic Resonance Spectroscopy (NMR) Results.....	74
3.3.3 Differential Scanning Calorimetry (DSC) Results.....	77
3.3.4 Thermogravimetric Analysis (TGA) Results	78
3.3.5 Mechanical Test Results.....	82
3.4 Polyacrylonitrile-Polyethyl acrylate Copolymers	84
3.4.1 Fourier Transform Infrared Spectroscopy (FTIR) Results.....	85
3.4.2 Nuclear Magnetic Resonance Spectroscopy (NMR) Results.....	87
3.4.3 Differential Scanning Calorimetry (DSC) Results.....	90
3.4.4 Thermogravimetric Analysis (TGA) Results	91
3.4.5 Mechanical Test Results.....	94
3.5 Polyacrylonitrile-Polymethyl acrylate Copolymers	97
3.5.1 Fourier Transform Infrared Spectroscopy (FTIR) Results.....	97
3.5.2 Nuclear Magnetic Resonance Spectroscopy (NMR) Results.....	98
3.5.3 Differential Scanning Calorimetry Results (DSC).....	100
3.5.4 Thermogravimetric Analysis Results (TGA)	101
3.5.5 Mechanical Test Results.....	103
3.6 Filtration Membranes	106
3.6.1 Nanocomposite membranes	108
3.6.2 Fracture Morphology of the Nanocomposites Nanoporous Memb.....	111
3.6.3 Swelling and Electrical Properties of the Nanocomposites Memb.....	112
3.6.4 Performances of Nanocomposite Membranes.....	114
3.7 Structure Property Relationship	121

3.7.1 Composition-Comonomer-Glass Transition Temperature.....	121
3.7.2 Composition-Comonomer-Mechanical Properties.....	123
4. CONCLUSION.....	126
5. SUGGESTED FUTURE RESEARCH.....	129
REFERENCES.....	130
CURRICULUM VITAE.....	140

LIST OF TABLES

Table 2.1 Recipe for Emulsion polymerization of acrylonitrile based copolymers and homopolymers	38
Table 3.1 Theoretical and experimental composition and intrinsic viscosity data of PAN-PHEA copolymers	49
Table 3.2 Thermal decomposition properties of homo- and copolymers (heating rate 10°C/min, N ₂ atmosphere)	55
Table 3.3 Mechanical Test Results for PAN-PHEA copolymer films.....	58
Table 3.4 Equilibrium swelling ratio and densities of copolymers at various percent HEA loadings	59
Table 3.5 Composition and intrinsic viscosity of PAN-PBA copolymers.....	63
Table 3.6 Thermal decomposition characteristics of acrylonitrile-butyl acrylate copolymers (heating rate 10 °C/min; N ₂ atmosphere).....	68
Table 3.7 Mechanical test results for Pan-Pba copolymer films.....	71
Table 3.8. Composition and intrinsic viscosity of PAN-PtBA copolymers.....	74
Table 3.9 Thermal decomposition properties of homo- and copolymers (heating rate 10°C/min, N ₂ atmosphere)	80
Table 3.10 Mechanical test results for PAN-PtBA copolymer films.....	84
Table 3.11 Composition and intrinsic viscosity of PAN-PEA copolymers	88
Table 3.12 Thermal decomposition properties of homo- and copolymers (heating rate 10°C/min, N ₂ atmosphere)	92
Table 3.13 Mechanical test results for PAN-PEA copolymer films	96
Table 3.14 Composition and intrinsic viscosity of PAN-PMA copolymers	99
Table 3.15 Thermal decomposition properties of homo- and copolymers (heating rate 10°C/min, N ₂ atmosphere).....	102
Table 3.16 Mechanical test results for PAN-PMA copolymer films	106
Table 3.17 Percent Cr removal of Asymmetric membranes	108
Table 3.18 Nanocomposite membrane type and flux time values	109

Table 3.19 Swelling Ratios and Sheet Resistivities of Copolymer and Nanocomposite Membranes	112
Table 3.20 Pure Water and Permeate Fluxes of Nanocomposite Membranes at Various Chromium (VI) concentrations and pHs	115
Table 3.21 Fouling Analysis for 10 percent PANI Loading Nanocomposite Membranes PAN88coPMA12-PANI(10)	120
Table 3.22 Glass Transition Temperatures and intrinsic viscosities of homo and copolymers at three different compositions	122
Table 3.23 Mechanical Properties of Acrylonitrile based copolymers	125

LIST OF FIGURES

Figure 1.1 Schematic representation of an emulsion polymerization system.....	8
Figure 1.2 Schematic representation of a) dead end filtration, b) crossflow filtration	23
Figure 1.3 Relative Sizes of materials that can be separated in memb. processes...	24
Figure 1.4 Pressure driven memb. processes and their separation characteristics...	25
Figure 2.1 Schematic representation of experimental apparatus.....	34
Figure 2.2 Rxn scheme for the copolymerization of acrylonitrile and acrylates	35
Figure 3.1 Chemical structure of polyacrylonitrile-co-polyhydroxyethyl acrylate (PAN-PHEA) copolymer	45
Figure 3.2 FTIR spectrums of the copolymers and homopolymers; monomers were successfully incorporated to chemical structure.....	47
Figure 3.3 ¹ H-NMR spectrum of AN-HEA copolymers with different compositions; chemical structure was proved by ¹ H-NMR.	50
Figure 3.4 ¹³ C-NMR spectrum of AN-HEA copolymers with different compositions, showing theoretical and actual compositions were comparable.....	51
Figure 3.5 DSC thermogram of (a) PHEA, (b) homopolymer of PAN and copolymers. Glass transition temperature of PAN was successfully lowered from about 104 to 70 °C . Heating rate 10 °C/min, nitrogen atmosphere.	52
Figure 3.6 Weight loss temperatures for homo- and copolymers; copolymers were thermooxidatively stable.	53
Figure 3.7 Derivative weight loss curves for homo- and copolymers versus temperature.....	54
Figure 3.8 Elastic modulus of PAN-PHEA copolymer films	56
Figure 3.9 Ultimate Tensile Strength of PAN-PHEA copolymer films.....	57
Figure 3.10 EAB of PAN-PHEA copolymer films	58
Figure 3.11 Degree of swelling versus time curves for various PAN-PHEA copolymers	60
Figure 3.12 Chemical structures of copolymers PAN-PBA	61

Figure 3.13 FTIR spectrum exhibited characteristic peaks of PAN-co-PBA	62
Figure 3.14 ¹ H-NMR spectrum of AN-BA copolymers with diffe. compositions ..	64
Figure 3.15 ¹³ C-NMR spectrum of AN-BA copolymers with diff. compositions ...	65
Figure 3.16 DSC thermograms of (a) PBA, (b) homopolymer of PAN and copolymers	66
Figure 3.17 Weight loss curves for homo- and copolymers versus temperature	67
Figure 3.18 Effect of copolymer composition on the percent weight loss during TGA analysis.....	69
Figure 3.19 Stress-Strain deformation curves for PAN-PBA copolymer films.....	70
Figure 3.20 Chemical structure of PAN-PtBA copolymers.....	72
Figure 3.21 FTIR spectrum exhibited characteristic peaks of PAN-co-PtBA.....	73
Figure 3.22 ¹ H-NMR spectrum of AN-tBA copolymers with diff. compositions ...	75
Figure 3.23 ¹³ C-NMR spectrum of AN-tBA copolymers with diff. compositions ..	76
Figure 3.24 DSC thermograms of (a) PtBA, (b) (1) PAN(84)-PtBA(16), (2) PAN(88)-PtBA(12), (3) PAN(92)-PtBA(8), (4) PAN	78
Figure 3.25 Weight loss curves for homo- and copolymers versus temperature	79
Figure 3.26 Effect of copolymer composition on the percent weight loss during TGA analysis.....	81
Figure 3.27 Elastic Modulus of PAN-PtBA copolymers	82
Figure 3.28 Ultimate Tensile Strength of PAN-PtBA copolymer films	83
Figure 3.29 Elongation at Break (%) of PAN-PtBA copolymer films.....	83
Figure 3.30 Chemical structure of PAN-PEA copolymers	85
Figure 3.31 FTIR spectrum exhibited characteristic peaks of PAN-co-PEA	86
Figure 3.32 ¹ H-NMR spectrum of AN-EA copolymers with different compositions; chemical structure was proved by ¹ H-NMR.	87
Figure 3.33 ¹³ C-NMR spectrum of AN-EA copolymers with different compositions, showing theoretical and actual compositions were comparable	89
Figure 3.34. DSC thermograms of homo and copolymers (PAN-PEA)	90
Figure 3.35 Weight loss curves for homo- and copolymers versus temperature	91

Figure 3.36 Effect of copolymer composition on the percent weight loss during TGA analysis.....	93
Figure 3.37 Elastic Modulus of PAN-PEA copolymers	94
Figure 3.38 Ultimate Tensile Strength of PAN-PEA copolymers	95
Figure 3.39 Elongation at Break (%) of PAN-PEA copolymers.....	96
Figure 3.40 Chemical structure of polyacrylonitrile-co-polymethyl acrylate (PAN-PMA) copolymer.....	97
Figure 3.41 FTIR spectrum exhibited characteristic peaks of PAN-co-PMA	98
Figure 3.42 ¹ H-NMR spectrum of AN-MA copolymers with diff. compositions .	100
Figure 3.43 DSC results demonstrating the effect of MA content in the copolymer on Tg. Heating rate 10 °C/min, N ₂ atm.	101
Figure 3.44 Weight loss curves for homo- and copolymers versus temperature ...	102
Figure 3.45 Effect of copolymer composition on the percent weight loss during TGA analysis.....	103
Figure 3.46 Elastic Modulus of PAN-PMA copolymers	104
Figure 3.47 Ultimate Tensile Strength of PAN-PMA copolymers	105
Figure 3.48 Elongation at Break (%) of PAN-PMA copolymers	106
Figure 3.49 Cross-section morphologies of 92% PAN-PBA asymmetric memb. .	107
Figure 3.50 Cross-section morphologies of 84% PAN-PtBA asymmetric memb. .	107
Figure 3.51 Cross-section morphologies of 88% PAN-PEA asymmetric memb. .	107
Figure 3.52 Chemical Structures of Emeraldine base and salt of PANI (X is dopant anion).....	110
Figure 3.53 FTIR spectroscopy of a. PAN(88)-co-PMA(12) copolymer,	111
b. PAN(88)-co-PMA(12)-PANI(5) c. PAN(88)-co-PMA(12)-PANI(10).....	111
Figure 3.54 Fracture morphology of a. PAN(88)-co-PMA(12) membrane, b. PAN(88)-co-PMA(12)PANI(5) c. PAN(88)-co-PMA(12)PANI(10)	113
Figure 3.55 Influence of pH and hexavalent chromium concentration on formation of hexavalent chromium species	117
Figure 3.56 Percent chromium removal of PAN(88)-co-PMA(12)-PANI(5) nanocomposites membranes at various pHs.....	118

Figure 3.57 Percent chromium removal of PAN(88)-co-PMA(12)-PANI(10)
nanocomposites membranes at various pHs..... 119

ABBREVIATIONS

APS	Ammonium persulfate
CMC	Critical Micelle Concentration
CT	Chain Transfer Agent
DSC	Differential Scanning Calorimetry
DMA	Dynamic Mechanical Analyses
DMF	Dimethylformamide
E	Elastic Modulus
EAB	Elongation at Break
FTIR	Fourier Transform Infrared Spectroscopy
IRFL	Irrversible Flux Loss
IPA	Isopropyl alcohol
IV	Intrinsic Viscosity
MF	Microfiltration
NF	Nanofiltration
NMR	Nuclear Magnetic Resonance
NMP	1-methyl-2-pyrrolidone
PAN	Polyacrylonitrile
PANI	Polyaniline
PBA	Poly-n-butyl acrylate
PHEA	Polyhydroxyethyl acrylate
PEA	Polyethyl acrylate
PtBA	Polytertiary butyl acrylate
PMA	Polymethyl acrylate
PRF	Percent Flux Recovery
q	Swelling degree
R	Rejection (retention)

RFL	Reversible Flux Loss
RO	Reverse Osmosis
S	Surfactant
SEM	Scanning Electron Microscope
TFL	Total Flux Loss
TGA	Thermogravimetric Analysis
UF	Ultrafiltration
UTS	Ultimate Tensile Strength
WU	Water Uptake

CHAPTER 1

INTRODUCTION

1.1 Free Radicalic Polymerization

In terms of production of synthetic high polymers, free-radical polymerization is a significant industrial method. We can define it as a chain polymerization method, which depends on free-radical reactions to obtain chain development. Within the framework of this method, monomers with carbon-carbon double bonds sensitive to free-radical attack and splitting are benefited from. A double bond splitting arises in the end of a free radical attack; besides we observe the monomer unit and the previous radical unit at one of the previous splitting areas and radical stabilization occurs at the other splitting site.

As far as many monomer and polymer types are concerned, development and commercialization of various industrial free-radical polymerization processes are in question. Commercial use of many monomers and polymerization processes is in question. Besides, in the last two decades, improvement has been obtained in terms of synthesizing of polymers with controlled architectures depending on free-radical polymerization. It can be said that block copolymers, graft copolymers, and radial polymers are among synthesized materials. The mentioned materials' fields of exploitation are many common industrial and household applications, which are adhesives, paints and coatings, textiles, nonwoven fabrics, personal care products, wallpaper, construction materials, specialty additives etc [1].

1.2 Polymerization Processes

Free radical polymerization takes place under both homogenous and heterogenous conditions. Insolubility of the polymer in the reaction media may cause the homogenously started systems to turn into heterogenous systems. Suspension and emulsion polymerizations can be an example for heterogenous process where mass and solution polymerizations are homogenous processes.

Emulsion polymerization will be discussed in detail in Chapter 1.3. Simply, polymerization of all monomers can take place by any of the processes discussed below. However, either one or two processes can be used to polymerize one monomer in commercial polymerizations.

1.2.1. Bulk Polymerization

One of the most basic types of polymerization with the minimum product contamination is the bulk or mass polymerization. However due to the unusual characteristics of radical chain polymerization bulk polymerization is barely controlled. Heat dissipation is difficult due to the highly exothermic nature that involves high activation energies that combines with a propensity toward the gel effect. Temperature control, which is vitally required in mass polymerization, is effected by the viscosity and the exotherm which causes temperature to be controlled with difficulty during the reaction [2].

1.2.2. Solution Polymerization

It is possible to eliminate the majority of the obstacles in the bulk polymerization processes through the polymerization of a monomer in a solvent. Solvent operates as a dilute and heat transformation in polymerization is facilitated. Besides through decrease of the viscosity of the reaction, easy stirring becomes available for the mixture. On the basis of a comparison, made with bulk polymerization, it can be

said that thermal control is much easier. But other difficulties like chain transfer to the solvent may arise as a result of application of a solvent as long as an accurate solvent is not selected. Besides obstacles to be encountered in elimination of the solvent leads to undesired purity levels [2].

1.2.3 Suspension Polymerization

In suspension polymerization, monomers (discontinuous phase) are suspended in the water (continuous phase) as droplets (50 – 500 μm). Within the scope of the majority of polymerizations, the range relevant for monomer weight is 1:1-1:4. Due to agitation and the surfactants, coalescing of monomer droplets to be turned into polymer particles is prevented. Within the framework of this type of polymerization, two types of surfactants are used, which are water soluble polymers and water-insoluble inorganic powders. Polyvinylalcohol and sodium polystyrene sulfonate are then components taking place within the scope of water soluble polymers; on the other hand substances such as sulfate and calcium phosphate are comprised by inorganic powders [2].

1.3. Emulsion Polymerization

The main field for use of emulsion polymerization is the manufacturing of a great variety of specialty polymers including, but not limited to adhesives, paints, binders for unwoven fabrics as well as admixtures for paper, textiles and building materials, impact modifiers for plastic matrices, diagnostic tests, and drug-delivery systems [3]. This branch of industry has been developed owing to both the probability of manufacturing polymers with unique properties and the environment-related issues and governmental directives to substitute solvent-based systems by the use of waterborne items. Since the 1930s, the emulsion polymerization process has been employed on a commercial basis. With respect to emulsion polymerization, the publication of the first-ever qualitative model was in 1947 by Harkins [4].

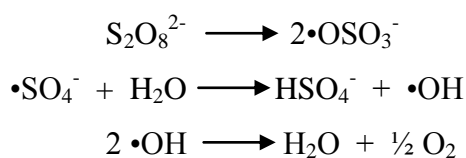
The control of nucleation, growth and stabilization of polymer particles is done by the free radical polymerization mechanism in combination with various colloidal events; that is the reason why emulsion polymerization is a rather complex process. Segregation of free radicals among the discrete monomer-swollen polymer particles, which will strongly decrease the possibility of bimolecular termination of free radicals and, thereby, give rise to a faster polymerization rate and polymer with a higher molecular weight, is the most remarkable feature of emulsion polymerization [5]. Emulsion polymerization cannot gain such advantageous property simultaneously in bulk or solution polymerization. In spite of the fact that the period of nucleation is fairly short, what plays a curial role in determining the final latex particle size and the particle size distribution is generation of particle nuclei during the early stage of the polymerization, and quality of latex products is also greatly influenced by it. A significantly challenging task to those who are involved in this impressive research area is the effective controlling of the particle nucleation process. The key factors governing the process of particle growth include conveyance of monomer, free radicals and surfactant to the growing particles and partition of such reagents among the continuous aqueous phase, emulsified monomer droplets (monomer reservoir), monomer-swollen polymer particles (primary reaction loci) and oil–water interface. From both the academic and the industrial points of view, the colloidal properties of latex products are noteworthy. The particle size and the particle size distribution, particle surface charge density (or zeta potential), particle surface area covered by one stabilizer molecule, conformation of the hydrophilic polymer physically adsorbed or chemically coupled onto the particle surface, type and concentration of functional groups on the particle surface, particle morphology, optical and rheological properties and colloidal stability are some of the representative properties [6].

The most widely encountered monomers exploited within the scope of this type of polymerizations have been split into groups. It can be said that within several groups, a single monomer may take place; but a general classification can be mentioned: Butadiene-styrene-acrylonitrile, Vinyl chloride-vinly acetate,

Vinylidene chloride, Acrylates and methacrylates, Water-soluble monomers: acrylic and methacrylic acids, acrylamide, other functional monomers.

In general, it is water which can be defined as the dispersing medium, where dispersion and stabilization of other materials through the emulsifying agent, also known as surfactant are observed. In order to obtain various objectives, addition of emulsifier to the system is necessary; the stabilization of monomer droplets in emulsion, the formation of monomer swollen micelles that would serve as nucleation sites, and stabilization of growing particles are among the said objectives. A long hydrocarbon ‘tail’ is a part of a standard surfactant molecule; it dissolves in hydrocarbon; besides a hydrophilic ‘headgroup’ that dissolves in polar solvents, which is primarily water, is a part of this structure. Surfactants are in general classified as ionic (cationic and anionic), non-ionic and amphoteric (zwitterionic). The reason why anionic and non-ionic surfactants are frequently used is compatibility. In order to increase the level of colloidal stability in commercial processes surfactant mixtures may be an alternative [7].

Initiators can be defined as the basis of free radicals, which are required for emulsion polymerization. Taking the stage, where free radicals production is in question, as a basis, initiators may be water or oil soluble. In order for an initiator to be defined as good quality, it should comprise of an effective free radical production at reasonable temperatures and it should remain stable at room temperature. Thermal homolytic dissociation of compound possessing bonds with dissociation energies between 100 and 170 kJ/mole can be defined as the most widely used initiation technique. Sodium, potassium and ammonium persulfates, which decompose in the range of 50-90°C are among water-soluble thermal initiators [8].



Oil soluble thermal initiators tend to be peroxides and azo compounds. Single electron transfer to or from an ion is an alternative method through which initiation arises; it is rather deemed as a redox reaction between the oxidizing and the reductant agents for production of free radicals. Persulfate-bisulfite and persulfate-hydrosulfite are two typical redox pairs beneficial to for emulsion polymerization [4].

In the course of synthesis or at a subsequent stage, addition of other components is in question for other targets. For pH regulation, buffers are added; for taking molecular weight under control, chain transfer agents are benefited from; to make some changes in latex features of a specific application or for prevention of degradation or decomposition, rheological modifiers, plasticizers, biocides, antioxidants and uv-absorbers are in general become a part of the structure subsequent to synthesis [4].

1.3.1 Emulsion Polymerization Process

In the course of emulsion polymerization components' spot can be deemed as one of the most significant features of this process. Upon addition of surfactant to water, micelles formation is in question in the event of exceeding of the critical micelle concentration (CMC) by the concentration in respect of a specific surfactant. 0.001-0.1 mole/liter is the CMC value range; most surfactants' values take place in the lower end of the mentioned range. The great part of the surfactant is in the micelles; because surfactant concentrations in the majority of emulsion polymerizations go beyond CMC by one or more orders of magnitude. Standard micelles dimensions amount to 2-10 nm; each micelle comprises of 50-150 surfactant molecules. According to the surfactant and its concentration, spherical and rodlike micelles are monitored. In the event of use of water-insoluble monomers, dissolution of a small part of the monomer in water is in question, another small part penetrate into the micelles; however monomer droplets stabilized by surfactant molecules adsorbed on the surface of the droplet are the location of

the largest amount. The amount of surfactant is the determinant of the number of micelles and their size. Larger numbers of smaller-sized particles are generated by large amounts of surfactant. When compared with micelles, monomer droplets are larger; but the micelles occupy a larger space than the droplets [4].

Initiator molecules, which can be solved in water, are located in the aqueous stage in the course of which production of free radicals is observed. Initiation does not arise before a free radical's meeting monomer molecules and forming growing chains; therefore it was the general view that initiation would take place in micelles upon primary radical penetration. Due to smaller total surface area of the droplets, no efficient competition of monomer droplets with micelles in capturing radicals produced in solution is in question. The micelles is where organic (oil-soluble) monomer and the water-soluble initiator meet. Due to their high monomer concentration compared to the monomer in solution, the micelles are exploited as the reaction site. In the course of progress of polymerization, through participation of monomer from the aqueous solution –the relevant concentration is consumed when monomer is dissolved from monomer droplets- the micelles develop. The Figure 1.1 represents a simplified scheme of an emulsion polymerization system. There are three types of particles within the system: monomer droplets, inactive micelles in which polymerization is not occurring, and active micelles in which polymerization are occurring. The latter are referred to as polymer particles rather than being regarded as polymer particles [3].

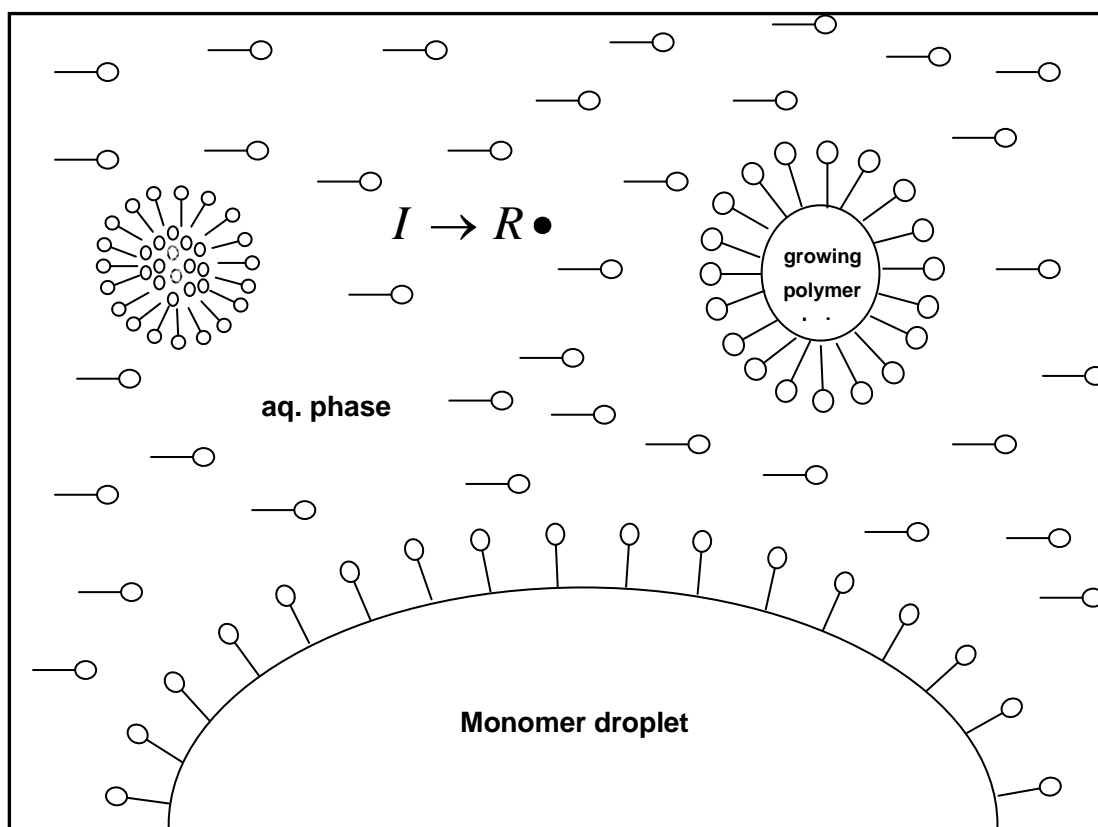


Figure 1.1 Schematic representation of an emulsion polymerization system.

Particle nucleation mechanism's progress depends on two simultaneous processes. One is penetration of radicals from the aqueous phase into the micelles. The other mechanism for particle nucleation comprises of precipitation of oligomers formed in the aqueous phase from the water and stabilization of them by surfactant; thereby new particles are formed, which is called homogeneous nucleation. Possibility of one type of nucleation or the other in a specific polymerization is highly dependent on water solubility of the monomer and on surfactant concentration. Monomers with high water solubility and low surfactant concentrations favor homogeneous nucleation. According to studies on highly water-insoluble monomers such as styrene, micellar nucleation is predominant; in terms of partially water-soluble such as methyl methacrylate or vinyl acetate, homogeneous nucleation is observed primarily [9].

1.3.2 Harkins-Smith-Ewart Mechanism

For the quantitative treatment of Smith and Ewart and other researchers [10-11-12-13], the original description of emulsion polymerization by Harkins [14] was relied on. According to Harkins, the emulsion polymerization process is classified into three intervals depending on the very important interaction between monomer droplets, inactive micelles (no polymerization taking place) and polymer particles (monomer-swollen micelles with growing chains).

With time in interval I, increase of the particle number is in question and then in the course of interval II and III, it is fixed. Interval I comprises of initiation and nucleation. In the course of this stage, growth of polymer particles in time is observed and a volume fraction of monomer is made sufficient for swelling of the polymer. The solution in water provides such a monomer; depending on continuous dissolution of monomer from monomer droplets, saturation of the solution in water is observed. In order to stabilize growing particles and form new ones, micelles provide the necessary surfactant. Interval I of the polymerization comprises of both the nucleation process and the depletion of micelles used up for particle formation. Before the end of interval I or very early in interval II absorption of all or almost all of the surfactant in the system by the polymer particles will take place. In the end, there is a relative instability in terms of monomer droplets and in the event that agitation comes to an end, they will unite. Interval I tends to be the shortest of the three intervals, the relevant duration changes in the range 2-15% conversion. Interval I is not related to low initiation rates anymore; because in order to obtain steady-state particle number, the level of time needed is high. The more water soluble monomers such as vinyl acetate in general help completion of the interval I more rapidly when compared with the less water soluble monomers [15].

The rate of polymerization may be fixed or may tend to increase slightly in the course of interval II. The latter action stems from a gel effect. While monomer droplets reduce, the polymer particles tend to increase. Interval II comes to an end

while the monomer droplets are invisible. In terms of passage from interval II to III, lower conversion can be mentioned; because there is an increase in the monomer water solubility and the extent of swelling of the polymer particles by monomer.

Within the scope of interval II and III, there is no change in the particle numbers; however there is a decrease in the monomer concentration with time; because monomer droplets are not available anymore. Gel effect existence goes on in the course of interval III. Final conversions are nearly 100 %, and spherical shape of particles can be observed and it ranges between 50 to 400 nm as far as diameter is concerned.

1.3.3. Quantitative Aspects

Emulsion polymerization's one of the most significant features is the possibility of simultaneously increasing polymerization rate and molecular weight of the polymer. Because of the increased number of polymerization sites (i.e. polymer particles) and the high monomer concentration within the particles, this issue is possible. The general free radical expression for the propagation step may be put forth as the grounds for the increase in size of one radical inside a particle.

$$r_p = k_p [M]_p \quad (1)$$

where k_p is the propagation rate coefficient and $[M]_p$ is the equilibrium swelling concentration of monomer in the particle. Since polymerization is occurring in all particles that have captured one radical, then the expression changes to:

$$R_p = \frac{\bar{n} N k_p [M]_p}{N_A} \quad (2)$$

where N is the total number of particles and \bar{n} is the average number of radicals per particle.

In the event that the polymerizing system is subject to subdivision many times, radicals growing are isolated into individual particles [16]; thereby upon penetration of another free radical into such particles, termination is in question without delay. The value of n in equation (2) is regarded as a significant parameter; because the rate and molar mass profiles during polymerization are determined by it. In general three limiting cases are touched upon. First of all, case 2 has to be handled; because it is in general valid for most emulsion polymerizations. In case 2, the level of radical penetration to the particles is too high and the rate is low. The average number of radicals per particle is $n = 0.5$; because since at any given moment either one or zero growing chains will take place within the scope of each particle. Upon its penetration into the particle, each radical is maintained and is multiplied until the penetration of another radical and the growing chain is ceased without delay [17,18]. Negligible desorption rates and the small particle size for accommodation of more than one radical favor this fact. This fact is valid for monomers such as styrene comprising of low transfer to monomer constants. Case 1 and values of $n \ll 0.5$ are correspondent. This is mostly encountered in monomers with high water solubility comprising of higher transfer constants and producing more active radicals such as vinyl acetate. It is valid in the event that a high radical desorption is observed in terms of penetration rate, and termination rates in water are not significant. In case 3, the value n is much higher than unity. The fact that particles are relatively large favors this fact; however what is more important is the time when termination constants are not high and termination in water and desorption of radicals are negligible.

Within the framework of the Smith-Ewart theory [10], the primary nucleation sites are surfactant micelles. The number of particles subject to stabilization is related to the total surface area of surfactant in the system, indicated as $a_s S$, where a_s is the interfacial surface area covered by a surfactant molecule and S is the total concentration of surfactant in the system. But the number of particles is at the same

related to the rate of radical generation R_i . Smith and Ewart defined the number of particles by equation 3.

$$N = k \left(\frac{R_i}{\mu} \right)^{0.4} \left(\frac{S}{S_0} \right)^{0.6} \quad (3)$$

where μ is the rate of particle growth and k is the proportionality constant.

1.4 Literature Review of Emulsion Copolymerization of PAN

Within the scope of special end use, macromolecules are greatly needed. Under these circumstances, the appropriate solution shall be copolymerization as well as used for the purpose of the preparation of macromolecules, synergistic combination of properties shall be in question, which will begin from two or more different monomers. For the purpose of preparation of most of the commercially important polymers such as NBR and SBR, the technique benefited from is emulsion copolymerization. In lieu of preparing novel and more expensive specialty homopolymers, cost-effective multicomponent systems have been designed. For the purpose of obtaining desirable characteristics, the said multicomponent systems' being changed through the total synthesis of new polymers easily can be proposed [19].

Filtration membranes, and current-generation carbon fiber precursors which are the base materials for acrylic textile fibers, are established by the copolymers of acrylonitrile and the minor molar concentrations of alkyl acrylates. For the purpose of upgrading the processability, introduction of comonomers into these materials can be in question. Observation of semicrystalline transitions close to 300 °C, which exceeds the PAN degradation temperatures, is possible at the usual molar concentrations of comonomer. There is a need to process these copolymers by solvent based spinning, because emergence of decomposition/cyclization below the crystalline melting point of about 300 °C by the long range order is observed. The

long range order, in terms of which quantification is difficult, can be subject to disruption by way of efficient utilization of comonomers. Reduction of semicrystallinity is possible and as a consequence, through interruption of the AN sequences to be performed by second monomer use like ethyl acrylate or methyl acrylate elimination will be observed [20]. The following sections describe the literature review for AN copolymer with various comonomers.

1.4.1 Polyhydroxyethyl acrylate Copolymers

Polyhydroxyethyl acrylate (PHEA) is a hydrogel and has been synthesized for medical applications. Mechanical properties of PHEA are poor due to the high tendency for absorbing water. Since PHEA suffers from bad mechanical properties, it is beneficial to improve the mechanical properties of PHEA as well as keeping its desired hydrogel properties to utilize them in many applications such as matrices for drug and human growth hormone delivery, biomaterials in tissue engineering and ophthalmics. Compared to other acrylic polymers, few studies have been reported on the copolymerization of HEA. Penlidis et al., investigated the styrene-HEA and styrene-HEA-ethyl acrylate copolymers in view of feed composition, reactivity ratio, effect of temperature and initiator concentration [21]. Tejedor et al., studied the dielectric relaxation spectroscopy, thermally stimulated depolarization currents and dynamic mechanical experiments for ethyl methacrylate-HEA random copolymers [22]. In another study, the temperature sensitive water soluble HEA-butyl acrylate copolymer were examined and it was found that the interaction between these copolymers and polyacrylic acid in aqueous solutions resulted in the formation of interpolymer stabilized by hydrogen bonds and hydrophobic interactions [23].

1.4.2 Polybutylacrylate Copolymers

Butyl acrylate is a monomer, which is significant in terms of production of polymers in many industrial applications like paints and adhesives; the low glass transition temperature of its polymer has to be given importance in this respect [19].

Copolymerization of butyl acrylate and acrylonitrile in emulsions is a field of study, followed by Capek and coworkers [24,25,26] and it was determined that the mechanism of the copolymerization deviated from the classical Smith-Ewart theory on account of the partitioning behaviour of acrylonitrile. Devi et al. conducted an investigation on the synthesis of stable, transparent/translucent butyl acrylate-acrylonitrile copolymer latexes comprising on relatively high weight ratio of polymer to surfactant through polymerizing precursor emulsions containing a water-soluble initiator potassium persulfate [27]. Suresh and coworkers put forth the impact of butyl acrylate on the glass transition, dynamic mechanical and thermal degradation behaviour of its copolymer with acrylonitrile [19].

1.4.3 Polyethylacrylate Copolymers

Polyethyl acrylate are oil-proof and rubbers, resisting against high temperature. The commercial products are presented in various levels, change may be observed in processability, in the chemical nature of the cure-site or in the copolymer designed for the lower temperature application.

Reactivity levels were put forth by Brar and Sunita [28] via EVM by benefiting from a computer programme, which was designed by O'Driscoll. The basic quantities like monomer composition, diad and triad sequence distribution, conditional probabilities and number--average sequence lengths of A/E copolymers have been found out within the framework of ^{13}C -NMR analyses and differences between the ones, calculated from reactivity ratios as determined from the EVM, were determined.

The field of study of Braun and Meyer [29] was random copolymers' phase separation to high conversion in the course of free radical copolymerization. Occurrence of phase separation was registered by taking the actual stage of copolymerization as a basis. Copolymers' structure at the beginning of phase

splitting and the miscibility of low conversion copolymer compositions were compared.

1.4.4 Polytertiarybutyl acrylate Copolymers

Recently t-butyl acrylate has been the centers of attention for preparation of block or graft copolymers; because copolymers containing hydrophobic and hydrophilic sections stem from subsequent hydrolysis of the t-butyl group. Besides the reason why the poly t-butyl acrylate block has attracted a high level of attention to the ease of hydrolysis into a polyacrylic acid block; however there is one more grounds, which is the fact that the subsequent neutralization of the acid groups with a variety of bases forms a direct method to the corresponding ionomer blocks [30]. To our knowledge, there are no reliable report concerning with polyacrylonitrile-polytert-butyl acrylate copolymer.

1.4.5 Polymethylacrylate Copolymers

There is a wide application field with respect to carbon fibers in the industrial sector. Nowadays, most carbon fibers manufacture is based upon use of carbon pitch materials or acrylonitrile based polymers. The requirement of the development of a melt PAN based carbon fiber, which can be spun, is a PAN material, which is subject to process, well below the temperature in the course of which the stabilization reaction arises. In order to attain this objective, the melting temperature of the crystalline phase in PAN has to be decreased by incorporating comonomer units. Many works touch upon polyacrylonitrile-polymethylacrylate. McGrath and his colleagues made an investigation on the melting process of PAN-PMA carbon fiber precursors [31-32-33-34].

Rakshit et al. used the solution polymerization method and investigated the acrylonitrile-methyl acrylate, acrylonitrile-ethyl acrylate and acrylonitrile-butyl acrylate copolymers and their homopolymers [35]. The characterization was done

by elemental analysis, FTIR, ^{13}C -NMR, DSC, DTA and TGA. Another important study about acrylonitrile copolymers was made by Rieger and Schneider [36]. It was found that the Gordon-Taylor equation describes the dependence of the glass transition temperature from the composition of the copolymers very well-apart from some exceptions. Donescu et al. studied the solubilization of several monomers in the mixture water-sodium dodecylsulfate in order to find the selectivity of solute/surfactant interactions [37]. In this study, we are proposing an efficient one step copolymerization reaction of acrylonitrile and various types of acrylates.

1.5 Membrane Technology and Advantages

1.5.1 Historical Background of Membrane Technology

Membranes were first studied in the 18th century by Friar Jean Antoine Nollet where a pig`s bladder was used to separate alcohol from water by osmosis [38-39]. In the 19th and the 20th centuries the usage of membranes were limited to laboratory scale applications to develop physical and chemical theories, however membranes did not possess significant value for industrial or commercial applications. A major example for this is the study on the limit law of Van`t Hoff in 1887 which explains the ideal dilute solution characteristics, where he used the membranes produced by Traube and Pfeffer to measure solution osmotic pressure. In 1907, methods for controlling the pore size of the collodian membranes were developed by Bechold as he controlled the rate of evaporation of the solvents and washed the film with water. Moreover, using air pressure for enhancing permeation rates was first suggested by him and using air pressure and surface tension measurements lead to the development of the methods for measuring pore diameters. He is also known as the creator of the term Ultrafiltration [38-39].

The most important change in the field of membrane technology was achieved in the period between 1960 and 1980. The original Loeb-Sourirajan technique

inspired several membrane formation processes for the production of high performance membranes such as interfacial polymerization and multilayer composite casting and coating. Today, membranes with 0.1 μm or less selective layer thickness are being produced commercially with these methods. Developments in methods of packaging membranes into wide membrane area including spiral wound, hollow fiber, capillary, plate and frame modules, had resulted in the improvement of membrane stability. By installing large plants globally, processes such as microfiltration, ultrafiltration, reverse osmosis and electrodialysis were all established up to 1980 [40].

1.5.2 Membrane Technology

Today, membrane technology and the wide application fields related to this technology have earned a significant place in chemical industry. The key feature of a membrane that is benefited mostly is its ability to control the permeation rate of a chemical species through itself. The objective of using membranes depends on the application to be used. Within the scope of separation applications, the relevant target is to ensure that one component of a mixture penetrates the membrane without any limitation and at the same time penetration of other components are prevented. In order to fulfill many splitting needs in the process industries membranes can be benefited from. In terms of this splitting, two general fields can be said; within the scope of the first one, materials exist as a number of stages and within the scope of the second one, dissolution of species in a single stage can be said.

Membrane separation processes possess highly progressive process engineering methods and they are used to separate specific materials that are difficult and expensive to separate. Being useful to separate materials that cannot be separated by conventional separation methods, membrane technology has proved to be an important and popular method in industry and a promising alternative in the future;

moreover this technology has already provided advantageous solutions compared to other methods like absorption, distillation, extraction, leaching, crystallization and adsorption [41].

1.5.3 Membrane Definition and Classifications

We can define a membrane as a thin sheet of natural or synthetic material, which penetrates into substances in solution. A permeable or semi-permeable membrane stage is mostly a thin polymeric solid limiting the movement of specific species. Thus, nowadays an average 60% of synthetic polymeric membranes are benefited from as a semipermeable barrier layers permitting permit certain components of solutions or suspensions in terms of rapid permeation when compared with others. The said added stage can primarily be deemed as an obstacle between the feed stream for separation and one product stream. The said membrane or obstacle via itself is responsible for control of relative rates of transport of many species and as it is valid for all separation cases, leads to depletion of one product in specific components, and concentration of the second product in the said components [39].

Various ways can be mentioned in terms of classification of a membrane. Primarily on the basis of the ultrastructure as either microporous or asymmetric, classification of membranes is made. Microporous membranes may be sometimes subject to classification as isotropic (comprising of uniform pores throughout the membrane body) or anisotropic (within the structure of which changing of pores in size from one membrane surface to the other is in question).

According to the observations, frequently made, when compared with the maintained particles, there are much larger pores. It is possible that the particles, whose sizes are almost the same, enter into the pores partially, and block them. The reason why microporous membranes are designed is to ensure that all particles are maintained above its rating. Frequent observations comprise of the fact that the

pores are larger than the maintained particles and on a membrane surface, pore sizes are disseminated [39].

The characteristic of asymmetric membranes is a thin ``skin`` on the surface of the membrane. The layers within the body of the skin may contain voids, which give a support to the skin layer. Rejection is observed solely at the surface; however due to its special ultrastructure, maintained particles or macromolecules above the nominal molecular weight cut off (MWCO) do not penetrate into the main body of the membrane. The said asymmetric membranes do not often get ``plugged`` like microporous membranes; however like all filters, flux-lowering phenomenon such as fouling and concentration polarization is applicable in respect of them.

Within the framework of membrane preparation method porous or nonporous structure of the skin layer is determined. It is probable that the skin layer to result from the phase-inversion process is porous; besides it is possible that those skin layers that are deposited from solution or plasma onto a porous support have a homogeneous structure.

Phase inversion process means a method of production of asymmetric membranes resulting in a solvent-cast structure, whose porosity depends on immobilization of the polymer gel before complete solvent evaporation or depletion. Practically, dissolution of the polymer in a suitable volatile solvent and addition of a swelling agent like magnesium perchlorate or formamide are in question. In the event of casting of this solution and permission of the solvent to evaporate, an increased concentration of polymer at the solution/air interface arises, because more rapid loss of the solvent from the surface is in question. Basically the polymer goes out of solution at the surface and the so-called skin layer, which is unique to asymmetric membranes, is formed. Subsequent to skin formation, it is possible for the remaining solvent in the bulk of the mixture to evaporate more slowly. Finally the swelling agent within the structure of the mixture starts separating out as a distinct stage, which results in two phases within the substructure: the polymer-solvent as

the concentrated phase and the swelling agent as the disseminated phase. Finally, both the solvent and the swelling agent separate from each other, the polymer coating loses its thickness to a high extent, and it ruptures as a result an open-celled structure arises [39].

1.5.4 Basic Principles of Membranes

Species mass transport along the membrane in the course of a membrane splitting process is subject to control primarily by a driving force and the membrane morphology. In the course of the membrane separation process, maintenance of the feed mixture is observed in connection with one side of a membrane. Solvents and species, having smaller molecular sizes when compared with the pore dimensions will go through the membrane, and they turn into “permeate”, which is removed from the other side of the membrane on a constant basis. Concentration of “retentate”, meaning the rejected species, in the feed stream on a progressive basis is in question [42].

Performance of a membrane depends on two factors, which are *flux* and *selectivity*. Within the scope of the term “flux”, the amount of fluid flowing through the membrane is described; the volumetric flow rate of the permeate, which is in general stated on the basis of volume per unit membrane area per unit time as follows [43].

$$J = \frac{1}{A} \frac{dV}{dt} \quad (4)$$

where,

J : flux (L/m²/h)

dV/dt : permeate flow rate (L/h)

A : effective membrane area (m²)

Membrane flux primarily gives the definition of its productivity; whereas the *selectivity* of the membrane gives a definition whether it will be useful or not as it is an indication of the level of purity of the product stream and the amount recovered at the desired purity. One of the two parameters: *retention* or *separation factor* in general expresses selectivity. In terms of dilute aqueous mixtures, comprising of a solvent (mostly water) and a solute, it is much more appropriate to define selectivity within the framework of maintenance towards the solute. While the solute is partially maintained, the solvent (water) molecules penetrate freely through the membrane [43]. The retention is given by:

$$R = \frac{C_f - C_p}{C_f} = 1 - \frac{C_p}{C_f} \quad (5)$$

where,

R : retention

C_p : solute concentration in the permeate

C_f : solute concentration in the feed

In a sense, membrane splitting process may be deemed as an extension of the standard filtration; however some differences turning the membrane separation into one of the brightest new technologies today mentioned. The primary difference distinguishing the membrane splitting process from standard filtration may be deemed as the flow pattern. Conventional filtration processes operate in dead-end flow. This is the standard filtration procedure, used for filtration of a precipitate with filter paper or for straining spaghetti; there is no abnormality in terms of flow to the face of the filter. The standard method to perform ultrafiltration is cross flow; the principle flow parallel to the surface of the filter medium is included. Practice of microfiltration is done through both ways. Crossflow operation can be defined neither as clear nor difficult and in order to develop a thorough understanding with regard to grounds for its use (Figure 1.2) [44].

Conversion per pass may be deemed as one basic difference in terms of operation of the said two schemes. Within the scope of dead-end filtration, basically all the fluid penetrating into the filter may be retained by the cake or arises as a permeate; thereby conversion is approximately 100%, all of which occurs in the first pass. In terms of cross-flow filter, it can be said that the majority of the feed passes past the membrane rather than through it, and the ratio for conversion per pass for a long string of filter elements in series tends to be 20%. Recycling permits the ultimate conversion to be much higher [44].

Within the scope of the crossflow, the fluid, which will be subject to filtration, is pumped along the membrane, parallel to its surface. The fluid actually passing across the membrane partially flows through it. Through keeping the velocity along the membrane, material retained by the membrane is swept off its surface. On account of the fact that little of accumulation of retained material at the membrane is in question, the membrane in general does not “blind”, and when compared with the same system operating in dead-end flow, it is possible that the output is maintained at a higher level. Cross flow may be deemed advantageous when it is likely that the retained material plugs the membrane [44].

The flux decline, arising due to two phenomena; *concentration polarization* and *fouling* can be deemed as two of the major problems in the operation of the membrane separation processes. *Concentration polarization* can be defined as the formation of solutes close to or on the membrane surface. Solute is moved to the membrane surface through convective transport; solutes larger than the MWCO of the membrane are maintained by the membrane; besides solutes smaller than the pores will freely or partially penetrate through the membrane. Accumulation of solutes not passing through the membrane will be in question, and this fact will lead to either an increased resistance to solvent transport or an increase in local osmotic pressure; in both cases, flux may be decreased, and membrane’s sieving characteristics may be possible.

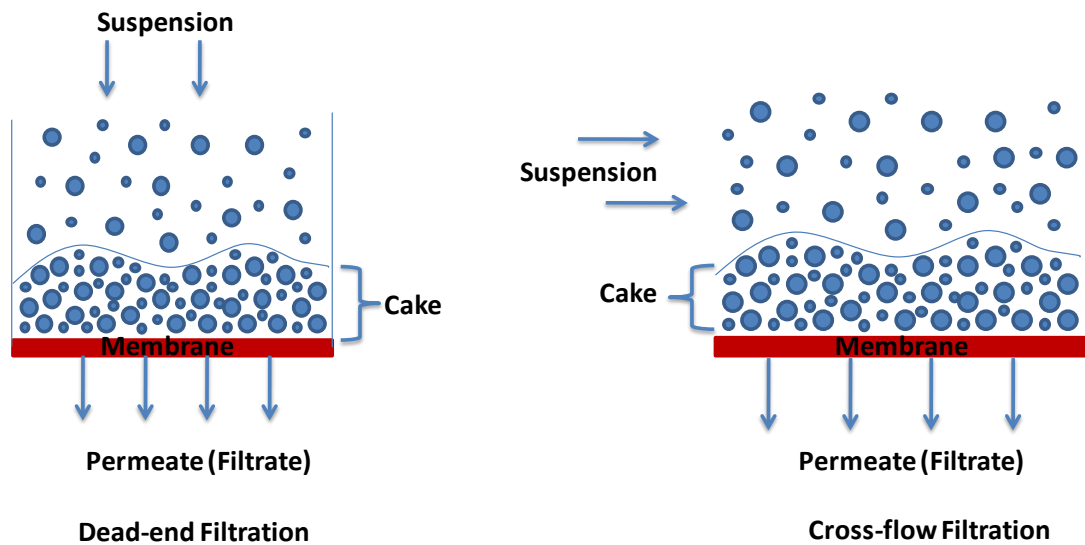


Figure 1.2 Schematic representation of a) dead end filtration, b) cross flow filtration [45].

Fouling may be defined as a phenomenon within the framework of which the membrane adsorbs or interacts through one way with the solutes taking place in the feed stream, and this fact leads to a decrease in membrane performance; flux lowering and/or increasing in solutes rejection within time. Fouling, is in general, definite and this fact makes it different from concentration polarization. Concentration polarization is affected by operating parameters such as velocity, pressure, temperature and feed concentration affects concentration polarization; however fouling basically depends on time and also partially on concentration. Overcoming the effects of fouling is only possible through shutting down the system and cleaning the membrane by chemical means [39-43]. The driving force for the pressure-driven membrane processes is *transmembrane pressure (TMP)* and it is defined as the pressure difference along the membrane.

1.5.5 Membrane Separation Processes

Species transfer between regions can be controlled by membranes and on the basis of the size range of separated materials and employed driving forces, classification can be made in this regard. Gradient pressure, concentration, electrical potential or temperature can be stated as the driving forces. Microfiltration (MF), ultrafiltration (UF), nanofiltration (NF) and reverse osmosis (RO) can be considered as the more common pressure driven membrane processes. The relative sizes of materials separated by these membrane separation processes are shown in Figure 1.3.

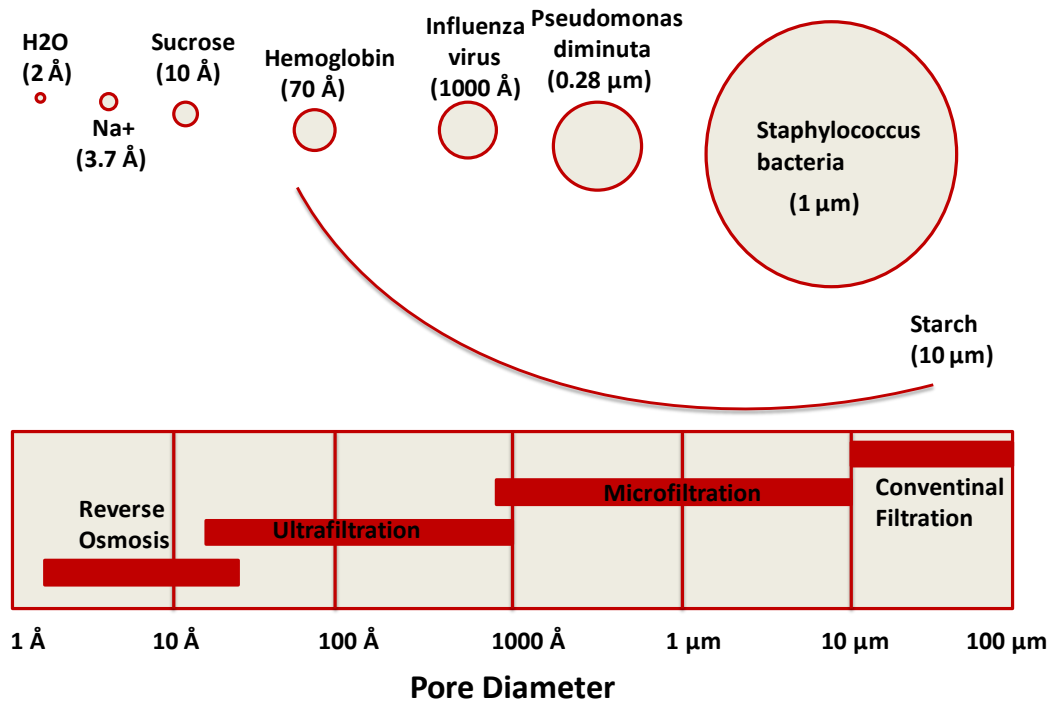


Figure 1.3 Relative Sizes of materials that can be separated in membrane processes [46].

The application of hydraulic pressure for the purpose of acceleration of the transport process is the component distinguishing the more common pressure driven processes. However, it is the nature of the membrane itself which controls the type

of components to be permeated and to be retained, shown in Figure 1.4. In reverse osmosis, all components other than the solvent itself can be retained; on the other hand through ultrafiltration solely macromolecules or particles larger than about 0.001-0.02 μm are retained. Besides the reason why microfiltration has been designed is to maintain particles in the micron range, which means suspended particles in the range of 0.1 μm to about 5 μm . Thus, to state from a broader perspective, reverse osmosis is basically deemed as a dewatering technique, on the other hand, ultrafiltration can be evaluated as a method for simultaneously purifying, concentrating, and fractionating macromolecules or as a fine colloidal technique, splitting suspended particles from dissolved substances, however the particles have to cover the size requirements related to microfiltration membranes. Nanofiltration can be deemed as a relatively new process depending on charged membranes with pores larger than RO membranes, however too small to permit penetration of many organic compounds like sugars [47].

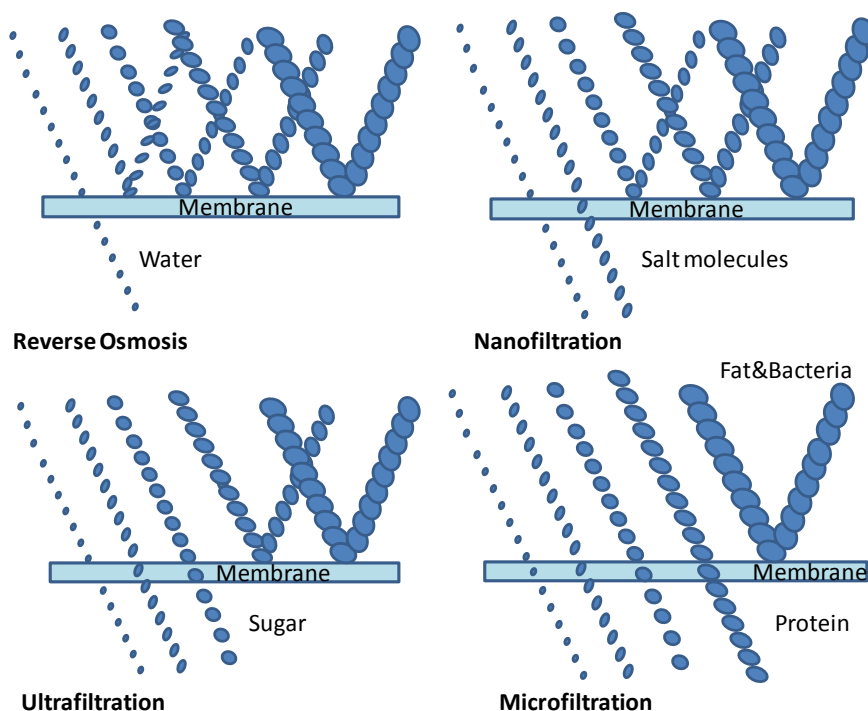


Figure 1.4 Pressure driven membrane processes and their separation characteristics[45]

Microfiltration

Pressure-driven flow through a membrane or other filter medium is benefited from for the purpose of separation of micron-sized particles from fluids, the process is named as microfiltration (MF). Despite the fact that the accurate size range is still subject to discussion, MF is in general defined as the filtering of a suspension comprising of colloidal or fine particles having linear dimensions within the framework of the approximate field of 0.02 to 10 μm . Within the scope of this size range, a wide variety of natural and industrial particles take place. The said particles in general have a larger structure when compared with the solutes separated on the basis of reverse osmosis and ultrafiltration. As a result, the osmotic pressure related to microfiltration cannot be defined as significant and the transmembrane pressure drop driving the microfiltration process is slight relatively (in general 1-50 psi). Besides, the membrane pore size and permeate flux tend to be larger for microfiltration when compared with ultrafiltration and reverse osmosis. As far as microfiltration is concerned, the imposed pressure drop, the driving force for the process, leads to passage of the suspending fluid and small solute species through the membrane or other filter medium and collection of them as permeate. Through a filter medium, the particles are maintained and collected as concentrated retentate. Maintenance mechanism, applicable for the particles is dependent on the type of filter medium and the structure of its interactions with the particles subject to filtration. In the event that a membrane with pores that are smaller than the particles is benefited from as the filter medium, a sieving mechanism is in question. Surface filtration is an alternative definition for the sieving mechanism [40].

Ultrafiltration

Basically ultrafiltration can be defined as a size exclusion based, pressure driven membrane splitting method. In general, the pore size for UF membranes is approximately 2-500 nm and the species in the molecular range from 3000 to 500 000 Da are maintained; on the other hand solvent goes through the membrane. UF

membranes skin structure is porous. The membrane productivity (flux) and the extent of separation can be considered as the most significant UF membrane features.

Unlike polymeric materials for RO and NF membranes in terms of which the macromolecular structures mainly depend on permeation properties such as salt rejection characteristics, selection of membrane material for ultrafiltration is related to impact of materials on the permeation properties.

The pore sizes and the pore size distributions of UF membranes are the issues, which are effective on membrane properties. Polysulfone (PS), polyether sulfone (PES), poly ether ether ketone (PEEK), cellulose acetate, polyacrylonitrile (PAN), polyimide (PI) can be uttered as standard UF materials [48].

Nanofiltration

Nanofiltration membrane usually have high rejections to most dissolved organic solutes having molecular weights higher than 100–200 and appropriate salt rejection at salt concentrations lower than 1000–2000 ppm salt. Also, the membranes have a two- to five-fold more permeability than brackish and sea water reverse osmosis membranes; thereby their operation at pressures as low as 50–150 psig is possible and production of useful fluxes can be observed. Due to the said issues, their basic application has been elimination of low levels of contaminants from relatively pure water. When evaluated from a broader perspective, similar membranes are benefited from for the purpose of softening municipal water through the elimination of sulfate and divalent cations or as a first pretreatment unit for an ultrapure water treatment plant [38].

Reverse Osmosis

Reverse osmosis is a method applied for the purpose of separation of the solute and the solvent components in the solution. The pore radius of the membrane is lower

than 1 nm. Water molecules, whose radius is approximately one tenth of 1 nm, can penetrate through the membrane freely; however electrolyte solutes like sodium chloride and organic solutes comprising of more than one hydrophilic functional group in the molecule are unable to penetrate through the membrane. The said solutes are removed from the membrane surface, or they are attracted to the solvent water phase to a high extension when compared with the membrane surface. The optional sorption of water molecules at the solvent-water membrane interface, arising on account of the interaction force operating between the membrane-solvent-solute, is on this account the relevant grounds for the separation. Polymeric materials like cellulose acetate and aromatic polyamide are in general benefited for the purpose of the preparation of reverse osmosis membranes.

When a membrane is placed between a pure water and an aqueous sodium chloride solution, the water flows from the pure water chamber to the sodium chloride solution chamber; however flow of sodium chloride does not occur. The water flow into the sodium chloride solution chamber, can increase the water level of the solution in question until the flow of pure water ceases at the standard level. In case of conversion to the hydrostatic pressure, the distinction between the water level of the sodium chloride solution and that of pure water at the fixed level is named as osmotic pressure. In case of application of pressure exceeding the osmotic pressure to the sodium chloride solution, reversal of the flow of pure water occurs; the flow from the sodium chloride solution to the pure water emerges. Flow of sodium chloride through the membrane does not occur. In conclusion, obtainment of pure water from the sodium chloride solution may be possible. The mentioned separation is named as reverse osmosis. The reverse osmosis process can be applied perfectly in the production of drinking water from seawater. This method is called seawater desalination [49].

1.5.6 Membrane Fouling

Fouling of the membrane can be deemed as a significant limiting stage within the scope of membrane technology. Fouling arises as a decline in flux with the progress of operation time. Literally, the flux decline should be observed in the event that all operating parameters like pressure, flow rate, temperature, and feed concentration are maintained fixed. The flux reduction is widely observed within the structure of MF and UF membranes.

The membranes will be fouled by nearly all feed components at a specific level. The characteristic and limit of membrane fouling highly depend on the physicochemical character of the membrane and the solutes. Surface chemistry, solute-solute and solute-membrane interactions are crucial in terms of understanding the fouling phenomenon. Within the phenomenological framework, a similarity may be found between membrane fouling and fouling of heat exchangers; however the surface of the membranes are more active; so it can be regarded as a more complex phenomenon [39].

1.5.7 Composite Membranes

Composite membranes comprise of at least two distinct materials. In general, deposit of a selective membrane material as a thin layer upon a porous sublayer, having the function of a support, is observed. The advantage of such membrane over the integrally skinned ones is that for the purpose of attainment of the desired membrane performance, independent optimization of each later is possible. There are many reliable techniques, targeting application of a thin top layer upon a support, which are dip-coating, spray coating, spin coating, interfacial polymerization, in situ polymerization, plasma polymerization, and grafting. Due to the versatility of preparation techniques, it is possible to use nearly all polymeric materials for the purpose of production of such membranes. The overall performance is improved by both the top layer and the support. High solvent

resistance is what makes PAN a good support material for thin film composite (TFC) membranes, which is evident from the following examples [50].

PAN supports preparation has been presented within the scope of the literature by Peinemann et al. [51], when an epoxidized PAN copolymer was applied ammonolysis providing highly solvent stable [including stability in dimethylformamide (DMF)] supports. A highly solvent-resistant UF membrane based on poly (acrylonitrile-co-glycidyl methacrylate) (PANGMA) was presented [52]. Phase inversion, followed by ammonolysis, was the method used for preparation of this membrane, and the said membrane was at a fixed level in DMF as well; thereby became an alluring support for preparation of organic solvent nanofiltration(OSN)-TFC membranes. Within the scope of lube oil dewaxing, composite membranes made of a support layer of PAN (10–80 mm thick), and a top, thermally cross-linked, elastomeric barrier layer of an adduct of maleic acid anhydride and a poly(aliphaticterpene) have been put forth as well [53]. Synthesis of PAN homopolymers or copolymers cross-linked with acids or bases, functionalized with amino, hydroxyl, or carboxylic groups, and covered by an additional hydrophilic or polyelectrolyte polymer layer has been performed [54]. The obtained composite membrane, was fixed in solvents like DMF, methylethyl ketone, and dichloromethane and could attain fluxes of 147.5 L/m²/h DMF and 99% congo-red dye rejections at 2.9 MPa and room temperature.

Industrial waste water often contains toxic transition and heavy metals other leachates which endanger the environment and the public health. One of the heavy metals, chromium, is considered as a toxic and a carcinogen nonbiodegradable environmental pollutant and usually exists in two oxidation states as chromium (III) and chromium (VI). Chromium (III) is in fact a relatively low toxic and is believed to be an essential nutrient for glucose metabolism in mammals [55-56]. In contrast to chromium (III), chromium (VI) is a strictly regulated pollutant contaminating the environment. Since it is detrimental to human health, the maximum level of

chromium (VI) in drinking water recommended by World Health Organization is 0.05 ppm [57-59]. Industries such as electroplating, metal finishing, dye, paint, paper are responsible for the hazardous effect of this significant environmental pollution [60]. Therefore, industries should use cost effective techniques to eliminate chromium (VI) in their water process to prevent damaging public health.

Traditional techniques such as, evaporation [61], adsorption [62], solvent extraction [63], ion exchange [64], electrochemical coagulation [65] and bioabsorption [66-67] require expensive equipment and controlling systems, although, these systems are found many times relatively successful in terms of separating chromium. Besides availability of these systems, these techniques produce large amount of sludge with high concentrations of chromium requiring problematic toxic sludge disposals [68-69]. On the other hand, almost complete chromium removal with membrane separation is one of the most reliable, sludge free energetically efficient ways. Membrane separation basically includes micro to nanofiltration as well as reverse osmosis and utilizes polysulfone, cellulose acetate, polyvinyl alcohol, polyamide and poly(methyl methacrylate) (PMMA) based membranes [70-76]. Recently, metal ion removals by several functionalized polymers are in great interest. Among these, amine functionalized polymeric membranes shows potentials in chromium removal. Several studies have been conducted for chromium removal using amine derivatives of acrylonitrile fibers, polyacrylamides, aniline formaldehyde condensate, short chain polyaniline on fiber [75-78]. Demirci Sankir et.al. have previously reported amine functionalized nanocomposites from polyaniline and ionically conductive sulfonated copolymers to tune their electrical conductivity [79].

1.6 The Aim of this study

Acrylonitrile copolymers have attracted much attention in academics and industry due to its well known commercial applications. It is important to utilize a suitable technique and optimize the conditions of polymerization especially in mass production for the synthesis of high performance acrylic polymers. In the present work, one step random copolymerization was proposed to produce different types of acrylonitrile copolymers. For such a typical system, controlling the molar composition results with tailoring the glass transition temperature. This is very crucial during thermal processing of these copolymers. This dissertation will mostly be concentrated on producing novel copolymeric materials specifically used in filtration technology. It is very important to point out that basic filtration membranes should possess following properties:

- High mechanical stability
- Chemical inertness
- Fouling resistance
- Morphology control
- Composite formation
- Fast filtration
- Less energy requirement with high flux rate at lower operation pressures
- Low price

This research demonstrates that acrylonitrile random copolymers and their novel composites can easily be converted in to high performance filtration membranes.

CHAPTER 2

EXPERIMENTAL

2.1 Acrylonitrile Copolymers Synthesis

2.1.1 Materials used for Homopolymer and Copolymer Synthesis

Acrylonitrile (AN, Aldrich 99%), butyl acrylate (BA, Acros 99.5%), hydroxyethyl acrylate (HEA, Aldrich 99.5%), tert-butyl acrylate (tBA, Acros 99.5%), ethyl acrylate (EA, Acros 99.5%) and methyl acrylate (MA, Acros 99.5%) were freshly distilled by vacuum distillation prior to use. Ammonium persulfate (APS, 99+%) water soluble initiator was provided from Acros Organics. 1-dodecanthiol (Merck) was used as a chain transfer agent (CT). DOWFAX 8390 solution surfactant (S) was used as received. Magnesium sulfate (97% anhydrous) and N,N- dimethyl formamide (DMF) (99.8%) and 1-methyl-2-pyrrolidone (NMP) (99%) were provided from Acros Organics and used as received. Deionized water was adopted as the polymerization medium. Emeraldine base polyaniline was purchased from Aldrich and directly used during nanocomposite preparations. Potassiumdichromate (cryst. Extra pure) was supplied from Merck. 1,5-Diphenyl carbazide from Merck was directly used for chromium detection.

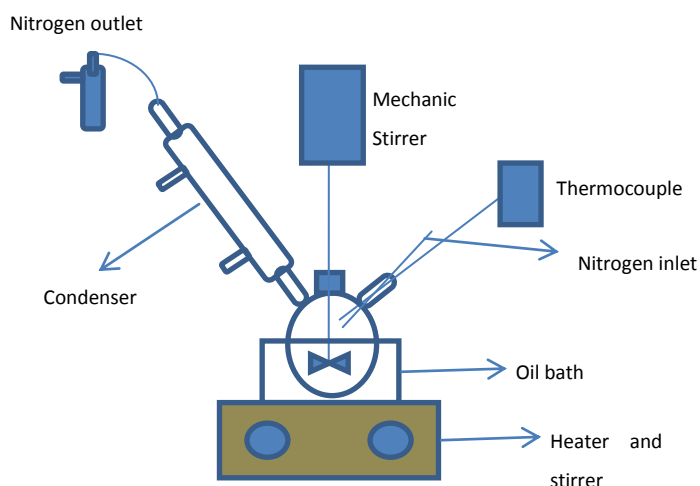


Figure 2.1 Schematic representation of experimental apparatus

2.1.2 Method for Homopolymer and Copolymer Synthesis

The copolymer and homopolymer synthesis was carried out in an aqueous medium via an emulsion polymerization route as described below (Figure 2.1);

A 250 mL reaction flask fitted with a condenser, glass stirrer, dropping funnel, nitrogen inlet tube and thermocouple probe was charged with water. The temperature was raised to 65 °C and the flask was purged with nitrogen for an hour, in order to remove all oxygen. The thermocouple regulated the temperature at a constant 65°C throughout the reaction. The surfactant, initiator (65% of total initiator) and mercaptan were added followed by the premix of the monomer mixture (20% of total monomer) to start the polymerization and then purged throughout the reaction. The remaining monomer mixture was added over a period of 2h. After addition of the monomer mixture, the remaining initiator was added through the dropping funnel. The latex was held at 65 °C for additional 30 min. The product was precipitated with 1% aqueous MgSO₄ solution and the copolymer was washed with distilled water for several times and then washed twice with 250

mL of methanol. The methanol removed any excess monomer that could still be present in the copolymer and also removed the water so that the copolymer could be dried much easier. Finally, the product was vacuum dried at 60 °C overnight. Various copolymers were prepared by using different type and amount of comonomer to examine the effects of the comonomer on the physical and chemical properties of the product. Table 1 shows recipe for the polymerization of homo and copolymers.

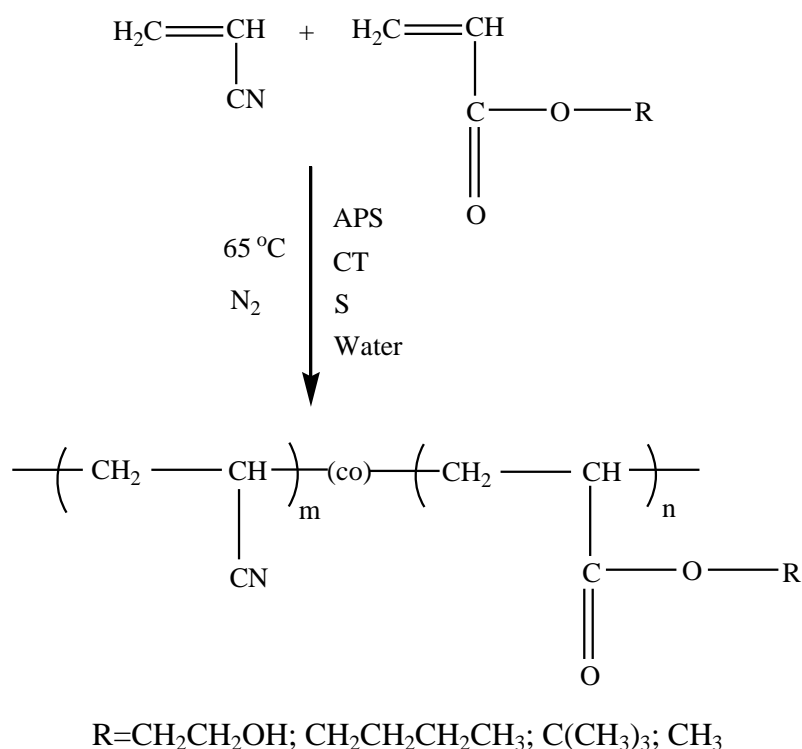


Figure 2.2 Reaction scheme for the copolymerization of acrylonitrile and acrylates

2.1.3 Film preparation for Mechanical Tests and Water Uptake Measurements

The copolymer films were prepared by casting from DMF (6% wt/wt) on a smooth glass plate under an IR lamp at about 60 °C and films were vacuum dried at 60 °C for 2 hours for further drying and used in mechanical tests. For water uptake

measurements, vacuum dried membranes (1x1 cm) were equilibrated for 24 h in water at room temperature prior to measurements, and water uptake of the membranes was calculated using following equation 1:

$$WU (wt \%) = \frac{M_w - M_d}{M_d} \times 100 \quad M_w = \text{Weight of wet membrane} \quad (1)$$
$$M_d = \text{Weight of dry membrane}$$

2.1.4 Nanocomposite Membrane Preparation

For a typical 5 percent PANI composite, emeraldine base PANI (0.06 gram) were dissolved in DMF (6.0 gram) and mixed overnight. Then, the required amount (1,14gram) of PAN(88)-co-PMA(12) copolymer (intrinsic viscosity of 1.6 dL/g) was added to the mixture to provide 5 percent PANI in the mixture. Polymer mixture was then poured on a smooth glass plate at room temperature. After this, plates were dipped in IPA solvent for an hour. Finally, copolymer nanocomposite membranes were soaked in water at room temperature overnight and doped with 0,5 M sulfuric acid solution for two hours then resoaked in water overnight. Membranes were permeated water at 689.5 kPa prior to performance tests.

2.2 Polymer Characterization Methods

2.2.1 Fourier Transform Infrared Spectroscopy (FTIR)

The polymerization reactions of the homopolymers and the copolymers were followed by a Bruker Vertex-70 FTIR spectrophotometer. Unknown samples are identified with matching reference spectrum by determination of functional groups. The white polymer was mixed with KBr to obtain pellets. FTIR spectra were taken directly. The PAN-based copolymers and homopolymers were analyzed over a

400-4000 cm^{-1} range with the resolution of 4 cm^{-1} . All spectra were averaged over 32 scans.

2.2.2 Nuclear Magnetic Resonance Spectroscopy (NMR)

^1H -NMR and ^{13}C -NMR spectra of polymers were obtained by Bruker 300 MHz NMR spectrometer (BioSpin, Ettlingen, Germany). DMSO- d_6 was used as a solvent. The sample concentration was approximately 8 mg/mL. The proton signals were referenced to tetramethylsilane (TMS) at 0 ppm as the internal standard. The data were evaluated by using XWINNMR software.

2.2.3 Differential Scanning Calorimetry (DSC)

The glass transition temperature (T_g) of homopolymers and copolymers were evaluated by Perkin Elmer Diamond DSC under nitrogen atmosphere at a heating rate of 10 $^{\circ}\text{C}/\text{min}$.

2.2.4 Thermogravimetric Analysis (TGA)

Thermal stability and thermal decomposition investigations of PAN-based copolymers and homopolymers were achieved by thermogravimetric analysis using a Perkin Elmer Pyris 1 TGA instrument (USA) under N_2 atmosphere with a heating rate of 10 $^{\circ}\text{C}/\text{min}$.

Table 2.1 Recipe for Emulsion polymerization of acrylonitrile based copolymers and homopolymers

Synonym	Full Name	AN	HEA	BA	Surfactant	APS	1-dodecanthiol	Water
PAN	Polyacrylonitrile	22.30 g	-		1.78 g	0.0223 g	0.42 g	42 mL
PHEA	Polyhydroxyethyl acrylate	-	22.40 g	-	1.79 g	0.0224 g	0.43 g	43 mL
PBA	Polybutyl acrylate	21.88 g	-		1.75 g	0.0219 g	0.42 g	42 mL
PAN(92) -co- PHEA(8)	92 molar percent PAN and 8 molar percent PHEA	22.15 g	4.22 g	-	2.11 g	0.0264 g	0.50 g	45 mL
PAN(88) -co- PHEA(12)	88 molar percent PAN and 12 molar percent PHEA	22.60 g	6.75 g	-	2.35 g	0.0293 g	0.56 g	44 mL
PAN(84) -co- PHEA(16)	84 molar percent PAN and 12 molar percent PHEA	22.13 g	9.23 g	-	2.51 g	0.0314 g	0.60 g	43 mL
PAN(92) -co- PBA(8)	92 molar percent PAN and 8 molar percent PBA	22.13g	-	4.65g	2.14 g	0.0268 g	0.51g	45 mL
PAN(88) -co- PBA(12)	88 molar percent PAN and 12 molar percent PBA	22.92g	-	7.55g	2.44 g	0.0305 g	0.58 g	43 mL
PAN(84) -co- PBA(16)	84 molar percent PAN and 12 molar percent PBA	22.18g	-	10.21g	2.59 g	0.0324 g	0.62 g	43 mL

Table 2.1 Continued

Synonym	Full Name	AN	tBA	EA	Surfactant	APS	1-dodecanthiol	Water
PtBA	Polytertbutyl acrylate	-	22.45 g	-	1.80 g	0.0225 g	0.43 g	46 mL
PEA	Polyethyl acrylate	-	-	22.66 g	1.81 g	0.0227 g	0.43 g	46 mL
PAN(92) -co- PtBA(8)	92 molar percent PAN and 8 molar percent PtBA	22.27 g	4.68 g	-	2.16 g	0.0269 g	0.51 g	45 mL
PAN(88) -co- PtBA(12)	88 molar percent PAN and 12 molar percent PtBA	22.23 g	7.32 g	-	2.36 g	0.0295 g	0.56 g	44 mL
PAN(84) -co- PtBA(16)	84 molar percent PAN and 12 molar percent PtBA	22.33 g	10.28 g	-	2.61 g	0.0326 g	0.62 g	43 mL
PAN(92) -co- PEA(8)	92 molar percent PAN and 8 molar percent PEA	22.14g	-	3.63g	2.06 g	0.0258 g	0.49g	45 mL
PAN(88) -co- PEA(12)	88 molar percent PAN and 12 molar percent PEA	22.26g	-	5.73g	2.24 g	0.0280 g	0.53 g	44 mL
PAN(84) -co- PEA(16)	84 molar percent PAN and 12 molar percent PEA	22.17g	-	7.97g	2.41 g	0.0301 g	0.57 g	44 mL

Table 2.1 Continued

Synonym	Full Name	AN	MA	Surfactant	APS	1-dodecanthiol	Water
PMA	Polymethyl acrylate	-	22.45 g	1.79 g	0.0225 g	0.42 g	47 mL
PAN(92) -co- PtBA(8)	92 molar percent PAN and 8 molar percent PMA	22.35 g	3.08 g	2.20 g	0.0254 g	0.48 g	45 mL
PAN(88) -co- PtBA(12)	88 molar percent PAN and 12 molar percent PMA	22.29 g	4.82 g	2.17 g	0.0271 g	0.51 g	45 mL
PAN(84) -co- PtBA(16)	84 molar percent PAN and 12 molar percent PMA	22.21 g	6.70 g	2.31 g	0.0289 g	0.55 g	44 mL

2.2.5 Mechanical Tests

Tensile tests were used to characterize the strength, the modulus, and the percent elongation of the homo and the copolymers at room temperature. The specimens had dimensions 0.6mmx1cmx6cm. An Instron 3361 operating at a constant extension rate of 10 mm/min was used to obtain the tensile data. The Instron 3361 is designed with a fixed or essentially stationary member carrying one grip and a movable member carrying a second grip. The ends of the specimens were placed in grips so that the long axis of the test specimen coincided with the direction of the applied pull through the centerline of the grip assembly. Specimens were aligned in the self-aligning grips in the direction of the applied pull. The modulus was determined from the slope of the initial linear portion of the stress-strain curve. The tensile strength at break was calculated by reading the maximum stress during process. Percent elongation at break of the specimen was calculated by reading the extension at break (%). For each type of sample, at least five experiments were performed and the average values of Young's modulus, tensile strength, and percent elongation at break were calculated.

2.2.6 Viscosity Measurements

Viscosity measurements were made in a thermostatic water bath at 30 °C using an Ubbelohde viscometer. A copolymer was dissolved in NMP, which had been exhaustively dried. For each polymer, the viscosity of the four concentrations was measured. Multiple readings were made at each concentration. Intrinsic viscosity was obtained by extrapolation of a plot of specific viscosity/concentration vs concentration to infinite solution.

2.2.7 Scanning Electron Microscopy (SEM)

The morphology of the membranes was examined using a Field emission scanning electron microscopy QUANTA 400F. For this purpose, after the casting membranes were dried for 24 h at room temperature and for the cross-section analysis they were fractured in liquid nitrogen. Before analysis, the samples were sputtered with gold/platinum about 2 nm.

2.2.8 Sheet Resistivity Measurements

Sheet resistivity of the nanocomposite membranes were measured using Lucas type Four Point Probe equipped with Keithley 2400 IV Source Measure Unit. Error resulting from film anisotropy was minimized by measuring the conductivity at different spots on the film. The average of these measurements has been reported in this study.

2.2.9 Water flux and Cr(VI) Removal Tests of Membranes

A dead end filtration apparatus (Sterlitech™ HP 4750) was used to measure both water and permeate flux at 689.5 kPa at three different concentrations as 50, 100 and 250 ppm. Analyses of aqueous solutions for chromium were performed calorimetrically using 1,5-diphenyl carbazide method [80] (Perkin Elmer Lambda 35 UV-Vis Spectrophotometer). Rejection of chromium (VI) was also measured at three different concentrations (50, 100, 250 ppm) for four different pH's (pH=2, 3, 5,7). The membrane size used in this study was 50 mm in diameter and the membrane area was 8,1 cm².

Water and permeate flux were calculated using the following equation (Equation 2) as a unit of L/m²h for 20 mL permeate volume by measuring the time interval.

$$J = \frac{V}{At} \quad (2)$$

where V is the volume of water or chromate solution (L), A is the active membrane area (m²) and t is time interval (h).

The chromium rejection, R, was calculated according to Equation 3;

$$R = 100x \left(1 - \frac{C_P}{C_F} \right) \quad (3)$$

C_P and C_F are the chromium concentration in permeate and in feed respectively.

Fouling analysis were performed with continuous permeation at 689.5 kPa. After 2h filtration, membranes were washed for 30 min at 25°C with deionized water. Then, the pure water flux of washed membranes (J_{w1}) measured to evaluate fouling capabilities of nanocomposite membranes.

Percent Flux Recovery (PFR) was calculated using following expression (Equation 4);

$$PFR = 100x \left(\frac{J_{w1}}{J_w} \right) \quad (4)$$

Fouling resistivity were also analysed by calculating total flux loss (TFL) (Equation 5) which is sum of reversible and irreversible flux losses;

$$TFL = \left(1 - \frac{J_P}{J_W} \right) \quad (5)$$

Reversible flux loss (RFL) can be seen in Equation 6,

$$RFL = \left(\frac{J_{WL}}{J_W} \right) - \left(\frac{J_P}{J_W} \right) \quad (6)$$

also, irreversible flux loss (IRFL) is defined by Equation 7,

$$IRFL = \left(1 - \frac{J_{WL}}{J_W} \right) \quad (7)$$

CHAPTER 3

RESULTS AND DISCUSSION

3.1 Polyacrylonitrile-Polyhydroxyethyl acrylate Copolymers

Polyacrylonitrile-co-poly(hydroxyethyl acrylate) copolymers (PAN-co-PHEA) at three different compositions (8, 12 and 16 molar percent of poly(hydroxyethyl acrylate) (PHEA)) and their homopolymers were synthesized by emulsion polymerization. Chemical structures and compositions were elucidated by FTIR, proton and carbon-13 NMR. Intrinsic viscosity measurements revealed that molecular weight of the copolymers were quite enough to form ductile films. Mechanical properties were also investigated. Thermal properties of copolymers were analyzed by DSC and TGA. Water uptake behaviors and densities of the copolymers were also evaluated. The chemical structure of copolymers is shown in Figure 3.1.

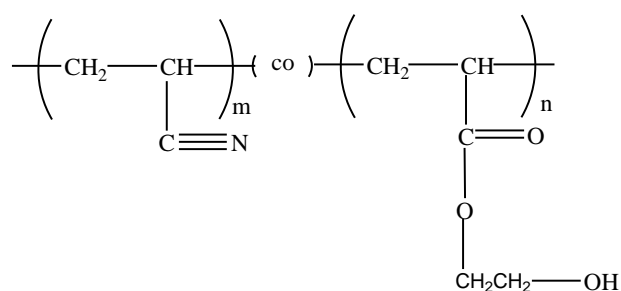


Figure 3.1 Chemical structure of polyacrylonitrile-co-polyhydroxyethyl acrylate (PAN-PHEA) copolymer

3.1.1 Fourier Transform Infrared Spectroscopy (FTIR) Results

The FTIR spectrum of the copolymers and the homopolymers can be seen in Figure 3.2. The broad peak at 3442 cm^{-1} corresponds to OH stretching, while OH bending can be seen at 1073 cm^{-1} . The aliphatic CH_x asymmetric and symmetric stretching peaks were observed at 2935 and 2864 cm^{-1} , respectively. The strong band at 1443 cm^{-1} corresponds to the CH_x bending. The characteristic $-\text{C}\equiv\text{N}$ stretching peak was seen at 2245 cm^{-1} and $-\text{C}=\text{O}$ stretching at 1731 cm^{-1} . The peaks between 1359 - 1078 cm^{-1} were assigned to C-C-O and O-C-C ester stretching vibrations. The chemical structures of the copolymers were confirmed by FTIR study. Also, from the FTIR spectrum; it can be concluded using the ratio of the band intensities of carbonyl to nitrile that there is a increased ratio from PAN(92)-co-PHEA(8) (1.5965) to PAN(88)-co-PHEA(12) (1.8208) and PAN(84)-co-PHEA(16) (2.0740) with an increased amount of HEA in the copolymer feed.

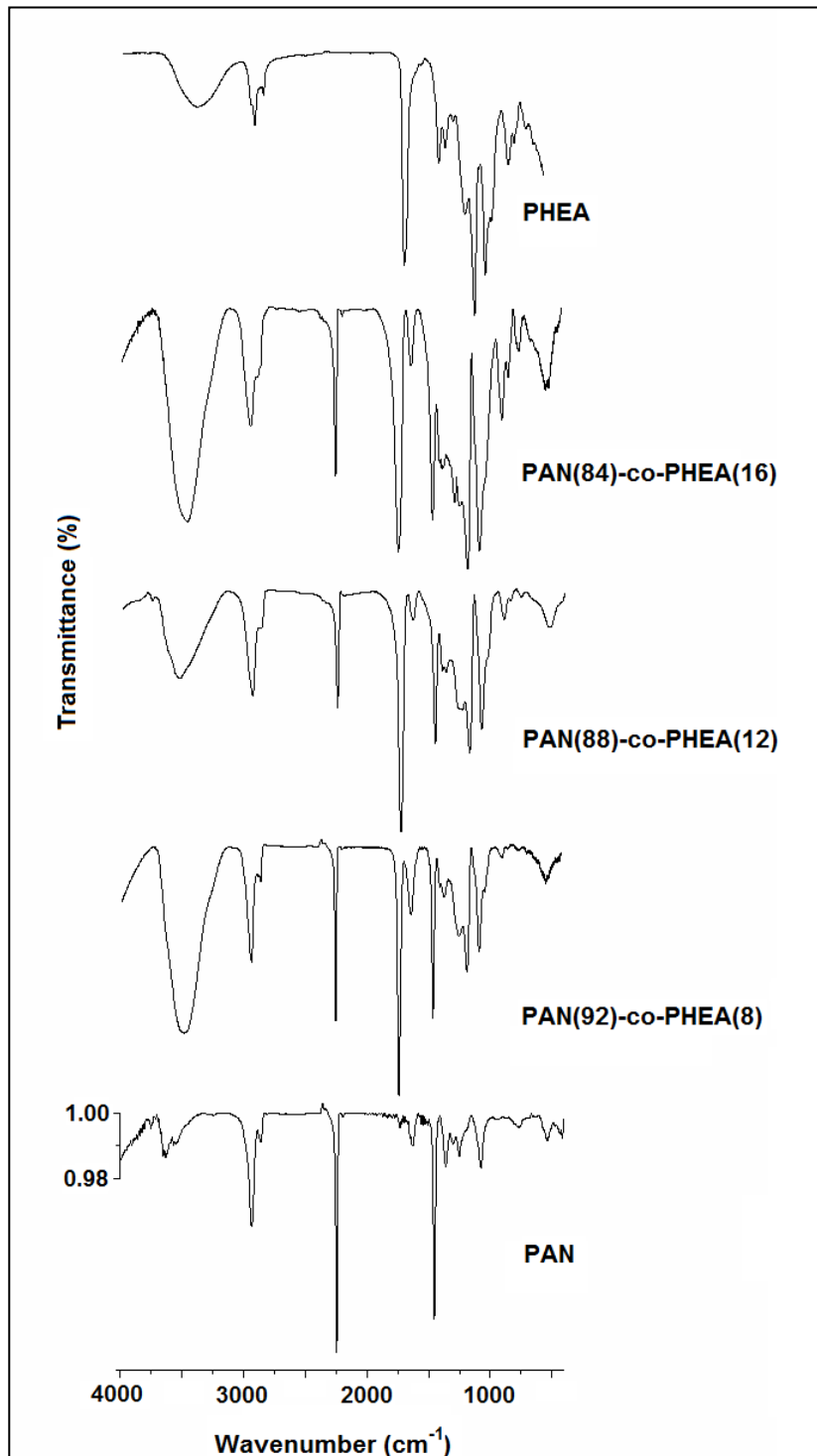


Figure 3.2 FTIR spectrums of the copolymers and homopolymers; monomers were successfully incorporated to chemical structure.

3.1.2 Nuclear Magnetic Resonance Spectroscopy (NMR) Results

¹H-NMR spectrum (Figure 3.3) of PAN-PHEA random copolymers at various molar ratios was performed for chemical conformation of copolymers. The resonance at 4.99 ppm was for the –OH of the hydroxyethyl group (g). The signals at 4.11 and 3.61 ppm were assigned to –CH₂ protons of the hydroxyethyl group (f and e). The –CH backbone protons of hydroxyethyl and the acrylonitrile group were ranged between 3.25 to 2.6 ppm (b and d), –CH₂ backbone protons were appeared between 2.4 to 1.37 ppm (a and c). The copolymer composition can be calculated by using the following peaks;

- i) –OCH₂ (f) and –CH (b,d) protons
- ii) –OH (g) and –CH (b,d) protons,
- iii) –OCH₂ (f) and –CH₂ (a,c) protons.

Observed values of integrals for the –OCH₂ (f) and –CH (b,d) peaks are labeled as n and m, respectively. The method for the composition calculation as follows:

Two protons from –OCH₂ peak give:

$$2y = n$$

$$y = n/2$$

Two protons from –CH peak of each monomer give:

$$x + y = m$$

$$x = m - \left(\frac{n}{2}\right)$$

Therefore the percent of incorporated HEA into the copolymer is calculated from the following equation:

$$\%HEA = \left(\frac{y}{x + y}\right) * 100$$

In order to obtain the percent of acrylonitrile that was incorporated into the copolymer, the value of the percent hydroxyethyl acrylate was subtracted from a value of 100%:

$$\%AN = \%100 - \%HEA$$

The theoretical and the actual compositions calculated from $^1\text{H-NMR}$ are summarized in the following equations and the results were tabulated in Table 3.1.

$$\begin{aligned} \text{i) } \text{Molar percent of HEA} &= \frac{I_{(f)}/2}{I_{(b,d)}} \times 100 \\ \text{ii) } \text{Molar percent of HEA} &= \frac{I_{(g)}}{I_{(b,d)}} \times 100 \\ \text{iii) } \text{Molar percent of HEA} &= \frac{I_{(f)}/2}{I_{(a,c)}/2} \times 100 \end{aligned}$$

Table 3.1 Theoretical and experimental composition and intrinsic viscosity data of PAN-PHEA copolymers

Sample (AN/HEA)	Monomer feed (molar ratio of AN to HEA)	Composition ^a (molar ratio of AN to HEA)	Composition ^b (molar ratio of AN to HEA)	Composition ^c (molar ratio of AN to HEA)
1	92/8	92.5/7.5	92.4/7.6	91.7/8.3
2	88/12	86.3/13.7	86.3/13.7	85.5/14.5
3	84/16	84.6/15.4	83.2/16.8	82.9/17.1

^a Calculated by $^1\text{H-NMR}$ from $-\text{OH}$ and $-\text{CH}$ peaks in $d_6\text{-DMSO}$

^b Calculated by $^1\text{H-NMR}$ from $-\text{OCH}_2$ and $-\text{CH}$ peaks in $d_6\text{-DMSO}$

^c Calculated by $^1\text{H-NMR}$ from $-\text{OCH}_2$ and $-\text{CH}_2$ peaks in $d_6\text{-DMSO}$

^{13}C -NMR spectrum (Figure 3.4) revealed that the characteristic signals of $-\text{C}=\text{O}$ and $\text{C}\equiv\text{N}$ were appeared at 173.4 (a) and 120.4 (b) ppm, respectively. Similarly, $-\text{OCH}_2$, $\text{CH}_2\text{-OH}$, $-\text{CH}_2$ and $-\text{CH}$ were detected at 66.3, 58.7, 32.6 and 22.07 ppm respectively. ^{13}C -NMR data showed that the HEA comonomer was reasonably incorporated to the copolymer structure.

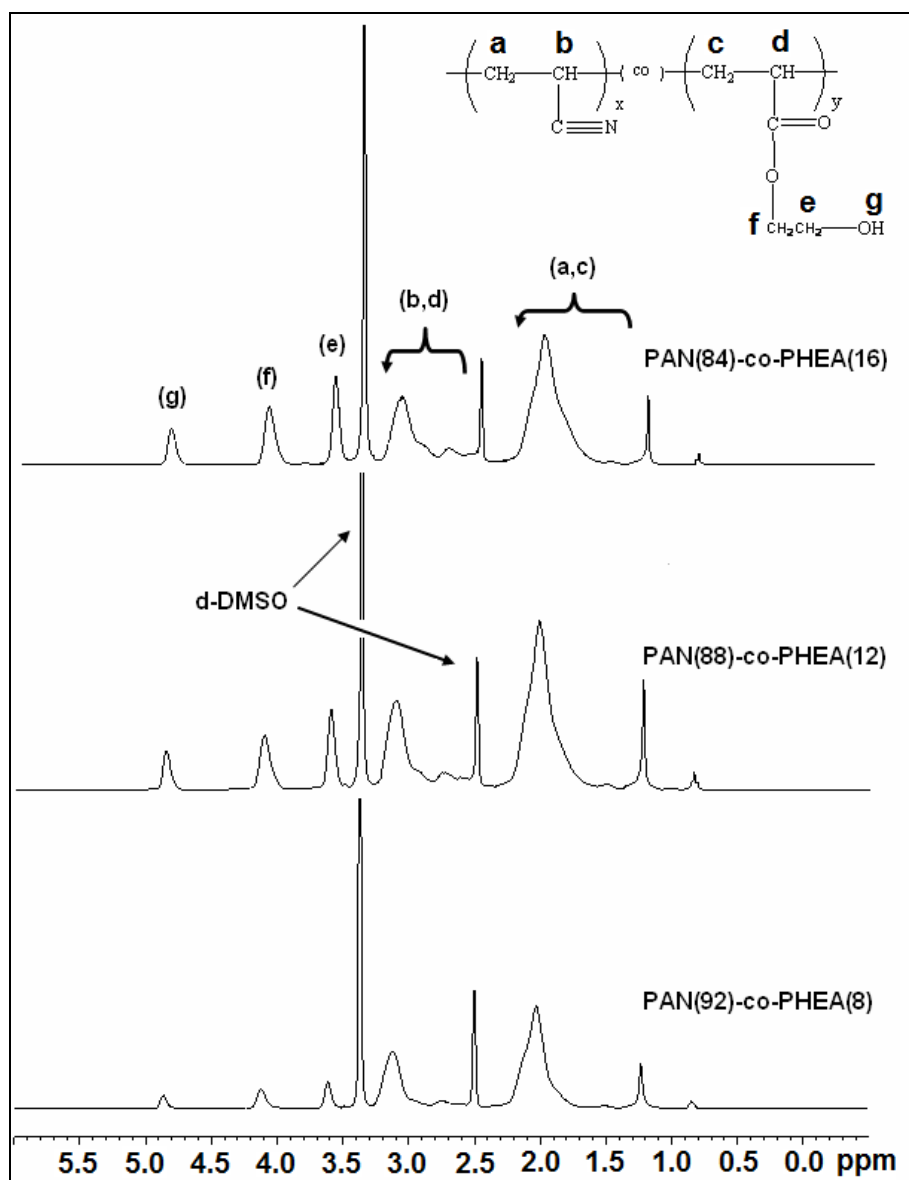


Figure 3.3 ^1H -NMR spectrum of AN-HEA copolymers with different compositions; chemical structure was proved by ^1H -NMR.

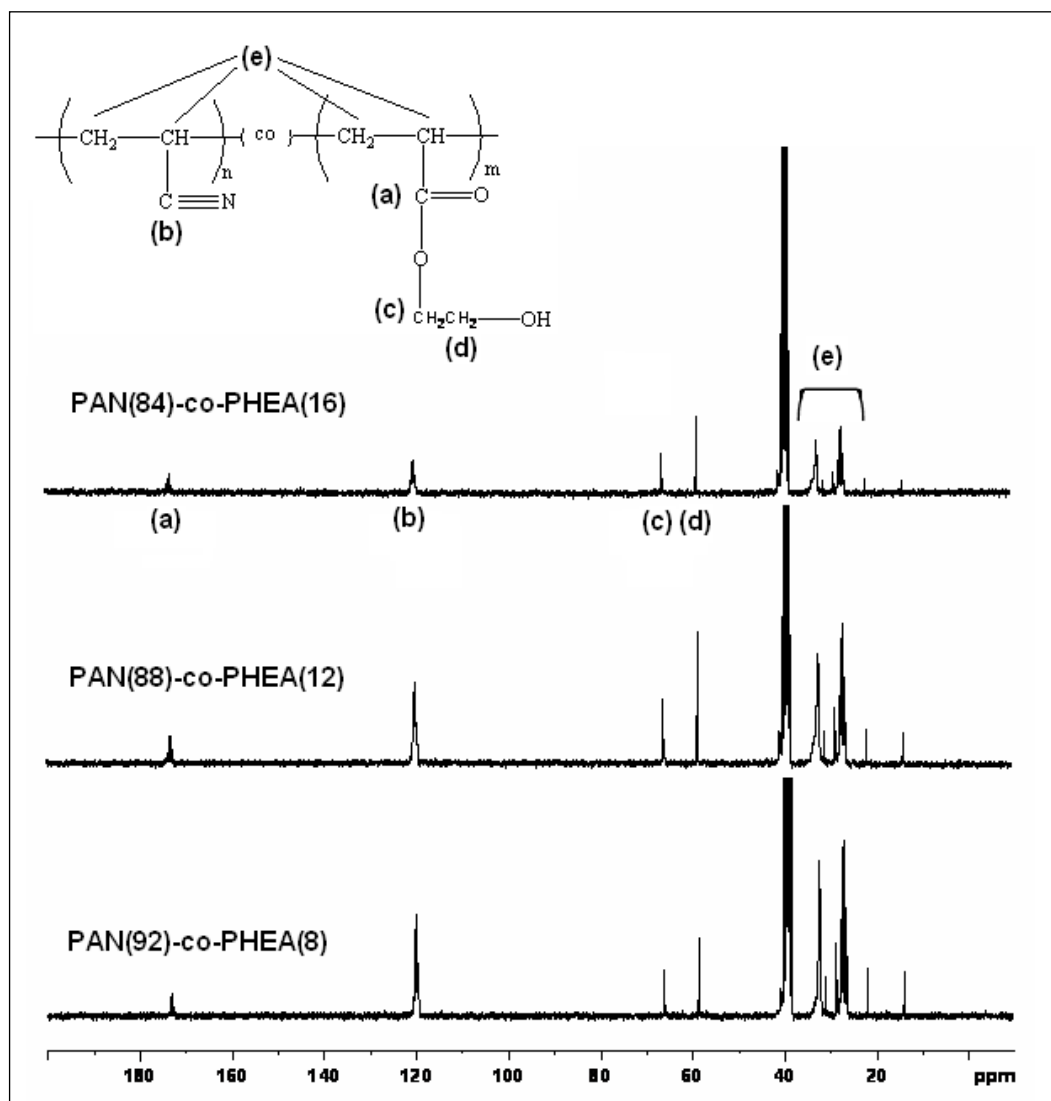


Figure 3.4 ^{13}C -NMR spectrum of AN-HEA copolymers with different compositions, showing theoretical and actual compositions were comparable

3.1.3 Differential Scanning Calorimetry (DSC) Results

The glass transition temperature (T_g) of the copolymers were determined from DSC. The determined values of T_g of copolymers lie between those of pure PHEA (3.5 °C) and pure PAN (104 °C) (Figure 3.5). The T_g values were found to decrease with

increase in the weight fraction of hydrophilic comonomer addition of HEA. Additionally the DSC thermograms of pure PAN and the copolymers showed that they do not decompose up to 240 °C. The T_g values of the copolymers of PAN and the polyacrylates have been reported by many workers [81-82]. However none of the previous reports have never issued the T_g of polyacrylonitrile-polyhydroxyethyl acrylate copolymer.

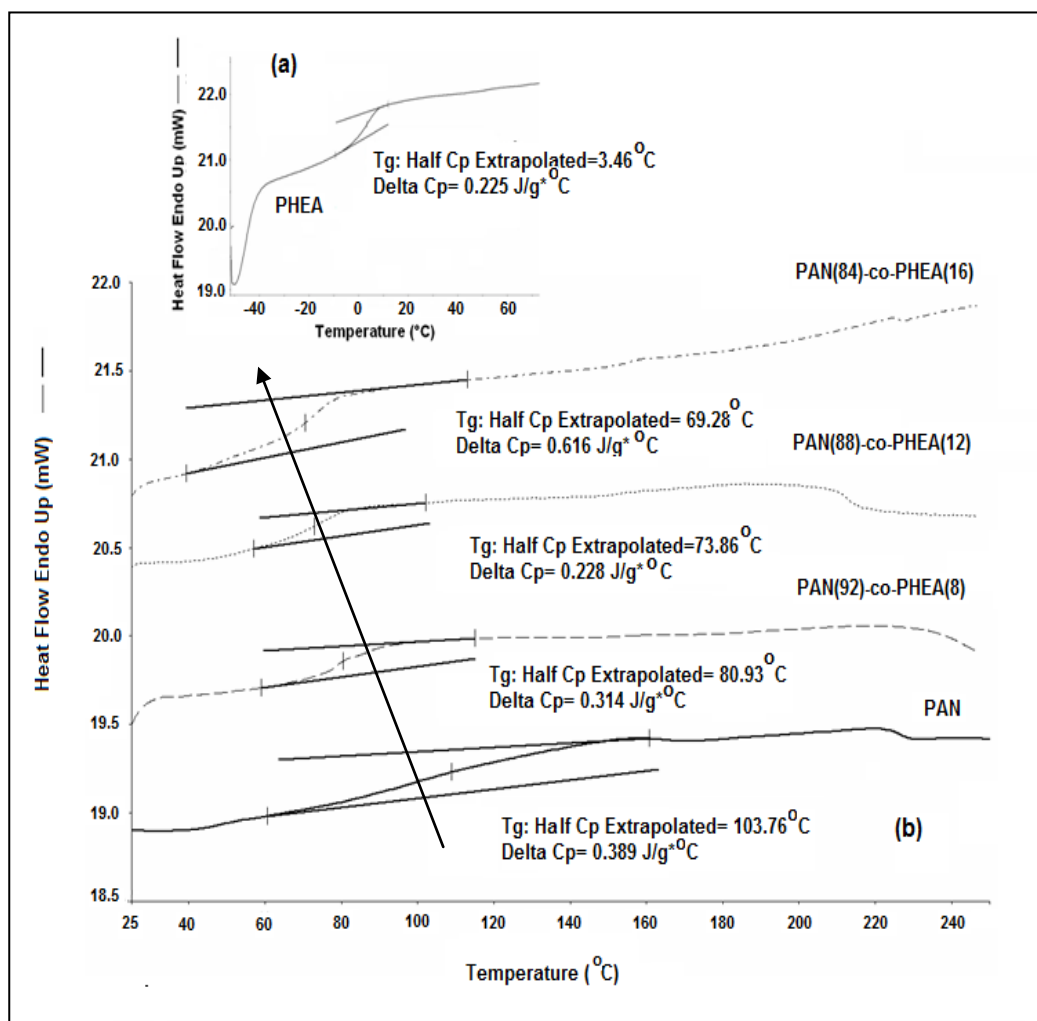


Figure 3.5 DSC thermogram of (a) PHEA, (b) homopolymer of PAN and copolymers. Glass transition temperature of PAN was successfully lowered from about 104 to 70 °C . Heating rate 10 °C/min, nitrogen atmosphere.

3.1.4 Thermogravimetric Analysis (TGA) Results

Thermal analysis of the homo and the copolymers were carried out to determine the degradation temperature and also the weight loss behavior during successive heating over a period of time. The study shows that thermal characteristics are affected by the weight % of the comonomer, as observed earlier for comparable systems [83-84]. The TGA thermograms of the synthesized copolymers and homopolymers are shown in Figure 3.6.

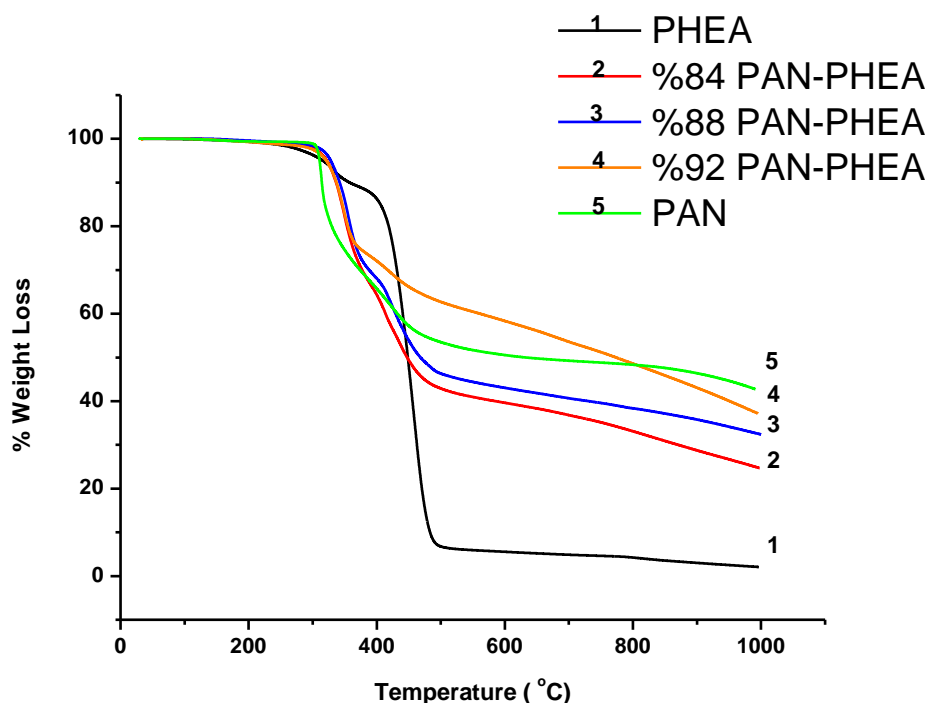


Figure 3.6 Weight loss temperatures for homo- and copolymers; copolymers were thermooxidatively stable.

There are two degradation steps for pure PAN. The thermal study of PAN was well studied before. The mechanism is quite complicated, but involves cyclization and aromatization of the polymer, followed by release of HCN [85-86]. The TGA thermogram of PHEA is typical for acrylate polymers where thermal degradation is

in the form of depolymerization [87]. All of the copolymers are thermooxidatively stable up to 330 °C which was high enough for many applications. Two step degradations was commonly observed for the copolymers, this can possibly be attributed to the side groups and the main chain degradation and more clearly seen in Figure 3.7. As the % weight of comonomer in the feed increases the thermal behavior of copolymers more resemble to pure HEA. Supplementally, 10% weight loss temperatures of copolymers (Table 3.2) are close to each other and in the range of pure PAN and pure PHEA.

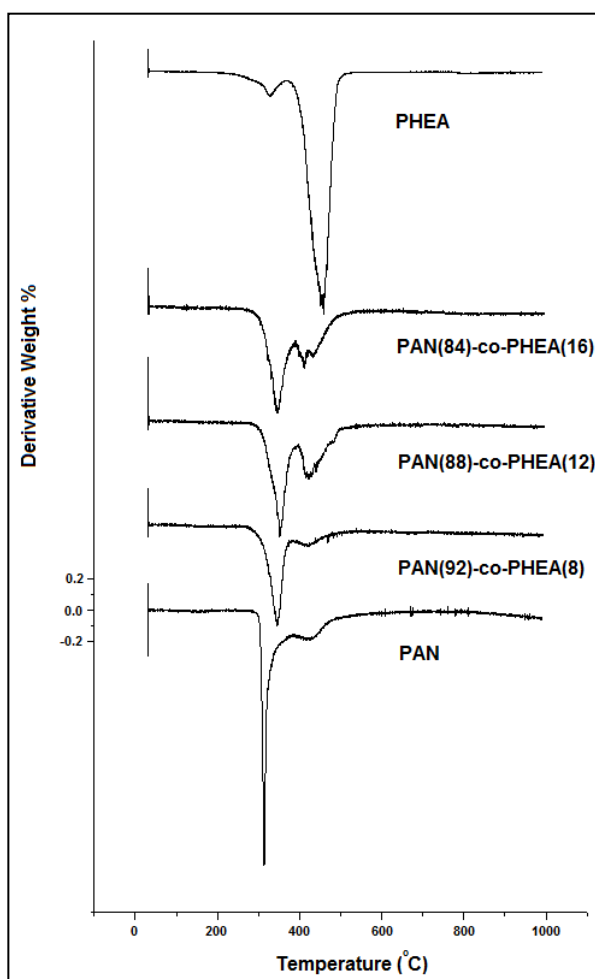


Figure 3.7 Derivative weight loss curves for homo- and copolymers versus temperature

Table 3.2 Thermal decomposition properties of homo- and copolymers (heating rate 10°C/min, N₂ atmosphere)

Sample name	T ₅ ^a (°C)	T ₁₀ ^b (°C)	T _{max} ^c (°C)	Char yield at 800°C
PAN	310	314	314	48
PAN(92)-co-PHEA(8)	317	337	349	38
PAN(88)-co-PHEA(12)	320	342	353	33
PAN(84)-co-PHEA(16)	324	336	348	32
PHEA	316	358	461	4.2

^a Temperature for 5% decomposition

^b Temperature for 10% decomposition

^c Temperature of the maximum point

3.1.5 Mechanical Test Results

In mechanical tests, samples are subjected to a progressively increasing tensile force until it fractures. The strain is directly proportional to the stress and the specimen returns to its original length upon the removal of stress. In this region load is not enough to cause permanent shifting between the molecules. Beyond this elastic limit the applied stress produces plastic deformation, so the permanent extension remains by the removal of applied load. The tensile strength of a polymer is defined as the force required breaking a sample by tensile force. In the linear elastic regions, the ratio of applied stress to the amount of elongation gives modulus of elasticity. The maximum force which caused the break of the sample is reported as tensile strength, and the elongation is compared to the original sample is reported as percent elongation [88].

Different compositions of PAN-PHEA copolymers showed different mechanical properties. As expected, elastic modulus of the films decreased with increasing the HEA content, since the polymer structure becomes softer and the polymer chains

starts to flow under the load with the addition of HEA. The maximum elastic modulus, which is 785 MPa, was obtained for 92 % PAN containing films (Figure 3.8).

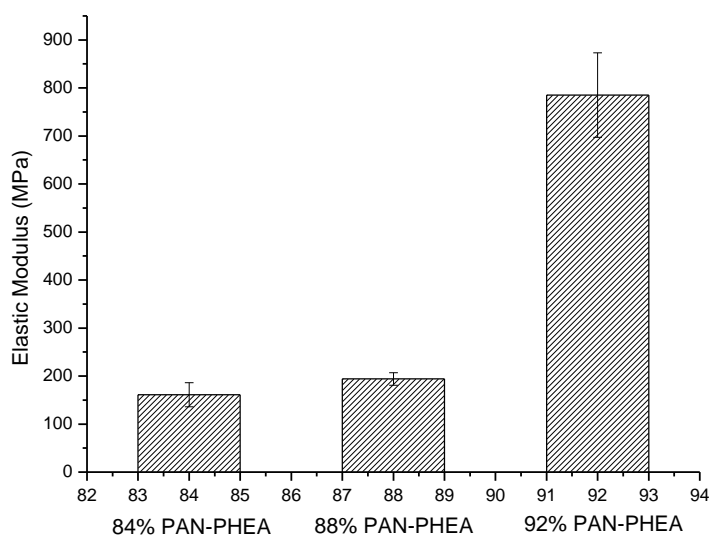


Figure 3.8 Elastic modulus of PAN-PHEA copolymer films

Ultimate tensile strength (UTS) values are given in Figure 3.9. Decrease in the AN unit in the copolymer content, decreases the UTS values leading to softer polymeric structures. As the AN content decreases to %92 PAN-PHEA, %88 PAN-PHEA and %84 PAN-PHEA, UTS values changed from 29.65 MPa, 22.03 MPa and 12.84 MPa, respectively. The decrease in the UTS values is due to the increase of the HEA content which has poor mechanical properties.

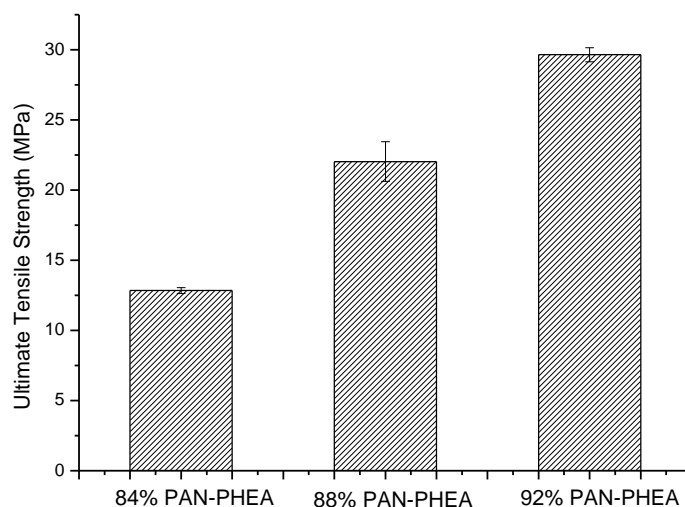


Figure 3.9 Ultimate Tensile Strength of PAN-PHEA copolymer films

The elongation at break (EAB) values of PAN-PHEA films are shown in Figure 3.10. EAB increased with increasing the HEA content from 8 to 12%. By further increasing the HEA content, besides the decrease in E and UTS, a decrease in EAB was obtained. This indicates a relative loss in the mechanical durability of the films compare to the films having 8 to 12% HEA. The PAN(88)-PHEA(12) sample showed the highest EAB value with 428.45%. As a result, it is possible to conclude that the mechanical properties of these films could be tailored with the addition of HEA. The values of E, UTS and EAB for all PAN-PHEA copolymers are given in Table 3.3.

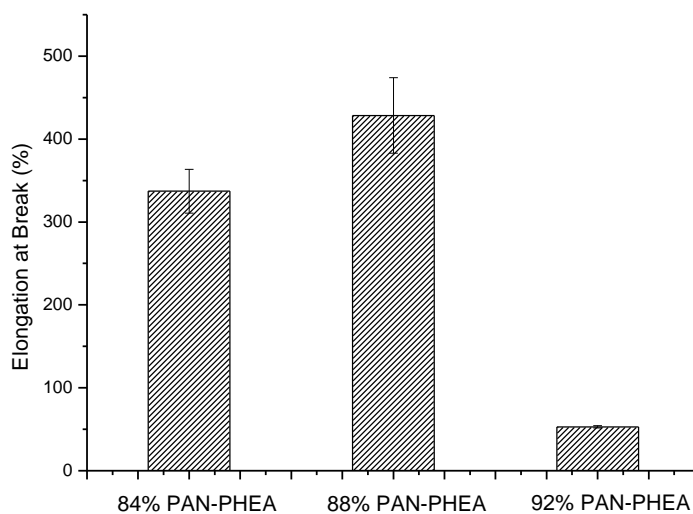


Figure 3.10 EAB of PAN-PHEA copolymer films

Table 3.3 Mechanical Test Results for PAN-PHEA copolymer films

Sample Name	UTS (MPa)	E (MPa)	EAB (%)
PAN(92)-PHEA(8)	29.65 ± 0.50	785 ± 87.5	52.89 ± 1.40
PAN(88)-PHEA(12)	22.03 ± 1.41	194 ± 13.4	428.45 ± 45.65
PAN(84)-PHEA(16)	12.84 ± 0.21	161 ± 25.1	337.17 ± 26.45

3.1.6 Swelling Behaviour Analysis of PAN-PHEA copolymers

Swelling behavior analysis of the polymer matrices is especially important for the design of controlled-release devices. In this study to obtain the hydrophilic property of copolymer, the HEA comonomer contributed into the PAN. It is possible to predict the drug release rate by determining the dynamic swelling properties of the polymer matrices [89]. In this study, the equilibrium swelling ratio and degree of swelling of the PAN-PHEA copolymers having various PAN content has been determined. Table 3.4 represents the equilibrium swelling ratios and the densities

of the solution cast copolymers at various percent HEA loadings. As expected, homopolymers of HEA absorb tremendous amount of water due to its hydrogel properties. It has been observed that the swelling ratio of the copolymers decreased with decrease in the HEA content. Also, increasing the HEA content lowered the density of the copolymers. This may correlate the decrease in the glass transition temperatures with increase in the HEA content.

Table 3.4 Equilibrium swelling ratio and densities of copolymers at various percent HEA loadings

HEA Content (%)	SR(%)	Density (g/cm ³)
8	7.94	1.15
12	10.31	1.11
16	21.82	1.06
100	1065	not applicable

Variations in the degree of swelling (q) with HEA content in the copolymer can be seen in Figure 3.11. As expected the degree of swelling decreased with the decreasing in the HEA content. Moreover, degrees of swelling reached a maximum in 1-6 hours. Then, a decrease in q was observed. Finally q values stabilized. This effect is called the overshooting phenomenon [90]. Basically, this phenomenon could be attributed to the polymer relaxation. Diffusion of the solvent into the hydrogel part (HEA) of the copolymer is faster than that of into the acrylonitrile chain. Therefore, initially more water was absorbed. Then, when the copolymer relaxes into the equilibrium conformation, membranes expelled some water.

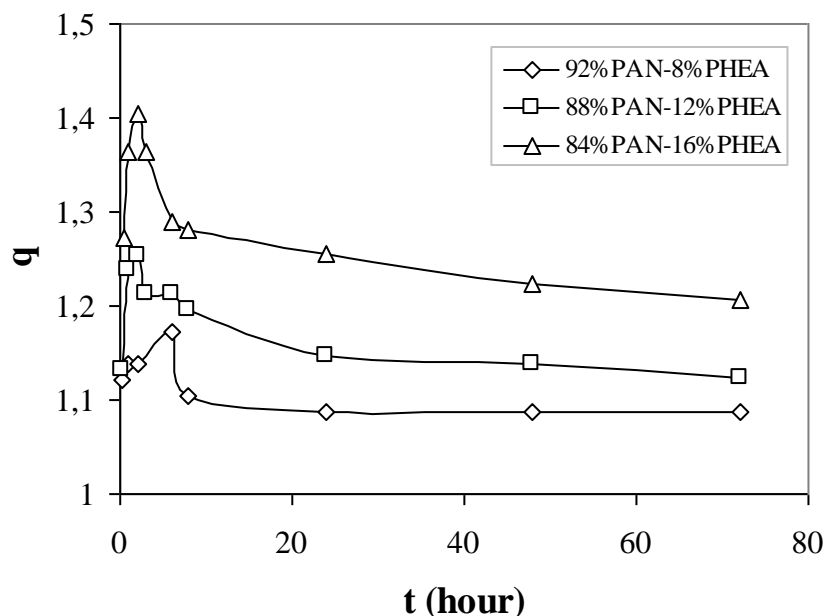


Figure 3.11 Degree of swelling versus time curves for various PAN-PHEA copolymers

3.2 Polyacrylonitrile-Polybutylacrylate Copolymers

Acrylonitrile based copolymers of polyacrylonitrile-co-polybutylacrylate were successfully synthesized using the emulsion polymerization technique. Chemical structures of the copolymers were checked by several characterization methods such as proton and carbon-13 NMR, FTIR. The experimental and the calculated compositions of copolymers were compared. Thermal behaviors of the copolymers were also monitored and compared with its homopolymer. The glass transition of copolymers was about 56 to 76 °C. TGA data showed that the copolymers were thermooxidatively stable. The 10 percent weight loss temperature was about 360 °C which was high enough for many applications. The intrinsic viscosity data showed that the molecular weight of the copolymers were in the range of the processing window. Mechanical properties were also investigated. The chemical structure of the synthesized copolymer is shown in Figure 3.12.

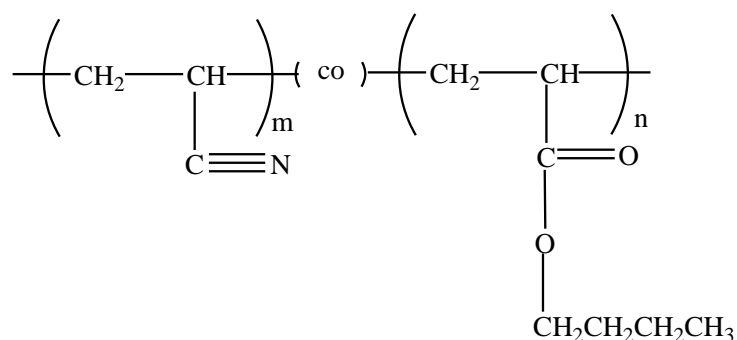


Figure 3.12 Chemical structures of copolymers PAN-PBA

3.2.1 Fourier Transform Infrared Spectroscopy (FTIR) Results

The chemical structure of both homo polymers and copolymers was investigated by FTIR spectroscopy in Figure 3.13. For the homopolymer of butyl acrylate; methylene and methane C-H stretching's are between $3000\text{-}2850\text{ cm}^{-1}$, C=O stretching is at 1733 cm^{-1} , the C-H deformation in methyl and methylene bands is at 1449 cm^{-1} , the C-H deformation in C-CH₃ band is between $1390\text{-}1300\text{ cm}^{-1}$ and C-O-C stretching of aliphatic ester band is between $1255\text{-}1130\text{ cm}^{-1}$. For the homopolymers of acrylonitrile, aliphatic C-H stretchings are between $2930\text{-}2850\text{ cm}^{-1}$, the characteristic peak of AN, CN is at 2251 cm^{-1} , the CH₂ stretching is at 1442 cm^{-1} , and the peak at 1069 cm^{-1} belongs to CN stretching. For the copolymers of the acrylonitrile/butyl acrylate FTIR spectra the C-H stretching are between $3000\text{-}2800\text{ cm}^{-1}$, the stretching vibrations due to nitrile group appear at 2245 cm^{-1} , C=O stretching is at 1733 cm^{-1} , at 1454 and 939 cm^{-1} methylene and butyl group of the main chain respectively. No band at $\sim 1635\text{ cm}^{-1}$ assigned to the C=C stretch vibration of the monomer is present, indicating that C=C is transformed to C-C completely and also it is shown in Figure 3.13 that the CN peak is stronger in PAN(92)-PBA(8) than in PAN(84)-PBA(16) due to the high content of acrylonitrile.

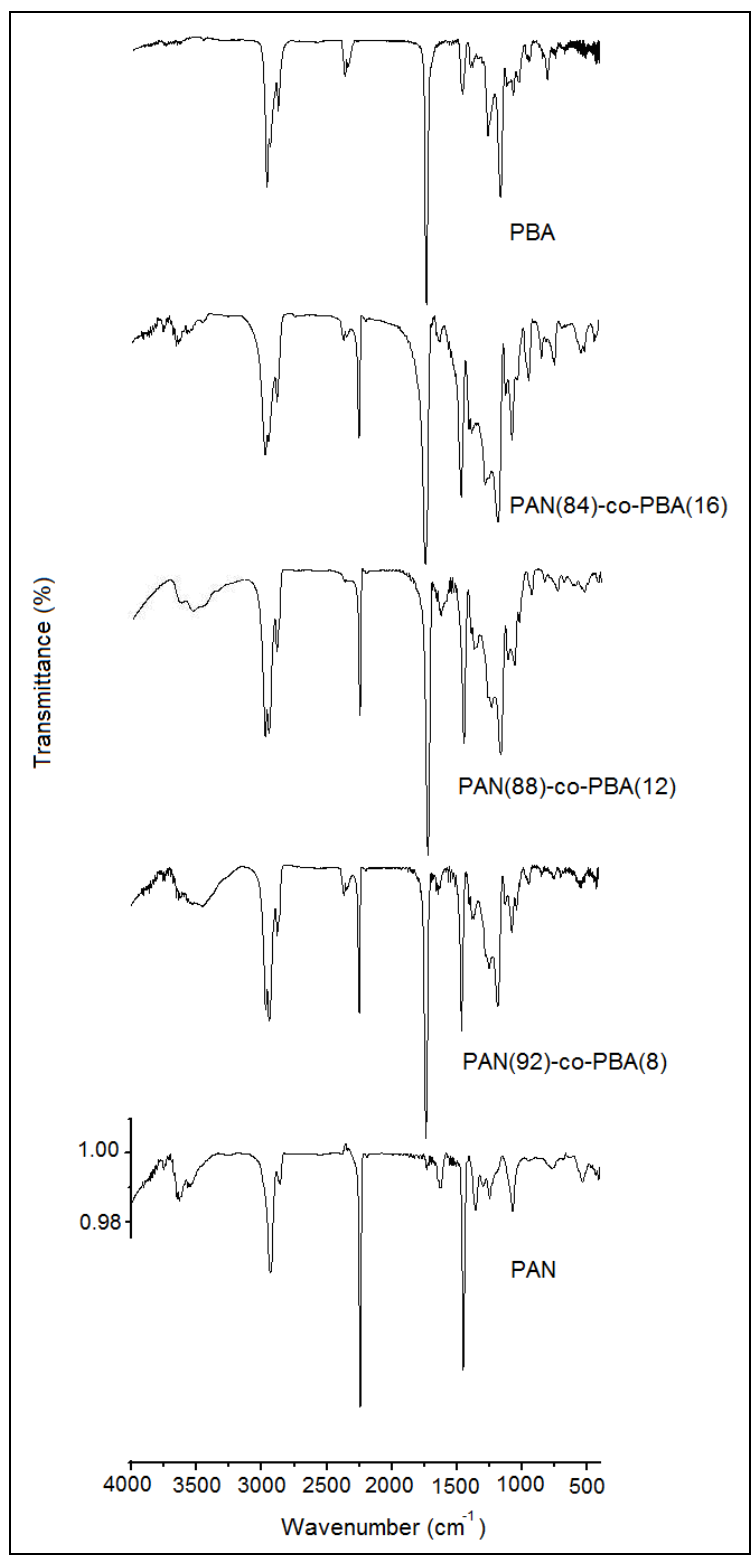


Figure 3.13 FTIR spectrum exhibited characteristic peaks of PAN-co-PBA

3.2.2 Nuclear Magnetic Resonance Spectroscopy (NMR) Results

The copolymer structure was clarified by $^1\text{H-NMR}$ and $^{13}\text{C-NMR}$. The Figure 3.14 shows that the $^1\text{H-NMR}$ spectrum of PAN-PBA random copolymers has different weight fractions. The OCH_2 stretching appeared at 4.1 ppm (e). The resonance between 3.1 to 2.4 ppm was belonged to $-\text{CH}$ backbone protons of acrylonitrile and butyl acrylate (b,d). The $-\text{CH}_2$ backbone protons were appeared between 2.2 to 1.2 ppm (a,c,g,f). Finally, $-\text{CH}_3$ (h) stretching was observed at 0.9 ppm. The average molar fraction composition of the copolymers were quantitatively determined from the integral area (I) of the peaks $-\text{OCH}_2$ and $-\text{CH}_2$ protons from the corresponding $^1\text{H-NMR}$ spectra of copolymer samples prepared with different molar feeds. The theoretical and the actual compositions calculated from $^1\text{H-NMR}$ by the following equation and results were tabulated in table 3.5.

$$\text{Molar percent of BA} = \frac{I_{(e)}/2}{\left[\frac{I_{(a,c,g,f)} - 6I_{(e)}/2}{2} \right] + I_{(e)}/2} \times 100$$

Table 3.5 Composition and intrinsic viscosity of PAN-PBA copolymers

Copolymer	Theoretical Composition	Experimental Composition	IV
PAN(92)-co-PBA(8)	92/8	92.6/7.4	1.04
PAN(88)-co-PBA(12)	88/12	88.4/11.6	1.36
PAN(84)-co-PBA(16)	84/16	81.1/18.9	0.90

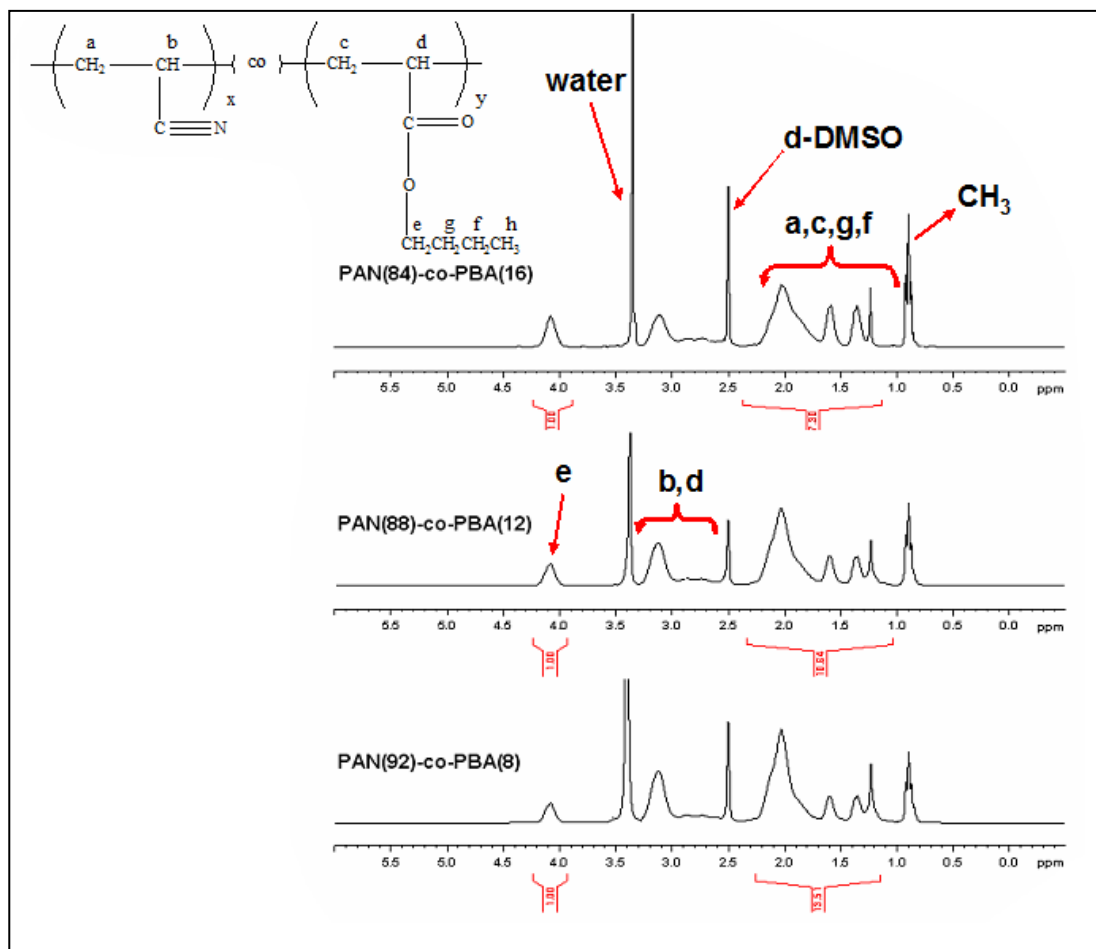


Figure 3.14 $^1\text{H-NMR}$ spectrum of AN-BA copolymers with different compositions

In the $^{13}\text{C-NMR}$ spectrum of PAN-PBA copolymers, the resonance signals around 13.52, 18.64, 29.94 and 64.47 ppm can be assigned to (f), (e), (d) and (c) carbons of butyl acrylate monomer (Figure 3.15). The resonance signals around 26.70-27.35 ppm and 32.57 to 33.28 ppm can be attributed to (g) and (j) carbons, respectively. The (k) and the partially (h) (41.54 ppm) carbons overlapped with the solvent $\text{d}_6\text{-DMSO}$. The carbonyl carbon in the copolymer appeared around 173.75 to 173.47 ppm (a) and the nitrile carbon of the acrylonitrile unit appeared around

120.14 to 120.88 ppm (b). It can be concluded that the butyl acrylate comonomer is completely collaborated into the copolymer structure.

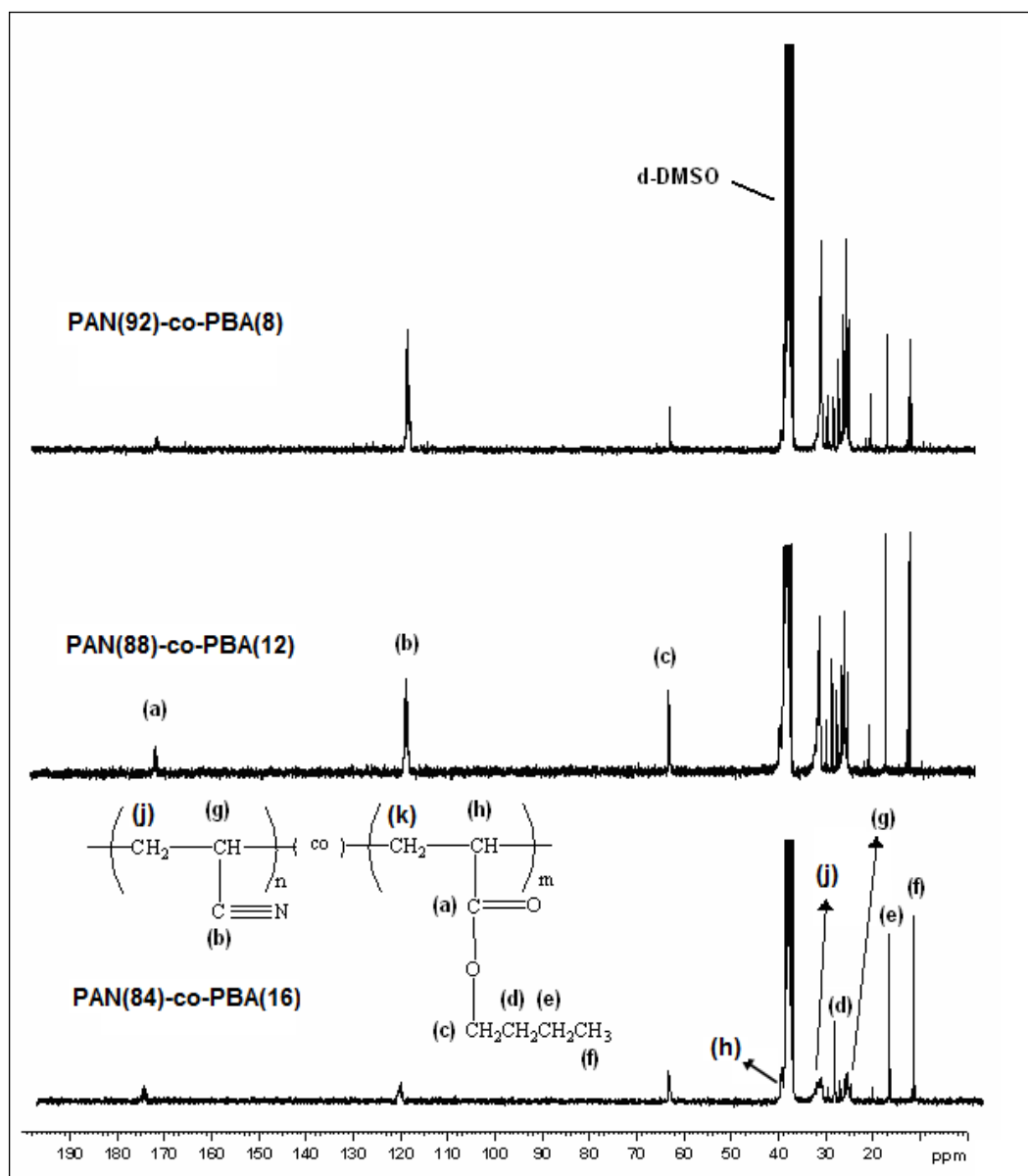


Figure 3.15 ^{13}C -NMR spectrum of AN-BA copolymers with different compositions

3.2.3 Differential Scanning Calorimetry (DSC) Results

The glass transition temperatures of the copolymers were determined from DSC. The determined values of T_g lie between those of pure PBA (-48.15 °C) and PAN (104 °C). BA and AN reactivity ratio values for bulk free radical copolymerization are reported to be 1.003 and 1.005 [91]. The product of the reactivity ratio values is close to unity which means that a growing chain has equal affinity to either of the two monomer units, so that the produced copolymers have a random structure. In general, as Figure 3.16 shows, as the weight fraction of the acrylonitrile in the feed increases T_g value increases.

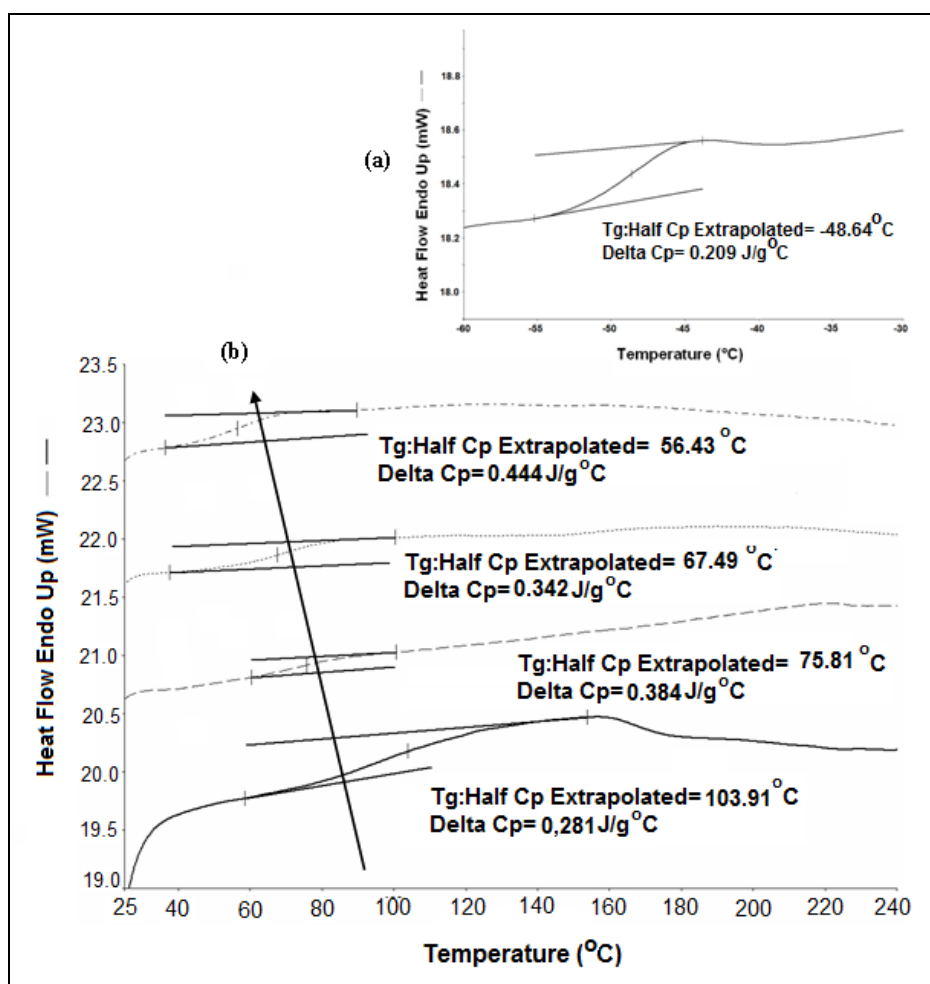


Figure 3.16 DSC thermograms of (a) PBA, (b) homopolymer of PAN and copolymers

3.2.4 Thermogravimetric Analysis (TGA) Results

The copolymer systems were studied by thermogravimetrically to access the thermal characteristics. The study shows that thermal characteristics are affected by the comonomer, as observed for comparable systems [92]. The TGA thermograms of the copolymers are shown in Figure 3.17. The copolymers were comparatively stable and they underwent generally one major step of decomposition at around 380 °C normally caused by a random scission of the polymer chain.

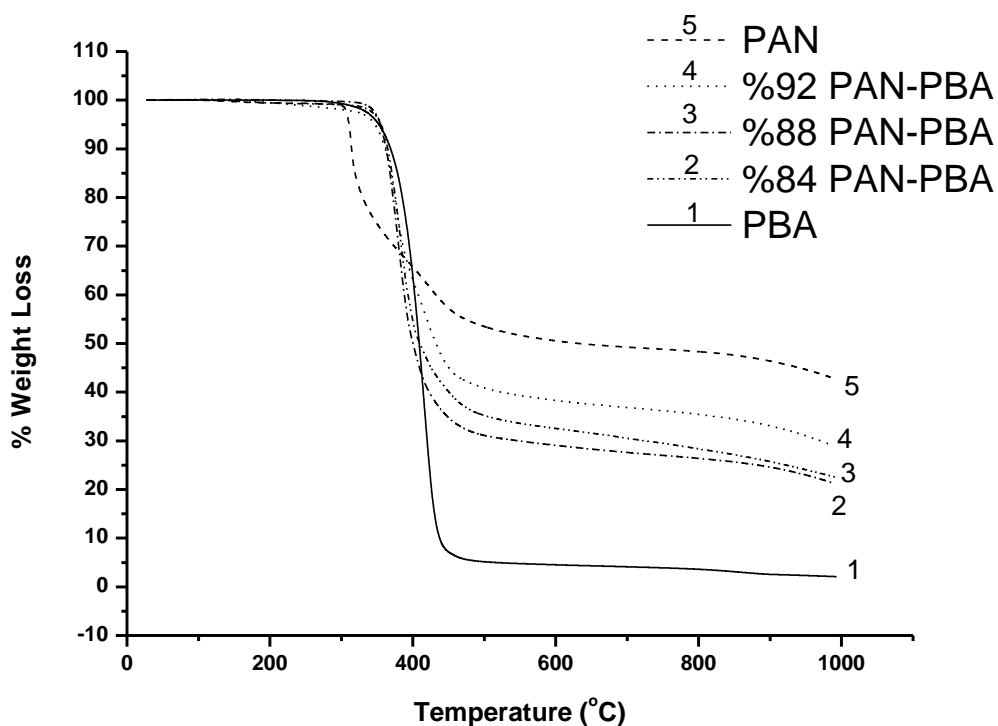


Figure 3.17 Weight loss curves for homo- and copolymers versus temperature

Table 3.6 Thermal decomposition characteristics of acrylonitrile-butyl acrylate copolymers (heating rate 10 °C/min; N₂ atmosphere)

Sample name	T ₅ ^a (°C)	T ₁₀ ^b (°C)	T _{max} ^c (°C)	Char yield at 800°C
PAN	310	314	314	48
PAN(92)-co-PBA(8)	347	365	376	35
PAN(88)-co-PBA(12)	354	363	379	26
PAN(84)-co-PBA(16)	355	361	384	28
PBA	352	366	412	3.6

^a temperature of 5% weight loss obtained from TGA

^b temperature of 10% weight loss obtained from TGA

^c temperature of the maximum point

It can be observed that as the acrylonitrile content increased the weight loss at the maximum temperature decreased (Table 3.6). The % weight loss at a given temperature is directly related to the copolymer composition. It is more clearly seen in Figure 3.18 that 92% PAN-PBA copolymer has one major and one minor decomposition step and it has the highest amount of acrylonitrile content and the most resemble one to pure PAN homopolymer decomposition mechanism. It is clear that the comonomer variation has a crucial effect on degradation mechanism. As the comonomer content increases, the copolymer decomposition temperature more resembles pure PBA homopolymer.

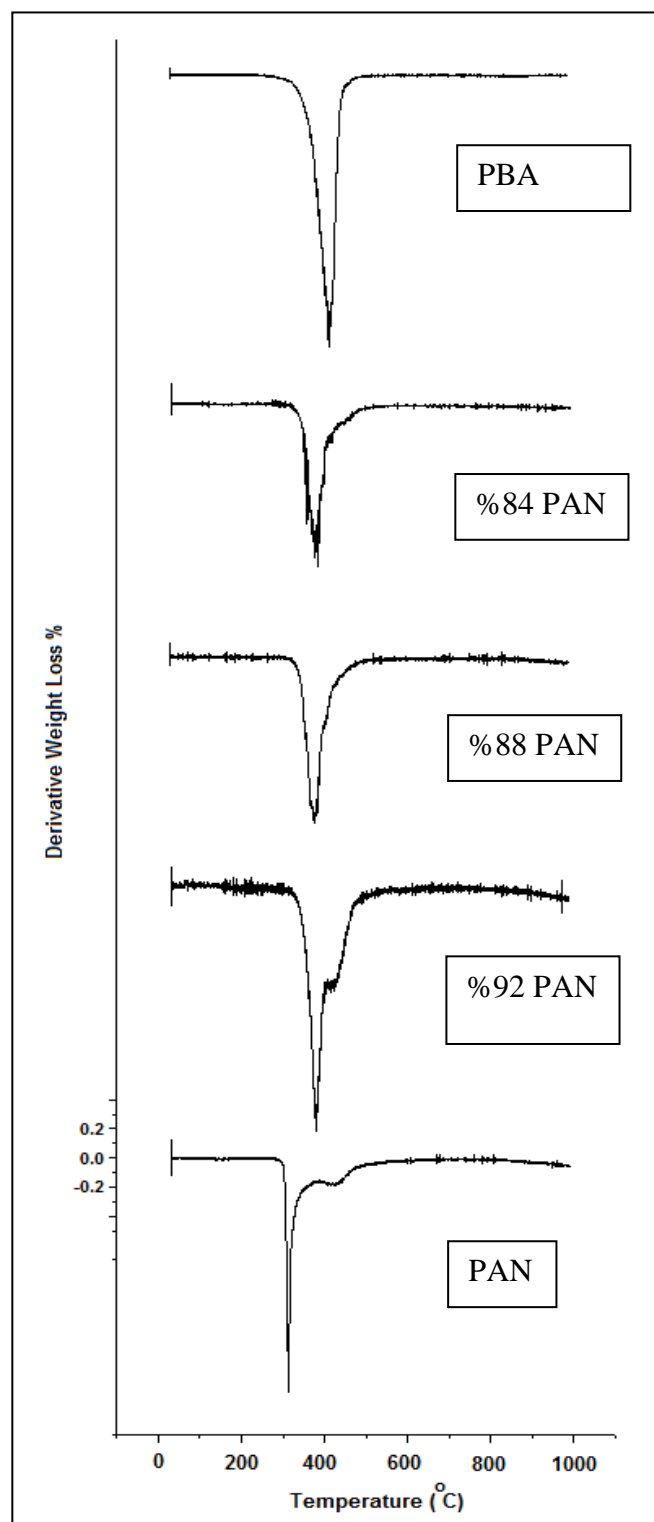


Figure 3.18 Effect of copolymer composition on the percent weight loss during TGA analysis

3.2.5 Mechanical Test Results

For both industrial assembling and practical application safety, mechanical properties are key factors. The stress- deformation curves obtained from PAN-PBA copolymer films are shown in Figure 3.19.

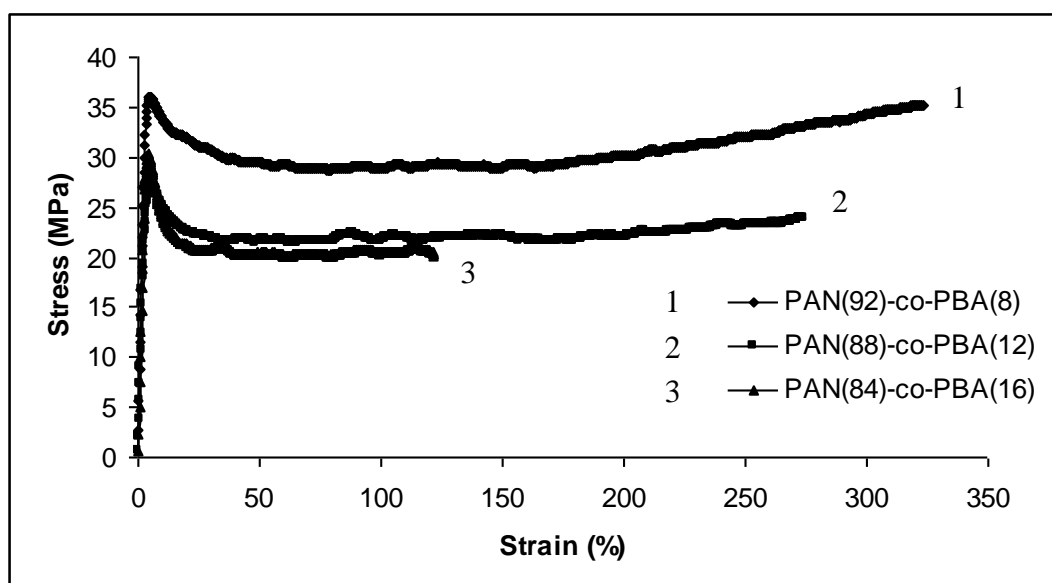


Figure 3.19 Stress-Strain deformation curves for PAN-PBA copolymer films

Toughness is defined as the amount of energy per volume that a material can absorb before rupturing. From Figure 3.19 we can conclude that the 92% PAN-PBA copolymers have higher strength and higher ductility than the other samples. It purely indicates that 92% PAN-PBA is tougher than the other samples. It is because increasing AN content in the copolymer there is a hardening effect on the rubbery PBA units, and so the copolymer behaves more like plastic than the others. This behaviour can also be anticipated from the rise in T_g value with the proportion of acrylonitrile. The values of E , UTS and EAB for all PAN-PBA copolymers are given in Table 3.7.

Table 3.7 Mechanical test results for PAN-PBA copolymer films

Sample Name	UTS (MPa)	E (MPa)	EAB (%)
PAN(92)-PBA(8)	36.62 ±0.58	1165 ±51.2	342.81 ±35.97
PAN(88)-PBA(12)	32.16 ±2.55	1103 ±50.8	273.58 ±71.26
PAN(84)-PBA(16)	30.57 ±0.62	1060 ±35.6	119.45 ±11.97

3.3 Polyacrylonitrile-Polytertbutylacrylate Copolymers

Polyacrylonitrile-co-polytert-butyl acrylate copolymers (PAN-co-PtBA) at three different compositions (8, 12 and 16 molar percent of polytert-butyl acrylate (PtBA)) and polyacrylonitrile (PAN) and PtBA homopolymers were synthesized by emulsion polymerization. Copolymers were characterized by FTIR, ¹H-NMR, ¹³C-NMR, intrinsic viscosity measurements, differential scanning calorimetry (DSC) and thermogravimetric analysis (TGA). Chemical structures and compositions were elucidated by FTIR, proton and carbon NMR. Intrinsic viscosity measurements revealed that the molecular weight of the copolymers were quite enough to form ductile film. The T_g values were decreases with increasing the weight fraction of tert-butyl acrylate. TGA results revealed that the stepwise thermal degradation was observed for copolymers and the decomposition temperatures rarely increased with decreased tBA content. Mechanical properties were also investigated. Figure 3.20 shows the chemical structure of PAN-PtBA copolymers.

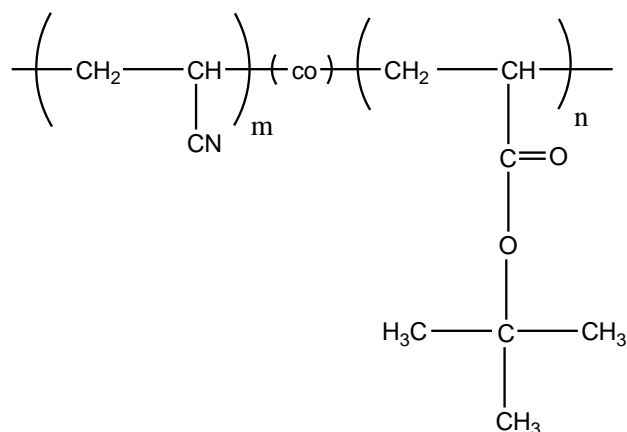


Figure 3.20 Chemical structure of PAN-PtBA copolymers

3.3.1 Fourier Transform Infrared Spectroscopy (FTIR) Results

Chemical structure was elucidated by FTIR, proton and carbon NMR. The FTIR spectrum of copolymers and homopolymers can be seen in Figure 3.21. The characteristic peaks of tert-butyl group, which exists only in PtBA, are at 2985 cm^{-1} (asymmetric CH_3) and $1395\text{-}1371\text{ cm}^{-1}$ symmetric CH_3 doublet peak [93]. The weak peaks at 2935 and 2869 cm^{-1} belong to the asymmetric and symmetric vibration modes of CH_x groups. Other characteristic peaks resulting from acrylonitrile and acrylate are $\text{-C}\equiv\text{N}$ stretching and -C=O stretching and they can be seen at 2243 and 1726 cm^{-1} respectively. The strong band at 1450 cm^{-1} can be assigned -CH bending and the peaks between $1284\text{-}1076\text{ cm}^{-1}$ correspond to C-C-O and C-O-C ester stretching vibrations. Non-existence of C=C stretching vibration at $\sim 1635\text{ cm}^{-1}$ implies that all the monomer was collaborated into the copolymer. Also, it is seen from the Figure 3.21, the CN peak is stronger in PAN(92)-PBA(8) than PAN(88)-PBA(12) than PAN(84)-PBA(16).

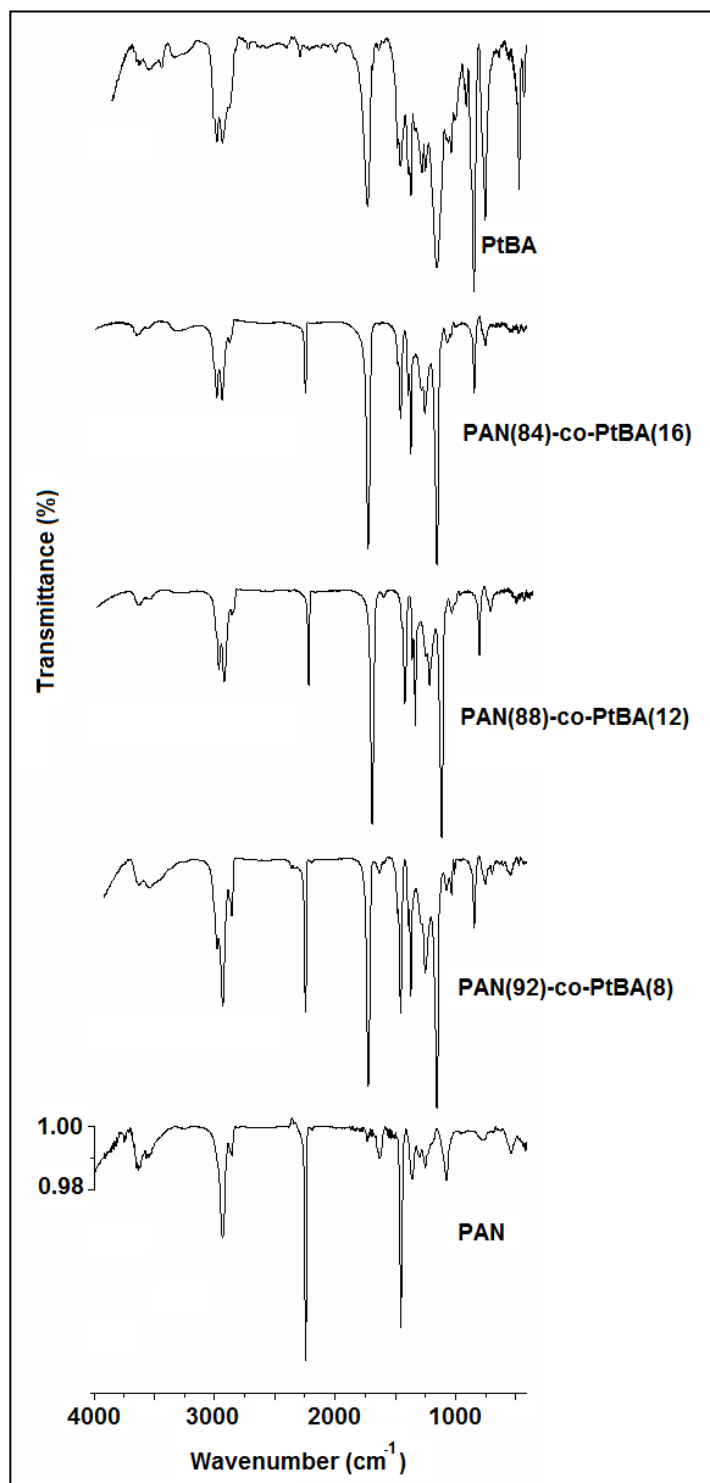


Figure 3.21 FTIR spectrum exhibited characteristic peaks of PAN-co-PtBA

3.3.2 Nuclear Magnetic Resonance Spectroscopy (NMR) Results

The copolymer structure was clarified by $^1\text{H-NMR}$ and $^{13}\text{C-NMR}$. The figure 3.22 shows the $^1\text{H-NMR}$ spectrum of PAN-PtBA random copolymers having different weight fractions. The resonance between 3.14 to 2.54 ppm was belong to $-\text{CH}$ backbone protons of acrylonitrile and tert-butyl acrylate (b,d). The $-\text{CH}_2$ backbone protons were appeared between 2.27 to 1.56 ppm (a,c). Finally, $-\text{CH}_3$ (e,f,g) protons of tert-butyl acrylate can be seen as a singlet between 1.52 to 1.38 ppm. The average molar fraction composition of the copolymers were quantitatively determined from the integral area (I) of the peaks $-\text{CH}$ and $-\text{CH}_3$ protons from the corresponding $^1\text{H-NMR}$ spectra of copolymer samples prepared with different molar feeds. The theoretical and the actual compositions calculated from $^1\text{H-NMR}$ by following equation and results were tabulated in table 3.8.

$$\text{Molar percent of tBA} = \frac{I_{(e,f,g)} / 9}{I_{(b,d)}} \times 100$$

Table 3.8. Composition and intrinsic viscosity of PAN-PtBA copolymers

Sample	Monomer feed	Composition ^a	$[\eta]^{\text{NMP}}_{30\text{ }^\circ\text{C}}$ (dL/g)
(AN/tBA)	(molar ratio of AN to tBA)	(molar ratio of AN to tBA)	
1	92/8	90.7/9.3	1.21
2	88/12	86.0/14.0	1.03
3	84/16	82.2/17.8	0.70

^a Calculated by $^1\text{H-NMR}$ in $d_6\text{-DMSO}$.

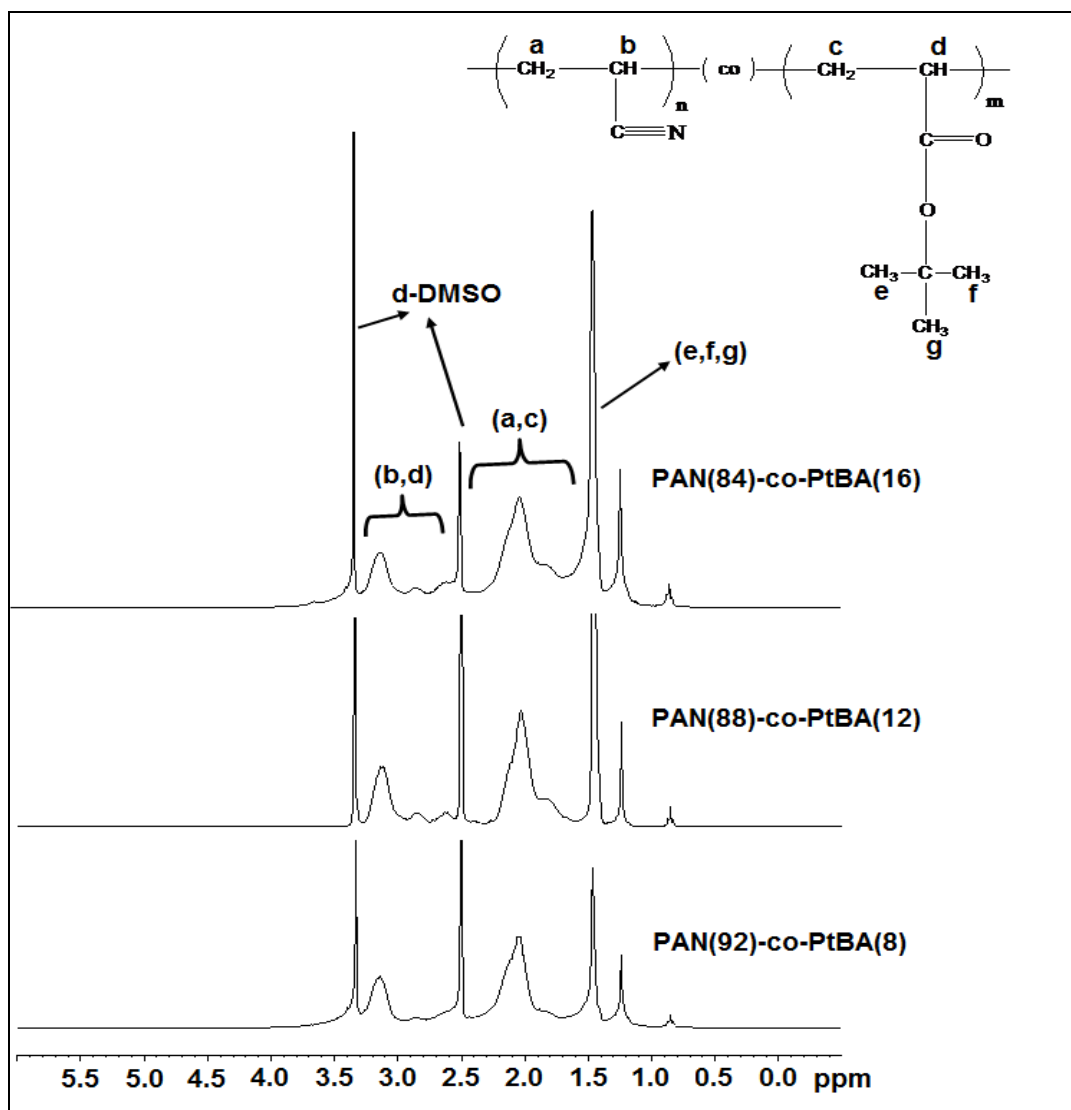


Figure 3.22 $^1\text{H-NMR}$ spectrum of AN-tBA copolymers with different compositions

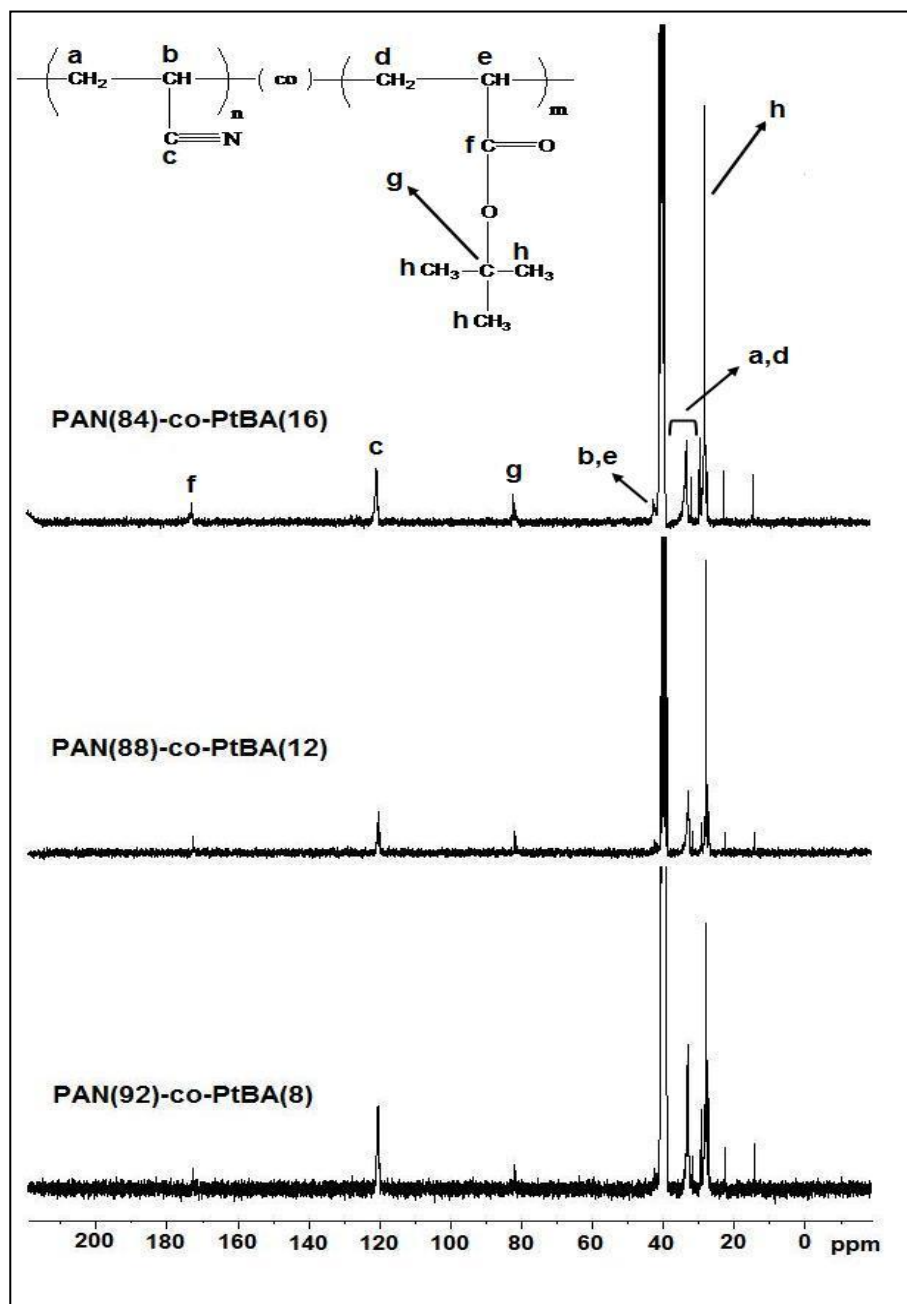


Figure 3.23 ^{13}C -NMR spectrum of AN-tBA copolymers with different compositions

^{13}C -NMR spectrum (Figure 3.23) revealed that the characteristic signals of $-\text{C}=\text{O}$ and $\text{C}\equiv\text{N}$ were appeared at 172.8 (f) and 120.6 (c) ppm, respectively. $-\overset{\text{C}}{\text{C}}-$ (g) was

detected at 81.9 ppm. The peak, located at 42.6 ppm, adjacent from the left hand side of the d-DMSO signal can be assigned as methine signal of tert-butyl acrylate and acrylonitrile. Similarly -CH₂ and -CH₃ peaks were detected at 31.76-33.09 and 29.17 ppm, respectively. The chemical structure of the copolymers was sured by ¹³C-NMR and ¹H-NMR.

3.3.3 Differential Scanning Calorimetry (DSC) Results

Differential scanning calorimetry was used to evaluate the thermal transition temperatures for the homopolymers and the copolymers [The heating rate was maintained at 10 °C/min]. PtBA is an amorphous polymer and its T_g is near 37.2 °C, lower than that of PAN. The T_g value of the copolymers with all composition range show a single T_g lying in between those of pure PtBA and pure PAN. It is seen in Figure 3.24 that, increasing the weight fraction of comonomer addition, decreases the T_g values of copolymers. Additionally, the DSC thermograms of the copolymers showed that they do not decompose up to ~200 °C. Moreover, the endothermic peak in the thermogram belonged to the degradation of t-BA parts in the copolymer. The presence of a single value for T_g may suggest that a random copolymer is formed.

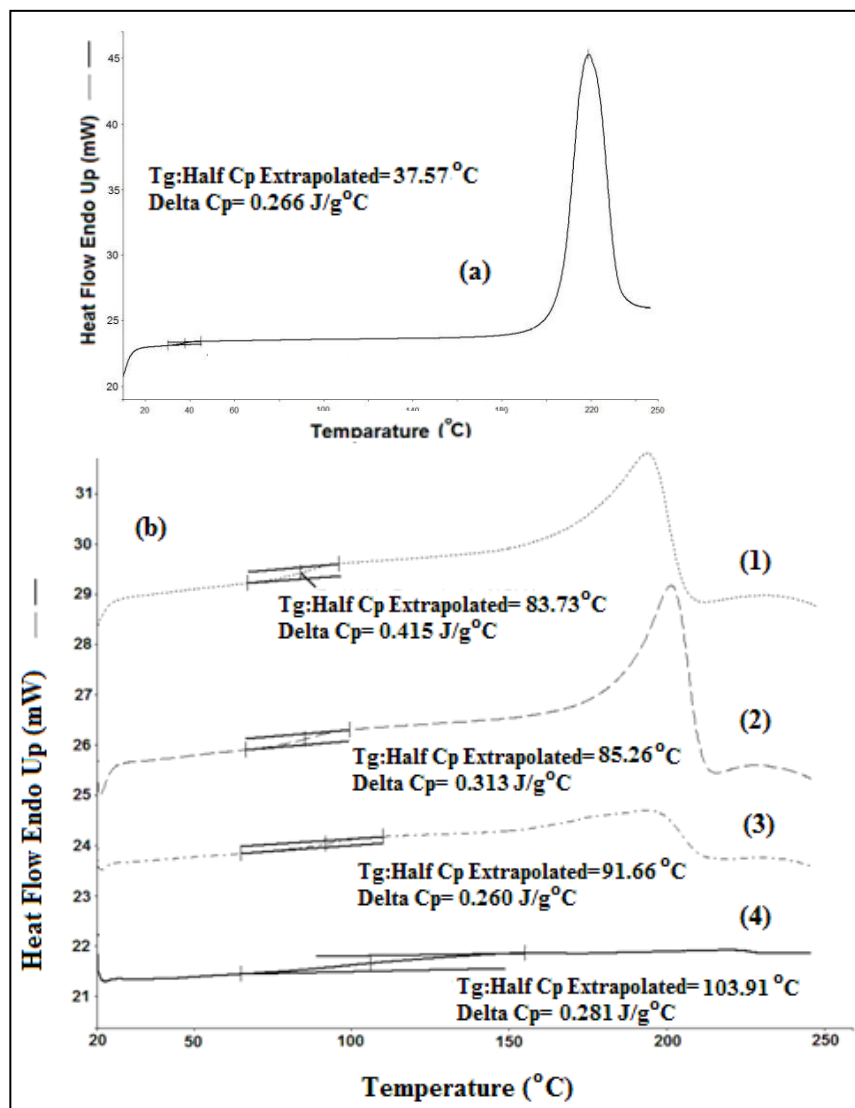


Figure 3.24 DSC thermograms of (a) PtBA, (b) (1) PAN(84)-PtBA(16), (2) PAN(88)-PtBA(12), (3) PAN(92)-PtBA(8), (4) PAN

3.3.4 Thermogravimetric Analysis (TGA) Results

The thermal stability of the copolymer was evaluated by TGA. Figure 3.25 shows the weight-loss curves for copolymers compared with PAN and PtBA homopolymers and the values of the decomposition temperature derived from TGA curves are included in Table 3.9. The results showed that the copolymers have

better thermal stability than pure PtBA homopolymer. The thermal decomposition of PtBA was studied by Schaeffgen and Sarasohn [94]. The degradation of PtBA is produced in two stages; in the initial step of the decomposition isobutylene was produced in a quantitative yield forming polyacrylic acid. The thermal degradation of poly(acrylic acid) was investigated by other authors [95-96] and they showed that a six-membered anhydride-type ring results from an intramolecular reaction between adjacent group.

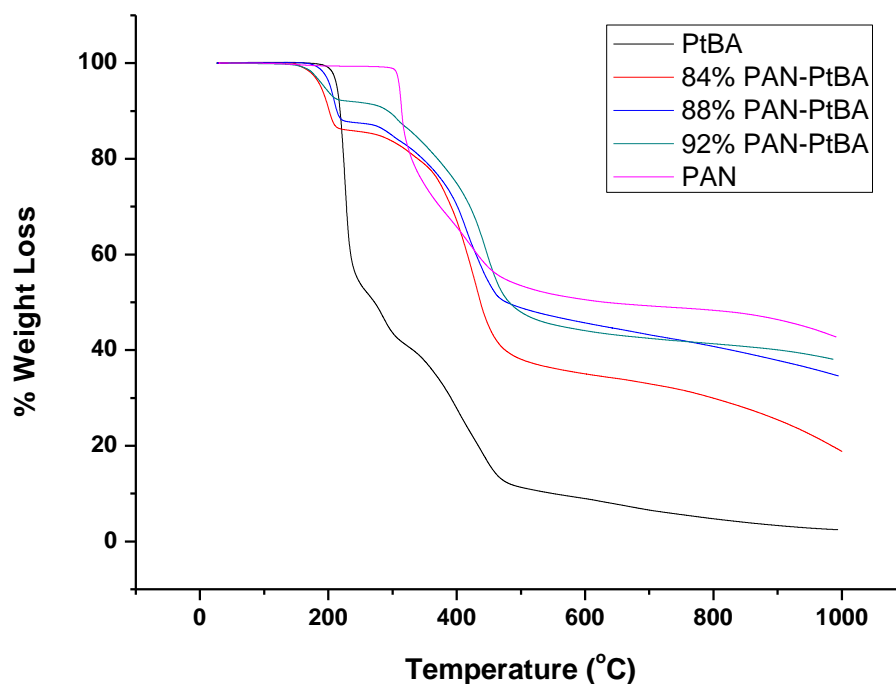


Figure 3.25 Weight loss curves for homo- and copolymers versus temperature

The TGA of the PAN-PtBA copolymers also displayed two main decomposition stages (Figure 3.26). There is hardly any weight loss before about 200 °C for all copolymers which confirms the DSC analysis. The first starts around at ~ 170 °C

and ends at approximately 240 °C, and the maximum decomposition temperature shifts to higher temperatures as the weight fraction of PtBA in the copolymer decreases. The weight loss at this first stage is generally interpreted as the release of the tert-butyl ester group giving polyacrylic acid [97]. The results showed that the copolymers have better thermal stability than PtBA homopolymer. Even though some information has been compiled, the decomposition mechanism is still not fully understood. Further investigations need to be made to clarify the mechanism.

Table 3.9 Thermal decomposition properties of homo- and copolymers (heating rate 10°C/min, N₂ atmosphere)

Sample name	T ₅ ^a (°C)	T ₁₀ ^b (°C)	T _{max} ^c (°C)	Char yield at 800°C
PAN	310	314	314	48
PAN(92)-co-PtBA(8)	201	307	207	43
PAN(88)-co-PtBA(12)	203	213	205	41
PAN(84)-co-PtBA(16)	188	201	199	30
PtBA	213	218	227	5

^atemperature of 5% weight loss

^btemperature of 10% weight loss

^ctemperature of the first maximum

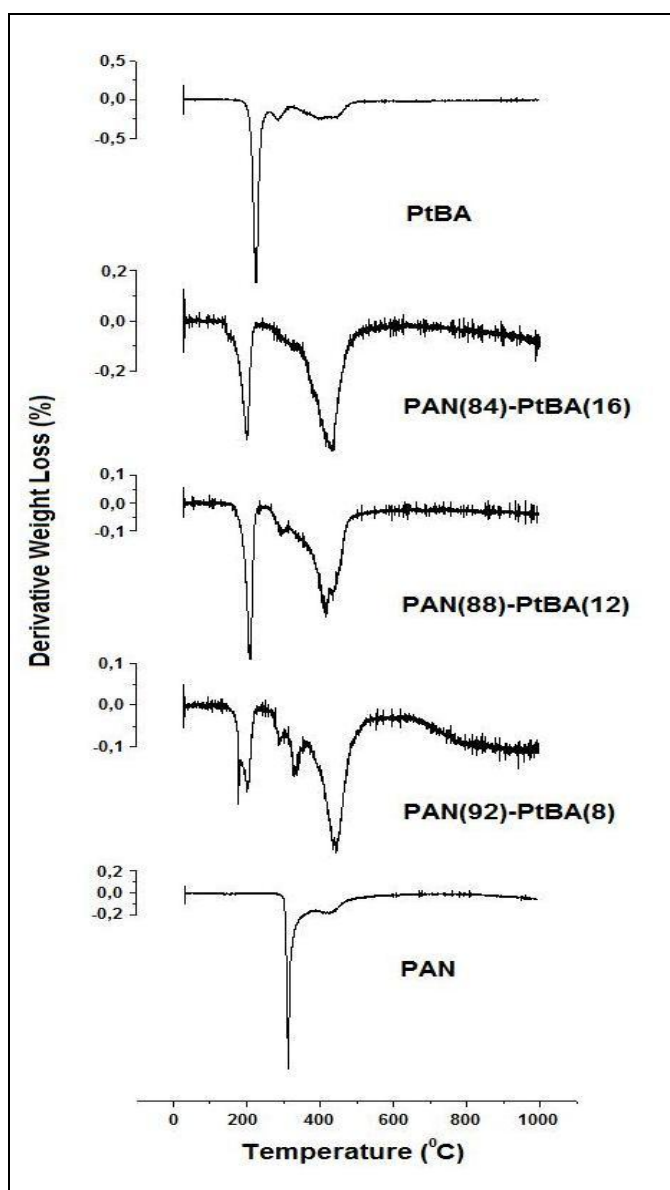


Figure 3.26 Effect of copolymer composition on the percent weight loss during TGA analysis

3.3.5 Mechanical Test Results

The elastic modulus (E) values found as 287 MPa, 228 MPa and 226 MPa for %92 Pan-Ptba, %88 Pan-Ptba and %84 Pan-Ptba respectively (Figure 3.27). It was observed that the elastic modulus decreased with an increase in the tBA content in the copolymers. Between 92% copolymer and 88% copolymer there is a detectable change in elastic modulus however, the addition of an extra 4 molar percent tBA after the 88% molar percent into the copolymer system has only a slight effect on the elastic modulus, that is one can use either 84% molar percent tBA or 88% molar percent tBA with respect to elastic modulus.

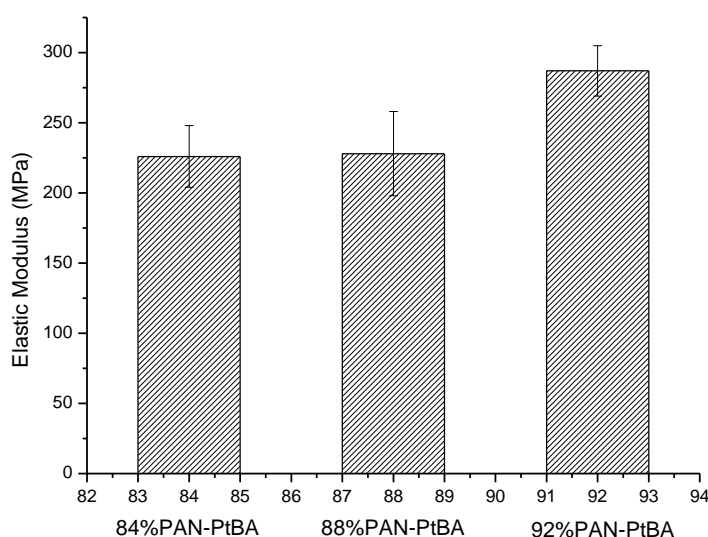


Figure 3.27 Elastic Modulus of PAN-PtBA copolymers

Figure 3.28 shows the variation of UTS with respect to the copolymer composition. A decreasing trend is observed with increasing the tBA content in the copolymer, it is more probable because more amorphous parts are incorporated into the copolymer.

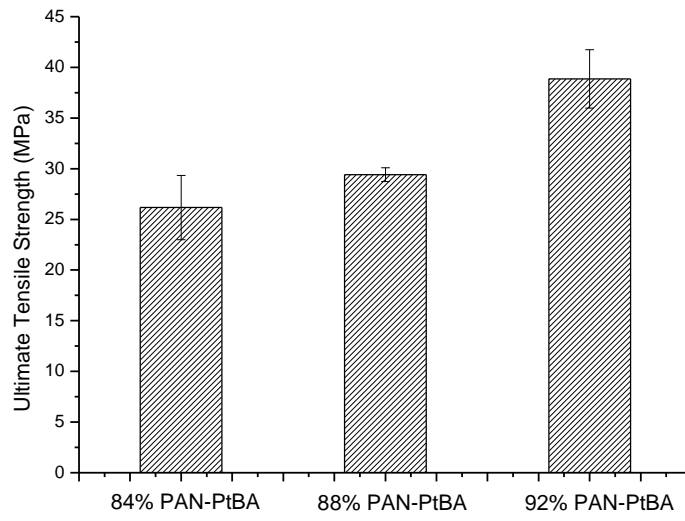


Figure 3.28 Ultimate Tensile Strength of PAN-PtBA copolymer films

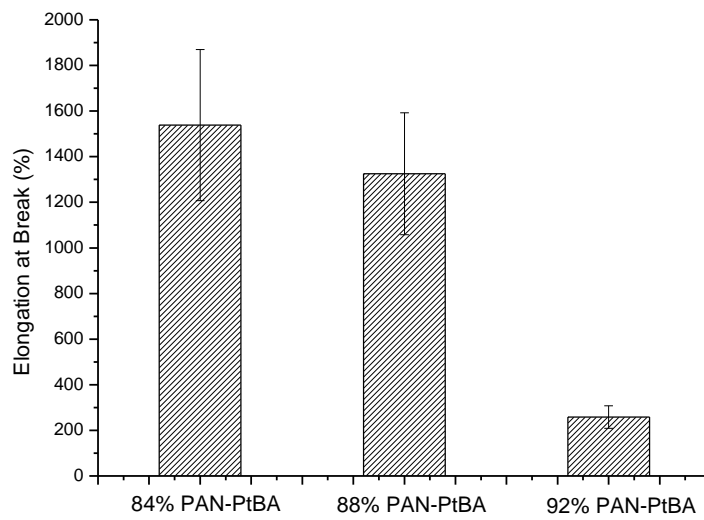


Figure 3.29 Elongation at Break (%) of PAN-PtBA copolymer films

The elongation at break vs copolymer composition graph is given in Figure 3.29. EAB values increases with increasing tBA content in the copolymer which results in more elastomeric structures. The rupture for the films occurs almost at the end of the cold-drawing. The values of E, UTS and EAB for all PAN-PtBA copolymers are given in Table 3.10.

Table 3.10 Mechanical test results for PAN-PtBA copolymer films

Sample Name	UTS (MPa)	E (MPa)	EAB (%)
PAN(92)-PtBA(8)	38.86 ±2.87	287 ±18.4	258.13 ±49.41
PAN(88)-PtBA(12)	29.41 ±0.69	228 ±30.7	1324.92 ±267.25
PAN(84)-PtBA(16)	26.17 ±3.17	226 ±22.3	1538.44 ±331.51

3.4 Polyacrylonitrile-Polyethyl acrylate Copolymers

Acrylonitrile based copolymers of polyacrylonitrile-co-polyethylacrylate were successfully synthesized using emulsion polymerization technique. Chemical structures of the copolymers were checked with several characterization methods such as proton and carbon-13 NMR, FTIR. Thermal behaviors of the copolymers were also investigated and compared with its homopolymer. The glass transition temperatures of copolymers were about 85 to 72 °C. TGA data showed that copolymers were thermooxidatively stable. The 10 percent weight loss temperature was about 350 °C which was high enough for many applications. Mechanical properties and intrinsic viscosity data were also done. The chemical structure of synthesized copolymer is shown in Figure 3.30.

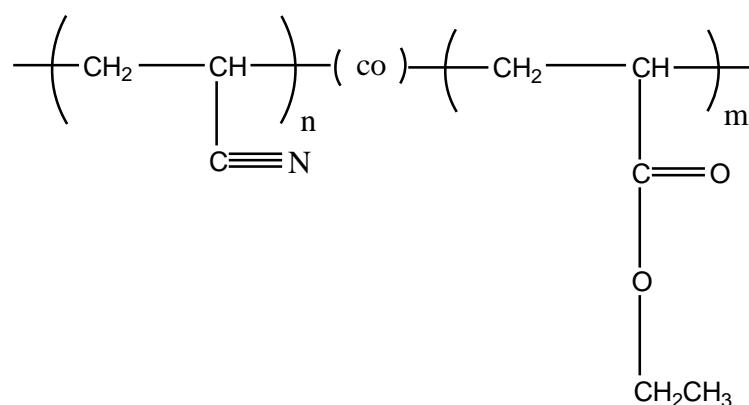


Figure 3.30 Chemical structure of PAN-PEA copolymers

3.4.1 Fourier Transform Infrared Spectroscopy (FTIR) Results

The FTIR spectrum for three copolymers and two homopolymers are represented in Figure 3.31. The aliphatic CH asymmetric and the symmetric stretching peaks are seen at 2987-2937 cm^{-1} respectively. The characteristic CN stretching is observed at 2245 cm^{-1} and C=O stretching vibration was seen at around 1728 cm^{-1} . The alkene CH scissoring gave a sharp peak at 1456 cm^{-1} . The broad bands around 1379-1178 cm^{-1} were caused by C-O-C ester group stretching's. The chemical structures of copolymers were evaluated by FTIR study. It is clearly seen from the Figure 3.31 that, the ratio of band intensities of carbonyl to nitrile is in the order of PAN(92)-PEA(8) to PAN(88)-PEA(12) to PAN(84)-PtBA(16) with increased amount of EA units in the copolymer feed.

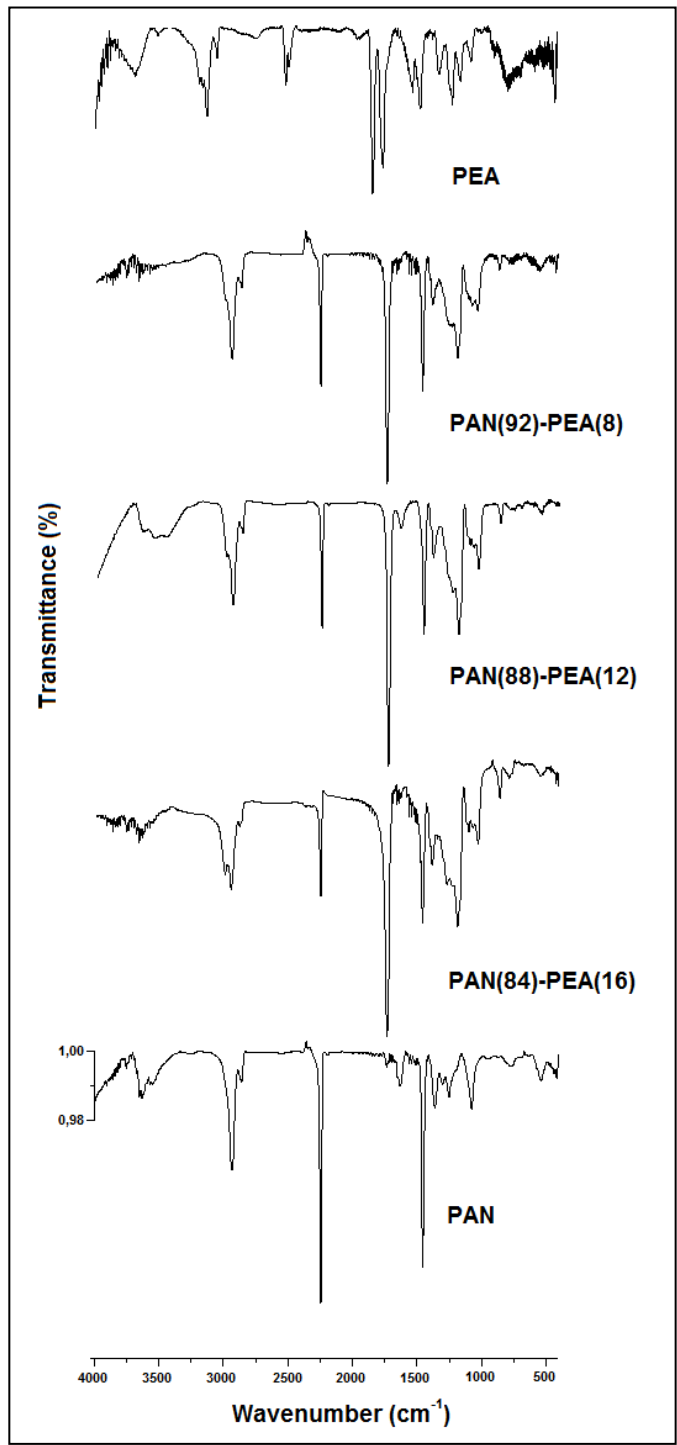


Figure 3.31 FTIR spectrum exhibited characteristic peaks of PAN-co-PEA

3.4.2 Nuclear Magnetic Resonance Spectroscopy (NMR) Results

The ^1H -NMR spectrum (Figure 3.32) of PAN-PEA random copolymers at various molar ratios was performed for the chemical conformation of copolymers. In the case of PEA, methyl ($-\text{CH}_3$) protons appeared around 1.14-1.23 ppm. $-\text{CH}_2$, $-\text{CH}$ and $-\text{OCH}_2$ proton signals appeared around 1.30-1.85, 2.10-2.40 and 3.90-4.15 ppm, respectively. In the case of PAN-PEA copolymer, $(-\text{CH}_3)_{\text{EA}}$ (f) and $(-\text{OCH}_2)_{\text{EA}}$ (e) protons appeared at around 1.24 and 4.12-4.18 ppm respectively. The two broad signals 1.50-2.28 ppm and 2.69-3.30 ppm can be attributed to $-\text{CH}_2$ (a,c) and $-\text{CH}$ (b,d) protons of both monomer units.

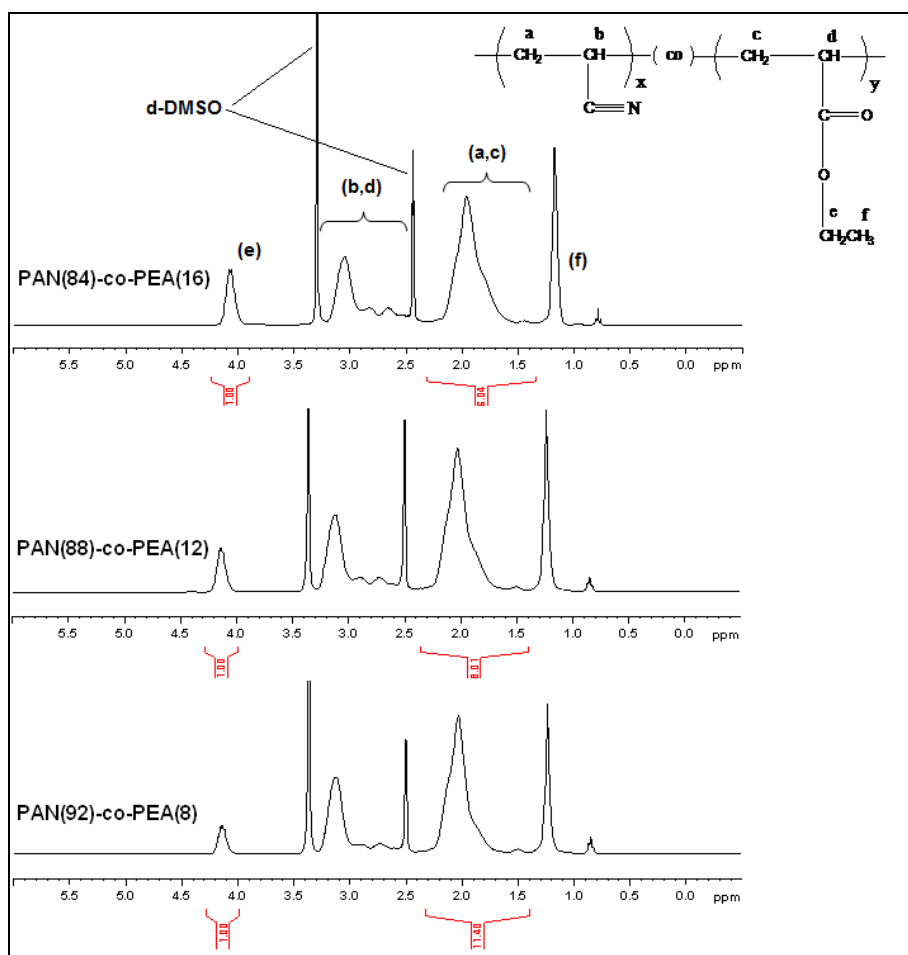


Figure 3.32 ^1H -NMR spectrum of AN-EA copolymers with different compositions; chemical structure was proved by ^1H -NMR.

The theoretical and the actual compositions calculated from $^1\text{H-NMR}$ are summarized in the following equations and the results were tabulated in Table 3.11.

$$\text{Molar percent of EA} = \frac{I_{(e)}/2}{I_{(a,c)}/2}$$

Table 3.11 Composition and intrinsic viscosity of PAN-PEA copolymers

Copolymer	Theoretical Composition	Experimental Composition	IV
PAN(92)-co-PEA(8)	92/8	91.2/8.8	1.79
PAN(88)-co-PEA(12)	88/12	87.5/12.5	1.07
PAN(84)-co-PEA(16)	84/16	83.4/16.6	1.09

The $^{13}\text{C-NMR}$ spectrum of the PAN-PEA copolymer recorded in $d_6\text{-DMSO}$ at room temperature is shown in Figure 3.33. The various resonance signals have been assigned by comparison with homopolymers. In the case of PAN, $-\text{CH}_2$ and $-\text{CH}$ carbons, appeared around 32.55 ppm and 26.70-28.98 ppm, respectively. The nitrile ($-\text{CN}$) carbon in PAN appeared in the region 119.53-120.91 ppm. In PAN-PEA copolymer, the signals around 14.21 ppm, 26.71-28.98 ppm, 31.26-32.73 ppm and 60.80 ppm can be assigned to $(-\text{CH}_3)_{\text{EA}}$, $(-\text{CH})_{\text{AN}}$, $(-\text{CH}_2)_{\text{AN}}$ and $(-\text{OCH}_2)_{\text{EA}}$ carbons respectively. The $(-\text{CH}_2)_{\text{EA}}$ and $(-\text{CH})_{\text{EA}}$ carbons of EA unit overlapped with the solvent $d_6\text{-DMSO}$ signals (38.59-40.94 ppm). The carbonyl carbon in PAN-PEA copolymer appeared around 172.62-173.25 ppm. The nitrile carbon of AN unit appeared from 119.66 to 120.41 ppm.

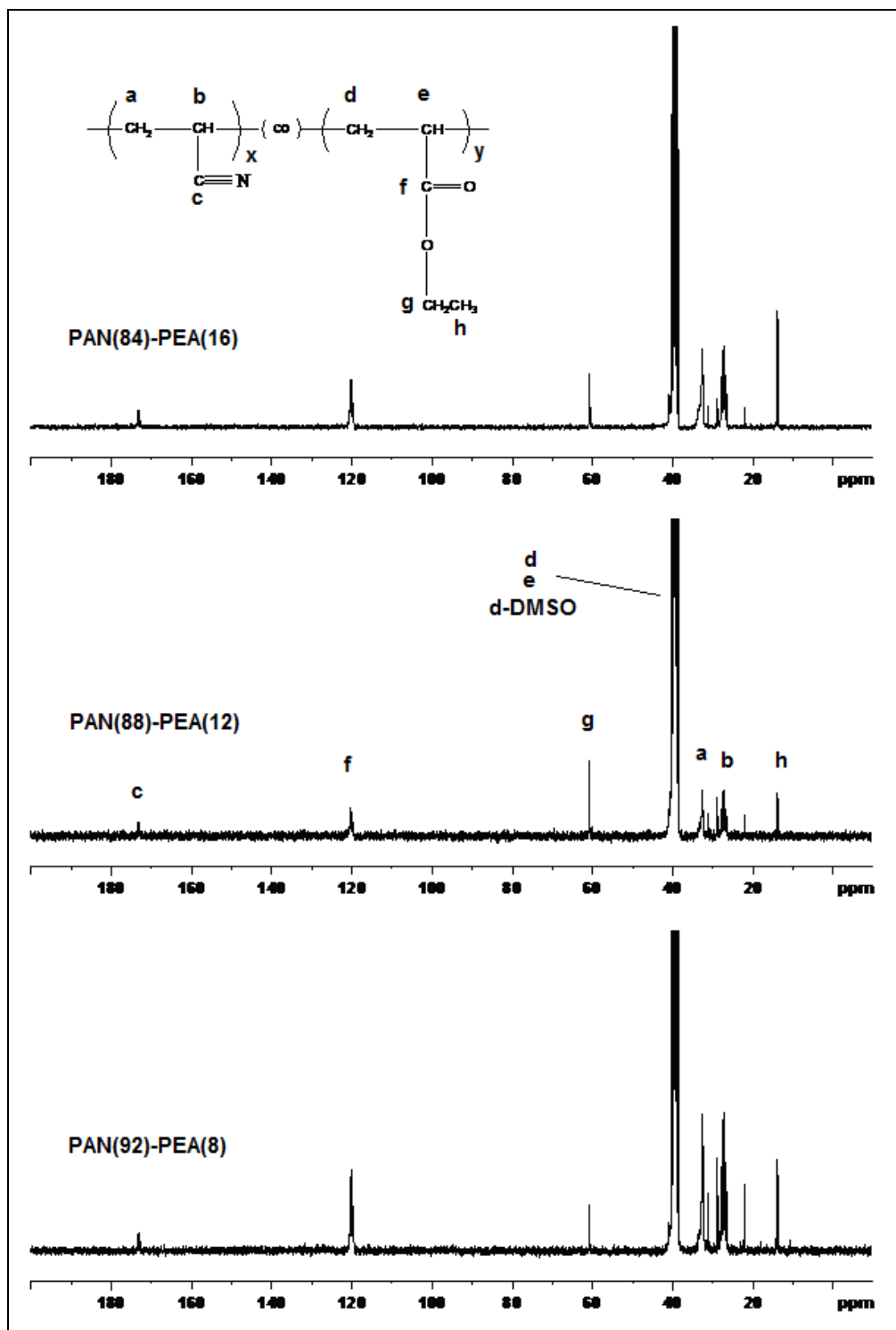


Figure 3.33 ^{13}C -NMR spectrum of AN-PEA copolymers with different compositions, showing theoretical and actual compositions were comparable

3.4.3 Differential Scanning Calorimetry (DSC) Results

Representative DSC thermograms of the copolymers of the ethylacrylate-acrylonitrile series and the observed glass transition values are given in Figure 3.34. DSC scan was performed from room temperature to 250 °C and the heating rate was maintained at 10°C/min. The T_g values were found to decrease with increasing acrylate content. This could be attributed to the effect of the bulkier comonomer acrylates.

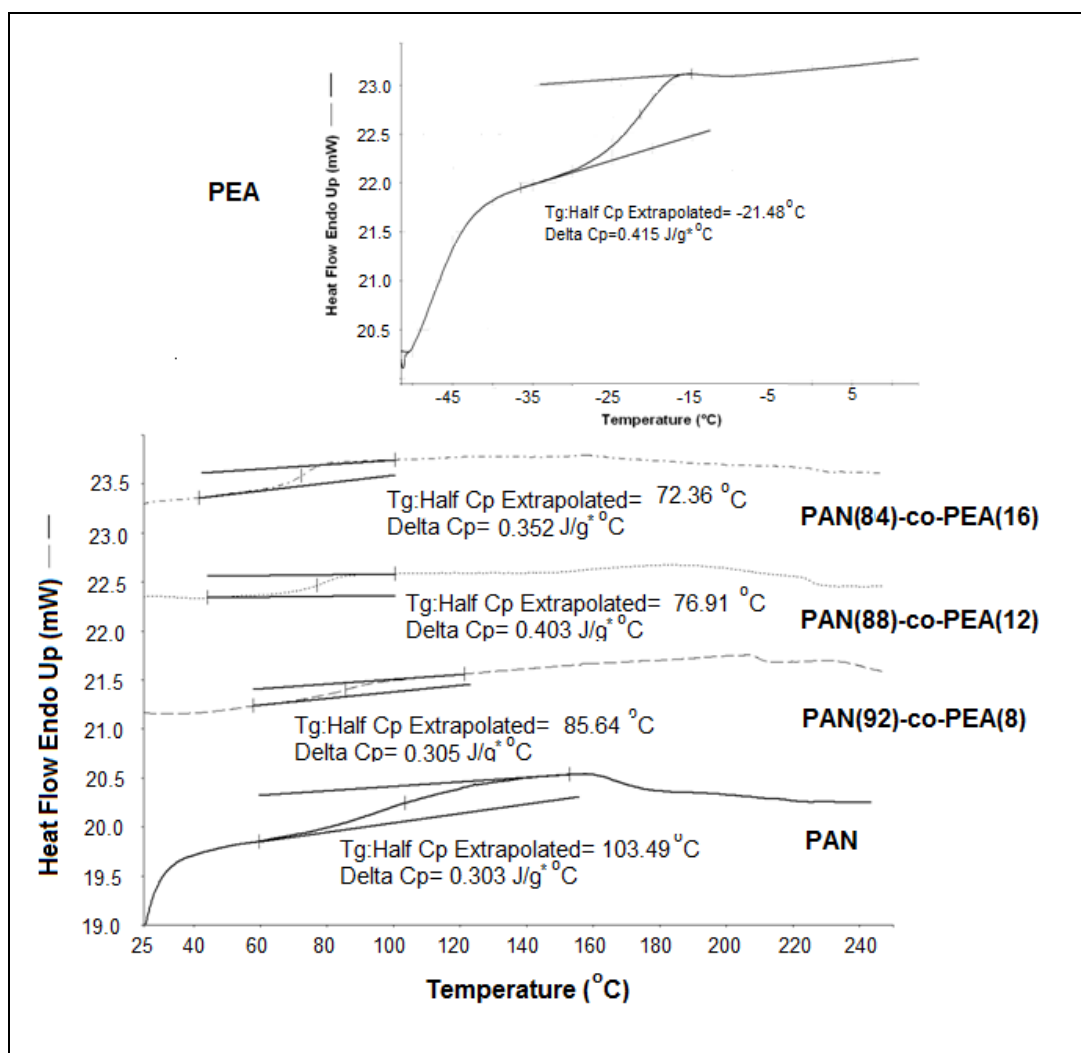


Figure 3.34. DSC thermograms of homo (PEA, PAN) and copolymers (PAN-PEA)

3.4.4 Thermogravimetric Analysis (TGA) Results

TGA diagrams of copolymers containing EA are shown in Figure 3.35. The thermal stability of the AN/EA copolymers increases with increase of the mole ratio of EA. The decomposition temperature increases with the increase of the molar ratio of EA. Increase in the mole ratio of EA disrupts the long order of AN chain, leading to increase of the amorphous region of the copolymers.

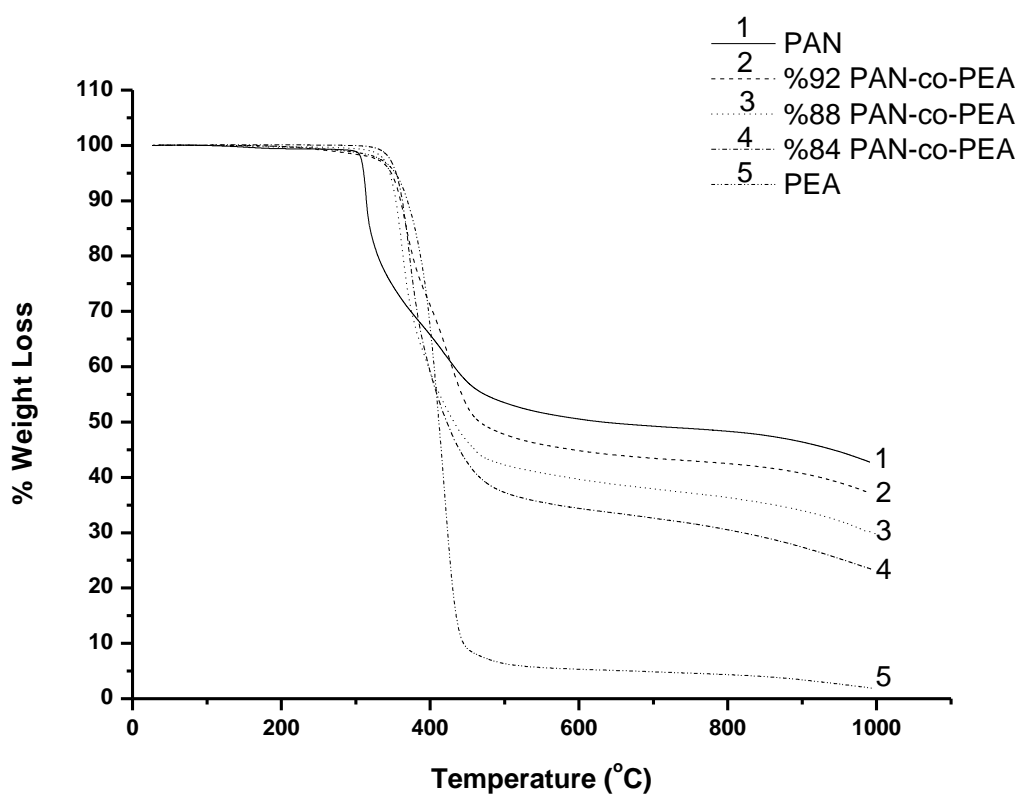


Figure 3.35 Weight loss curves for homo- and copolymers versus temperature

It can be seen that as the acrylonitrile content increased the weight loss at the maximum decomposition temperature decreases (Table 3.12). The % weight loss at a given temperature is directly related to the copolymer composition. It is more clearly seen in Figure 3.36 that with the addition of EA into the system, the thermal

degradation mechanism of the copolymers is changed. 92% PAN-PEA copolymer has one major and one minor decomposition steps and it has the highest amount of acrylonitrile content and the most resemble one to pure PAN homopolymer. On the other hand, 88 and 84 molar percent copolymers are much resembled to pure PEA. Also, from Figure 3.36, it is clearly seen that the char yield obtained at 800°C was found to increase with increased acrylonitrile content. This higher char yield is attributed to the formation of cyclic structures [31].

Table 3.12 Thermal decomposition properties of homo- and copolymers (heating rate 10°C/min, N₂ atmosphere)

Sample name	T ₅ ^a (°C)	T ₁₀ ^b (°C)	T _{max} ^c (°C)	Char yield at 800°C
PAN	310	314	314	48
PAN(92)-co-PEA(8)	348	360	360	43
PAN(88)-co-PEA(12)	346	354	362	36
PAN(84)-co-PEA(16)	339	363	371	31
PEA	353	369	421	4

^atemperature of 5% weight loss

^btemperature of 10% weight loss

^ctemperature of the first maximum

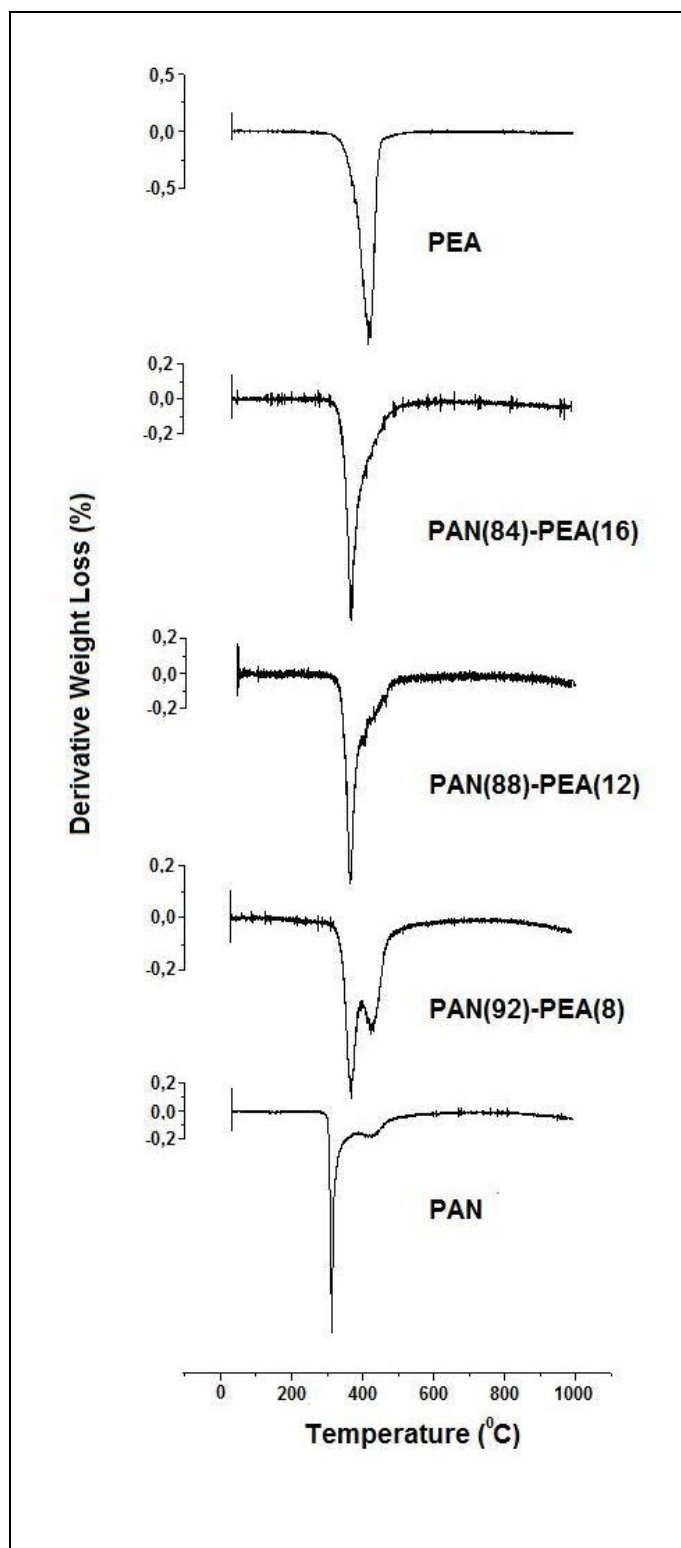


Figure 3.36 Effect of copolymer composition on the percent weight loss during TGA analysis

3.4.5 Mechanical Test Results

Variation of elastic modulus with respect to copolymer compositions can be seen in Figure 3.37. It is observed that elastic modulus values of copolymers decreases with increasing amounts of EA units in the copolymer content. This is because the polymer structure becomes softer with the addition of EA.

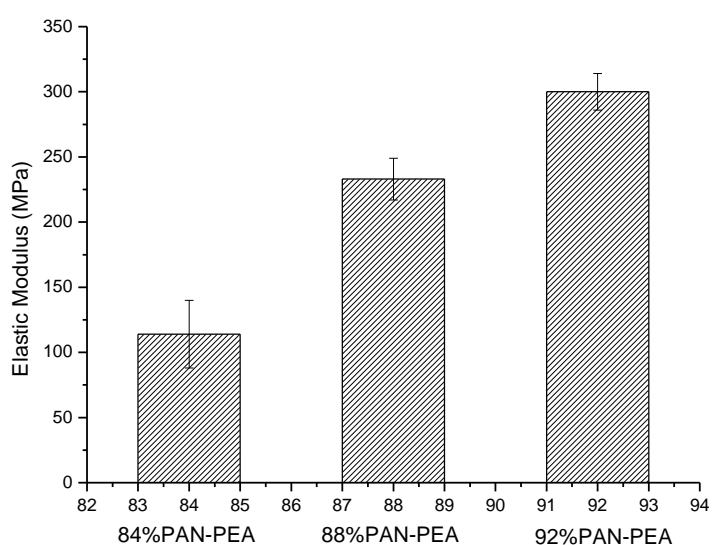


Figure 3.37 Elastic Modulus of PAN-PEA copolymers

Ultimate tensile strength (UTS) values are given in Figure 3.38. Decrease in AN unit in the copolymer content, decreases the UTS values leading to softer polymeric structures. As the AN content decreases to %92 PAN-PEA, %88 PAN-PEA and %84 PAN-PEA, UTS values changed from 37.65 MPa, 26.93 MPa and 19.10 MPa, respectively. The decrease in the UTS values is due to the increase of EA content caused by the increase of softer units in the copolymer feed.

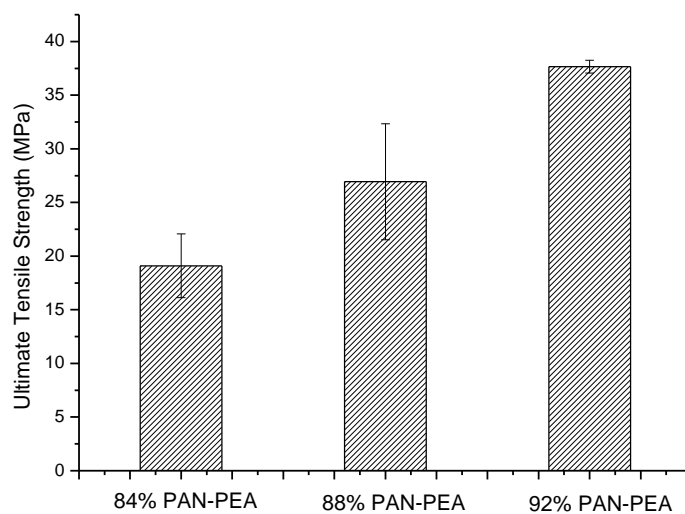


Figure 3.38 Ultimate Tensile Strength of PAN-PEA copolymers

The elongation at break (EAB) values of PAN-PEA films are shown in Figure 3.39. The PAN(88)-PEA(12) sample showed the lowest EAB value with 400.44% which can be due to the fact that it is the middle composition. That is as we go beyond the 88 molar percent of acrylonitrile; the copolymer behaves more like brittle acrylonitrile. On the other hand, when it comes to 84 molar percent the copolymer EA units seem to be dominant. The values of E, UTS and EAB for all PAN-PEA copolymers are given in Table 3.13.

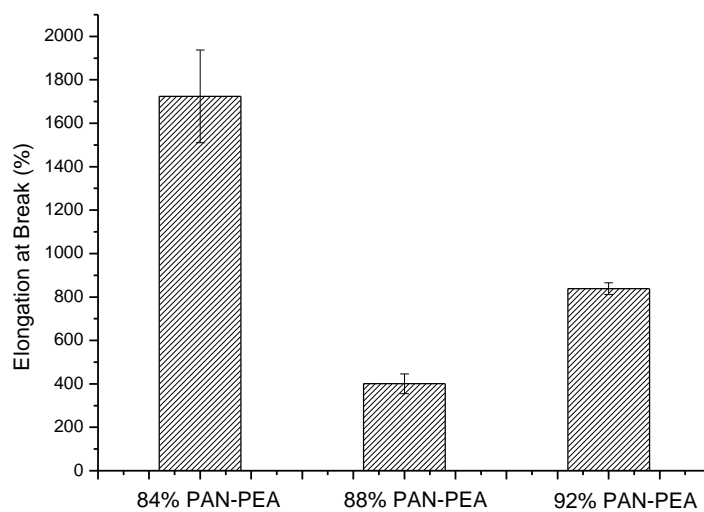


Figure 3.39 Elongation at Break (%) of PAN-PEA copolymers

Table 3.13 Mechanical test results for PAN-PEA copolymer films

Sample Name	UTS (MPa)	E (MPa)	EAB (%)
PAN(92)-PEA(8)	37.65 ± 0.60	300 ± 14.1	838.08 ± 27.43
PAN(88)-PEA(12)	26.93 ± 5.40	233 ± 16.7	400.44 ± 45.28
PAN(84)-PEA(16)	19.10 ± 2.97	114 ± 26.5	1723.91 ± 212.97

3.5 Polyacrylonitrile-Polymethyl acrylate Copolymers

Polyacrylonitrile-co-poly(methyl acrylate) copolymers (PAN-co-PMA) at three different compositions were synthesized by emulsion polymerization. Chemical structures and compositions were elucidated by FTIR, proton and carbon-13 NMR. Mechanical properties were also investigated. Thermal properties of copolymers were analyzed by DSC and TGA. The chemical structure of copolymers is shown in Figure 3.40.

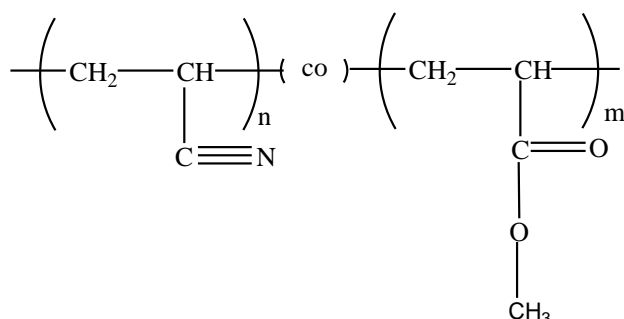


Figure 3.40 Chemical structure of polyacrylonitrile-co-polymethyl acrylate (PAN-PMA) copolymer

3.5.1 Fourier Transform Infrared Spectroscopy (FTIR) Results

The FTIR spectrum of copolymers can be seen in Figure 3.41. The aliphatic CH_x asymmetric and the symmetric stretching peaks were observed at 2934 and 2842 cm^{-1} , respectively. The strong band at 1443 cm^{-1} corresponds to the CH_x bending. The characteristic $-\text{C}\equiv\text{N}$ stretching peak was seen at 2245 cm^{-1} and $-\text{C}=\text{O}$ stretching at 1724 cm^{-1} . The peaks between 1359-1078 cm^{-1} were assigned to C-C-O and O-C-C ester stretching vibrations. The chemical structures of the copolymers were confirmed by FTIR study.

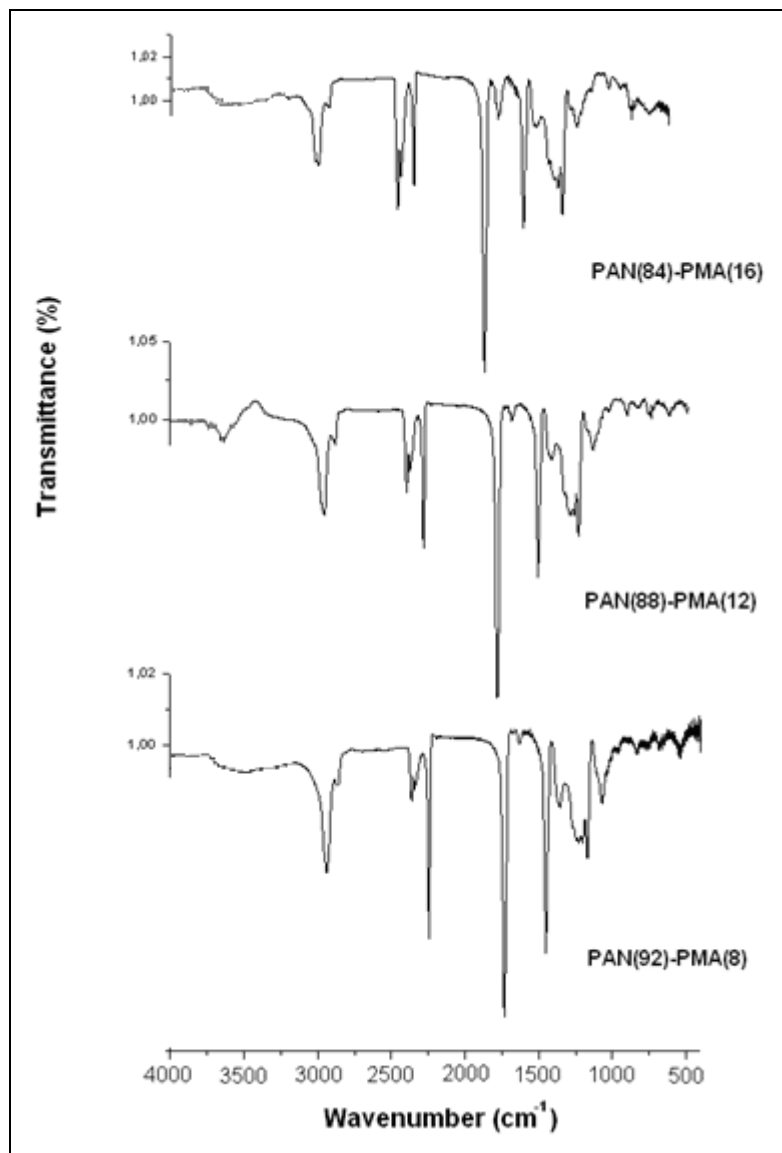


Figure 3.41 FTIR spectrum exhibited characteristic peaks of PAN-co-PMA

3.5.2 Nuclear Magnetic Resonance Spectroscopy (NMR) Results

The copolymer structure was clarified by $^1\text{H-NMR}$. The Figure 3.42 shows the $^1\text{H-NMR}$ spectrum of PAN-PMA random copolymers having different weight fractions. The $-\text{OCH}_3$ stretching appeared between 3.6-3.8 ppm (e). The resonance

between 3.2 to 2.5 ppm belonged to –CH backbone protons of acrylonitrile and methyl acrylate (b,d). The –CH₂ backbone protons appeared between 2.2 to 1.2 ppm (a,c). The average molar fraction composition of the copolymers were quantitatively determined from the integral area (I) of the peaks –OCH₃ and –CH protons from the corresponding ¹H-NMR spectra of copolymer samples prepared with different molar feeds. The theoretical and actual compositions calculated from ¹H-NMR by following equation and results were tabulated in table 3.14.

$$\text{Molar percent of MA} = \frac{I_{(e)}/3}{I_{(a,c)}/2}$$

Table 3.14 Composition and intrinsic viscosity of PAN-PMA copolymers

Sample (AN/MA)	Monomer feed (molar ratio of AN to MA)	Composition ^a (molar ratio of AN to MA)	[η] ^{NMP} _{30 °C} (dL/g)
1	92/8	92.4/7.6	1.61
2	88/12	89.2/10.4	1.47
3	84/16	85.8/14.2	1.48

^a Calculated by ¹H-NMR in *d*₆-DMSO.

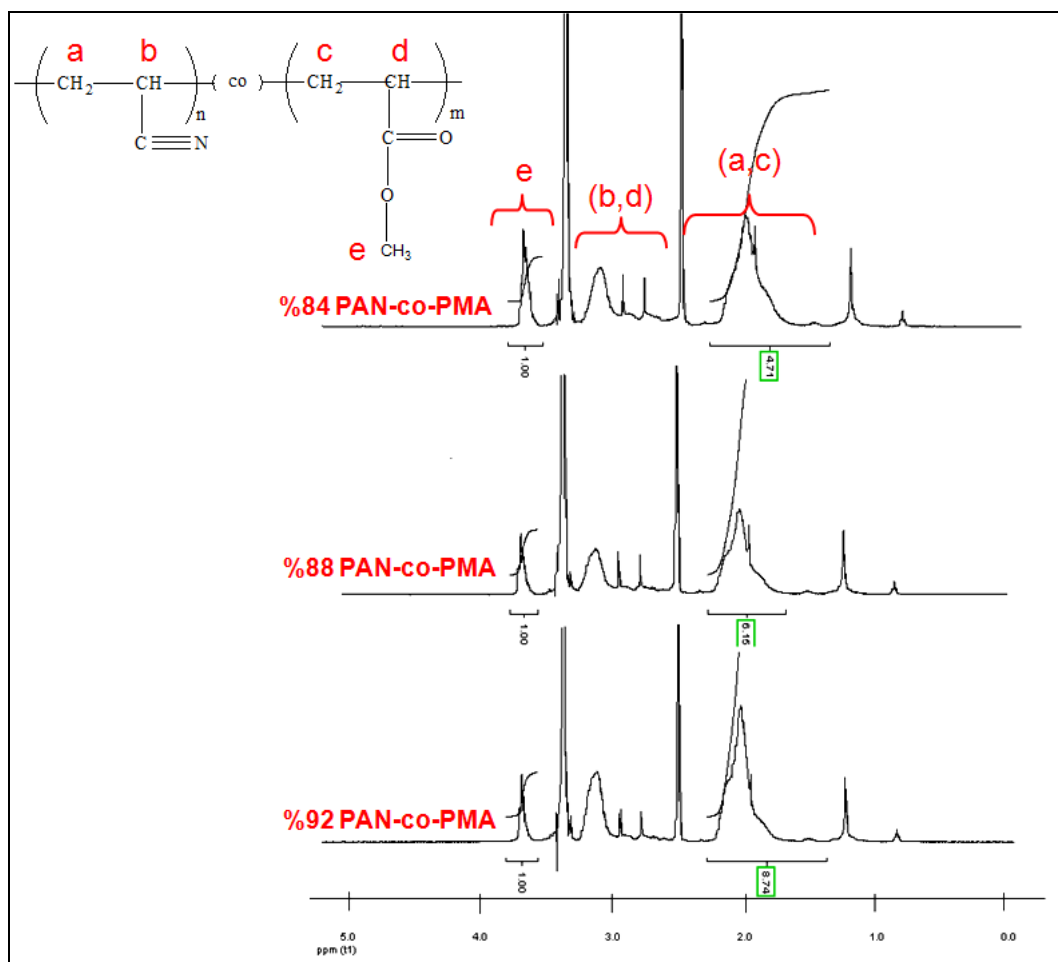


Figure 3.42 $^1\text{H-NMR}$ spectrum of AN-MA copolymers with different compositions

3.5.3 Differential Scanning Calorimetry Results (DSC)

The DSC curves of copolymers are shown in Figure 3.43. The T_g of polymethyl acrylate is well below that of polyacrylonitrile which is the reason of copolymer T_g 's was depressed relative to the pure PAN [33]. The incorporation of flexible MA monomers, which weakens the dipole-dipole interaction between $-\text{CN}$ and $-\text{CN}$, reduces the glass transition temperature of copolymers.

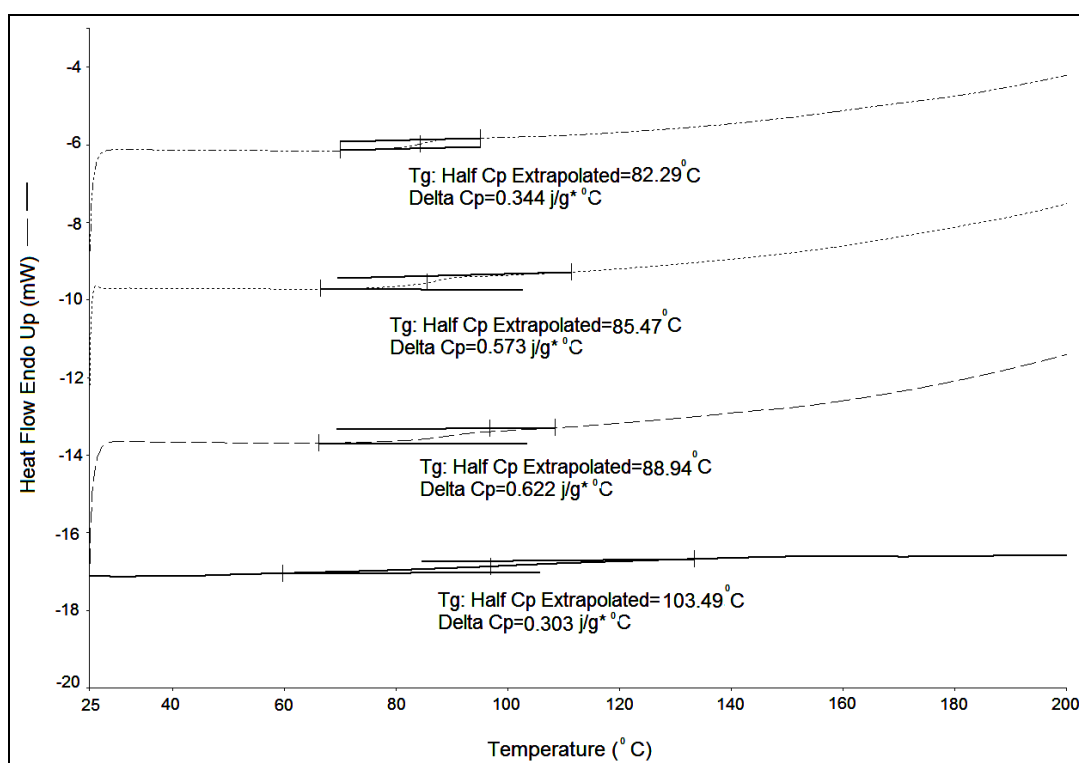


Figure 3.43 DSC results demonstrating the effect of MA content in the copolymer on Tg. Heating rate 10 °C/min, N₂ atm.

3.5.4 Thermogravimetric Analysis Results (TGA)

The TGA diagrams of copolymers containing MA are shown in Figure 44. The thermal stability of the AN/MA copolymers decreases with increase in the molar ratio of MA. The maximum degradation temperature (Table 3.15) increases as the molar ratio of MA increases; it is because of the amorphous region of the copolymers increasing. The copolymers are highly stable up to 300 °C, which is enough for some applications. It can be concluded that the presence of MA units reduces the char yield of the copolymers; it is because PAN chain is disturbed by MA units which inhibits the cyclization reaction of the PAN polymer to a certain degree [31-98]. The copolymers show a two degradation step which is more clearly seen in Figure 3.45.

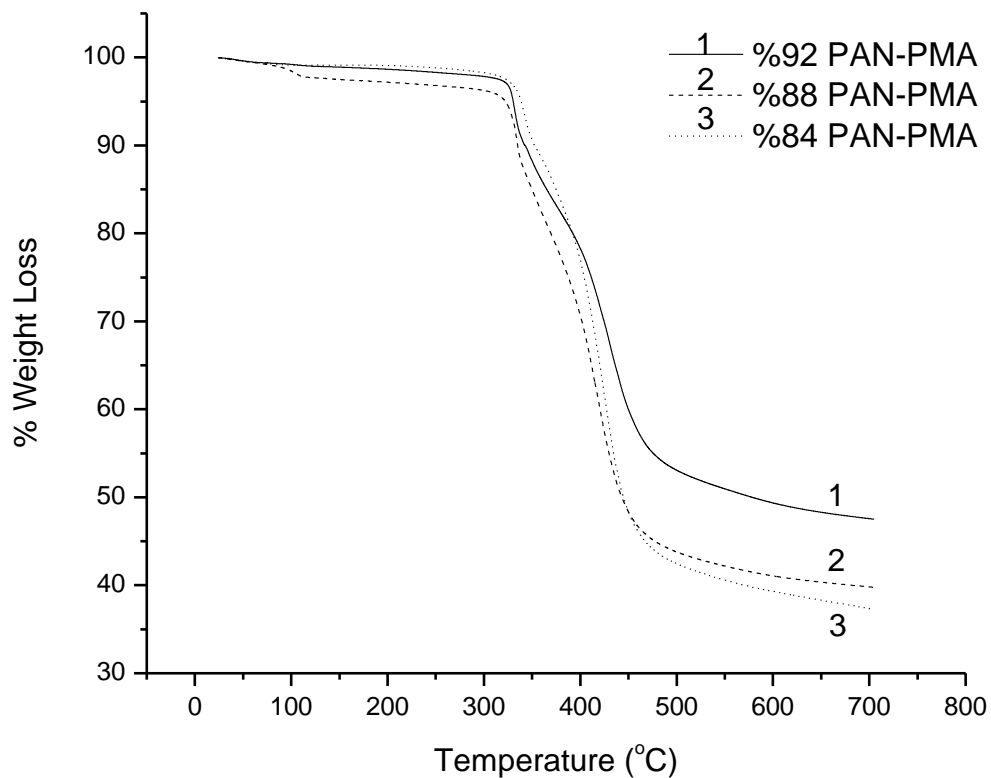


Figure 3.44 Weight loss curves for homo- and copolymers versus temperature

Table 3.15 Thermal decomposition properties of homo- and copolymers (heating rate 10°C/min, N₂ atmosphere)

Sample name	T ₅ ^a (°C)	T ₁₀ ^b (°C)	T _{max} ^c (°C)	Char yield at 700°C
PAN	310	314	314	48
PAN(92)-co-PMA(8)	330	343	333	47
PAN(88)-co-PMA(12)	322	335	335	40
PAN(84)-co-PMA(16)	339	353	343	37

^atemperature of 5% weight loss

^btemperature of 10% weight loss

^ctemperature of the first maximum

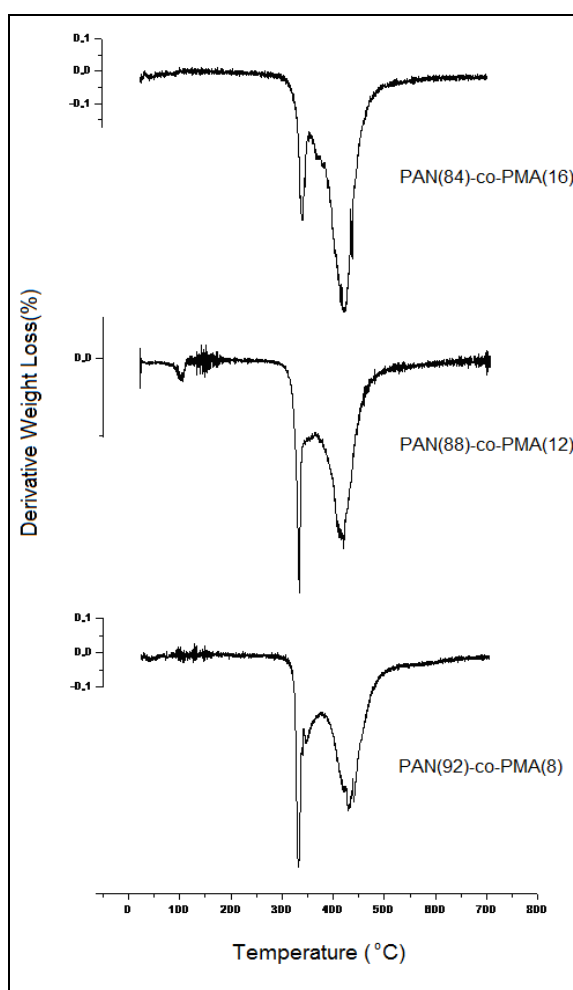


Figure 3.45 Effect of copolymer composition on the percent weight loss during TGA analysis

3.5.5 Mechanical Test Results

The tensile testing gives an indication of the strength and the elasticity of the copolymers, reflected by parameters such as tensile strength, modulus of elasticity and elongation at break. Different compositions of PAN-PMA copolymers showed different mechanical properties. The elastic modulus (E) values found as 200 MPa, 181 MPa and 53 MPa for %92 PAN-PMA, %88 PAN-PMA and %84 PAN-PMA

respectively (Figure 3.46). It was observed that elastic modulus for the copolymer %84 PAN-PMA drops to a much lower value compared to that of %92 PAN-PMA.

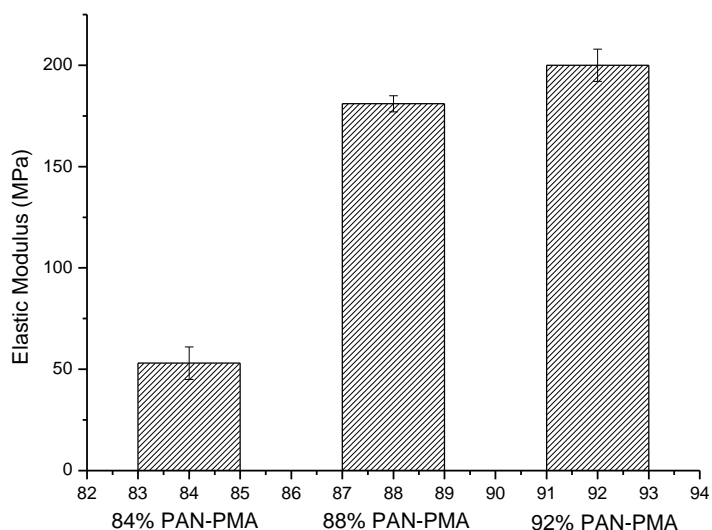


Figure 3.46 Elastic Modulus of PAN-PMA copolymers

Ultimate tensile strength (UTS) values are given in Figure 3.47. Decrease in AN unit in the copolymer content, decreases the UTS values leading to softer polymeric structures. As the AN content decreases to %92 PAN-PMA, %88 PAN-PMA and %84 PAN-PMA, UTS values changed from 127.80 MPa, 125.83 MPa and 135.25 MPa, respectively. The decrease in the UTS values is due to the increase of MA content.

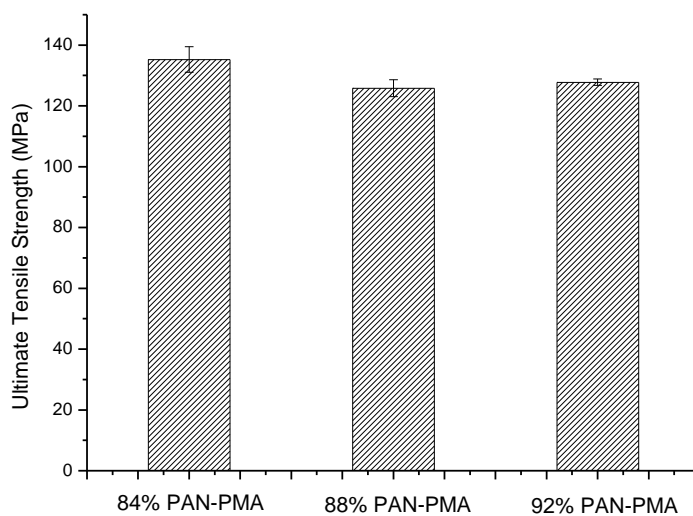


Figure 3.47 Ultimate Tensile Strength of PAN-PMA copolymers

The increase in the MA content in the copolymers rarely reduced the tensile strength and the modulus of elasticity but significantly increased the elongation at break, indicating that the copolymer membranes with 16 % MA content were weaker, more elastic, more flexible and softer. The elongation, for example, increased to 500% when the MA content in the copolymer changed from 8 to 16%. These results showed that the elasticity of PAN-PMA strongly depends on the amorphous phase fraction in the copolymer. The values of E, UTS and EAB for all PAN-PMA copolymers are given in Table 3.16.

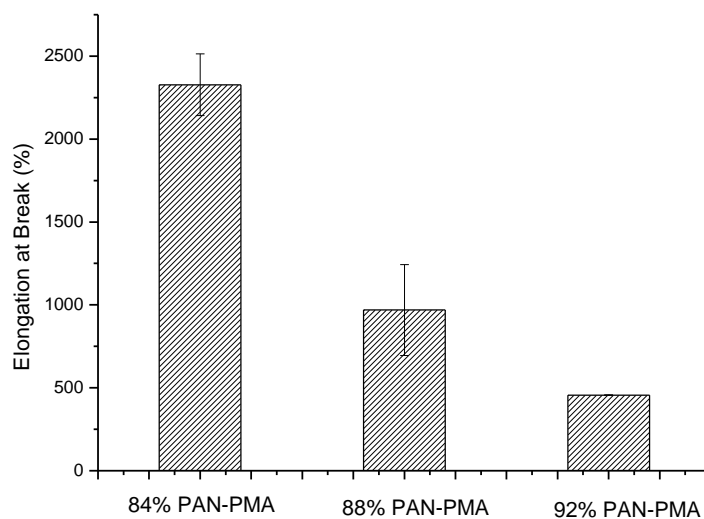


Figure 3.48 Elongation at Break (%) of PAN-PMA copolymers

Table 3.16 Mechanical test results for PAN-PMA copolymer films

Sample Name	UTS (MPa)	E (MPa)	EAB (%)
PAN(92)-PMA(8)	127.80 ± 1.03	200 ± 8.2	455.62 ± 0.86
PAN(88)-PMA(12)	125.83 ± 2.77	181 ± 4.5	968.97 ± 273.85
PAN(84)-PMA(16)	135.25 ± 4.23	53 ± 8.7	2327.15 ± 185.92

3.6 Filtration Membranes

Microscopic study through SEM analysis is carried out to have qualitative information regarding surface and cross-sectional morphology of the membranes. Asymmetric membranes with different copolymer types were prepared through phase inversion process. Figure 3.49, 3.50 and 3.51 shows the cross-sectional morphology of the membranes.

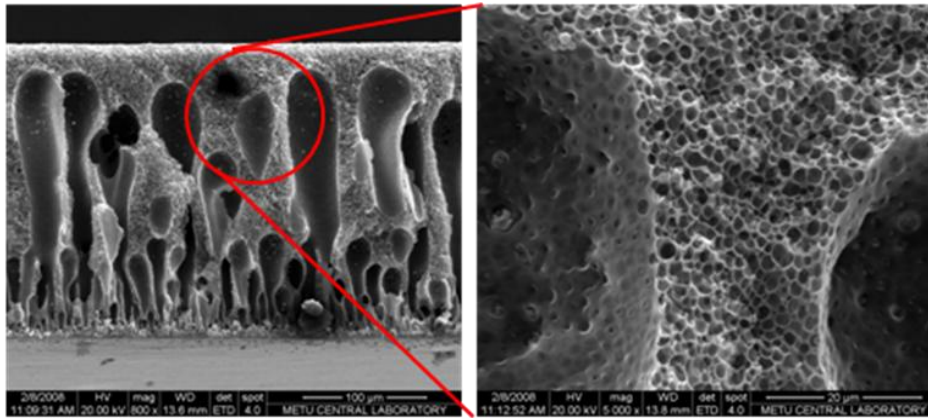


Figure 3.49 Cross-section morphologies of 88% PAN-PBA asymmetric membrane

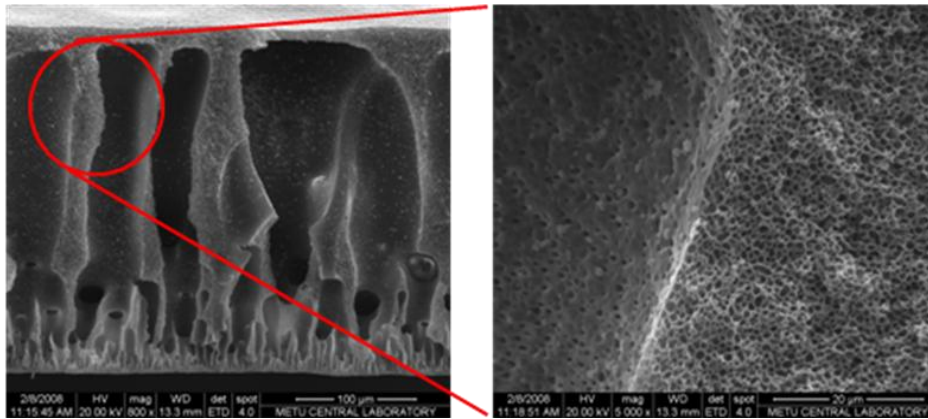


Figure 3.50 Cross-section morphologies of 88% PAN-PtBA asymmetric membrane

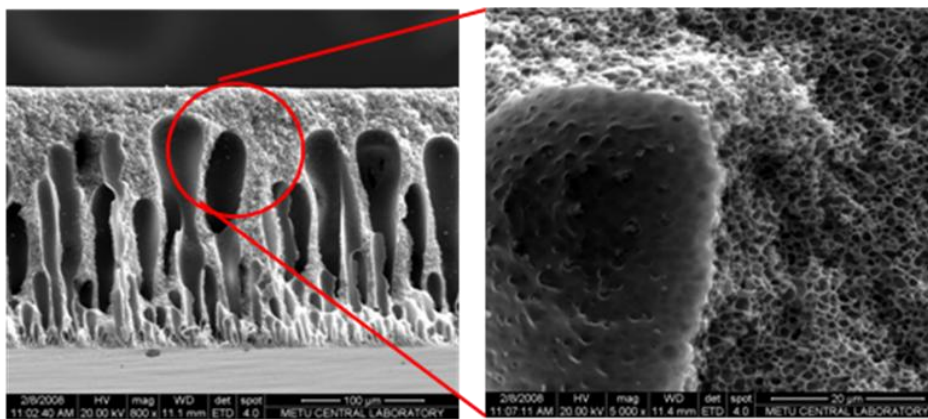


Figure 3.51 Cross-section morphologies of 88% PAN-PEA asymmetric membrane

Consequently, acrylonitrile copolymer membranes exhibits a typical asymmetric structure, composed of a thin and dense skin layer and a porous bulk that contains independent finger-like cavities enclosed in a porous solid matrix. The skin layer is responsible for the permeation or retention of solutes whereas the porous bulk acts as a mechanical support. These membranes were tested for waste water treatment such as, Cr removal from water. However, they are not useful for Cr removal (Table 3.17). For this reason, our route was changed from UF to NF.

Table 3.17 Percent Cr removal of Asymmetric membranes

Asymmetric Membrane Type	Percent Cr (VI) removal
PAN(88)-co-PBA(12)	less than 1 %
PAN(88)-co-PEA(12)	less than 1 %
PAN(88)-co-PtBA(12)	less than 1 %
PAN(88)-co-PHEA(12)	less than 1 %

3.6.1 Nanocomposite membranes

Conducting polymers are a new class of polymers used in the production of membranes. They have some advantages over conventional polymers, such as their electric conduction when in the doped state. However, these polymers do not have good mechanical properties, and should be used together with a conventional polymer in the membrane preparation. Polyaniline has been extensively studied as conductive polymer. Since these polymers have been used several times in Cr removal, PANI composites were investigated.

Among the other copolymer series, PAN(88)-PMA(12) and polyaniline nanocomposites membranes were the most successful ones due to their lower flux time (Table 3.18). For this reason, novel PAN(88)-PMA(12) and polyaniline

(PANI) nanocomposites were prepared at various PANI loadings to the remove chromium(VI) solution from water. The chemical structure (Figure 3.52), the swelling and fracture morphology of the nanocomposite membranes were also studied. PANI is well known as an electrically conductive polymer which was intrinsically doped in PAN(88)-co-PMA(12)copolymer matrix. The color of the membranes changed instantly from blue to green whenever membranes were dipped in the acid solution. This is the characteristic chemical change from emeraldine base to charged electrically conductive emeraldine salt form. It was observed that PANI had a great impact on the chromium removal. Permeate flux and the rejection of chromium(VI) was demonstrated for various pHs and chromium(VI) concentrations. The effect of solution pH on chromium(VI) removal was very significant. 99.5 percent chromium(VI) removal was observed at acidic pH with high flux as about 1500 L/m²h at 689.5 kPa. Low total flux losses indicated that membranes were fouling resistant.

Table 3.18 Nanocomposite membrane type and flux time values

Nanocomposite Membrane Type	Flux time (min)
PAN(88)-co-PBA-PANI(5)	8.50.20
PAN(88)-co-PEA-PANI(5)	10.12.25
PAN(88)-co-PtBA-PANI(5)	9.57.38
PAN(88)-co-PHEA-PANI(5)	12.12.23
PAN(88)-co-PMA-PANI(5)	1.25.13

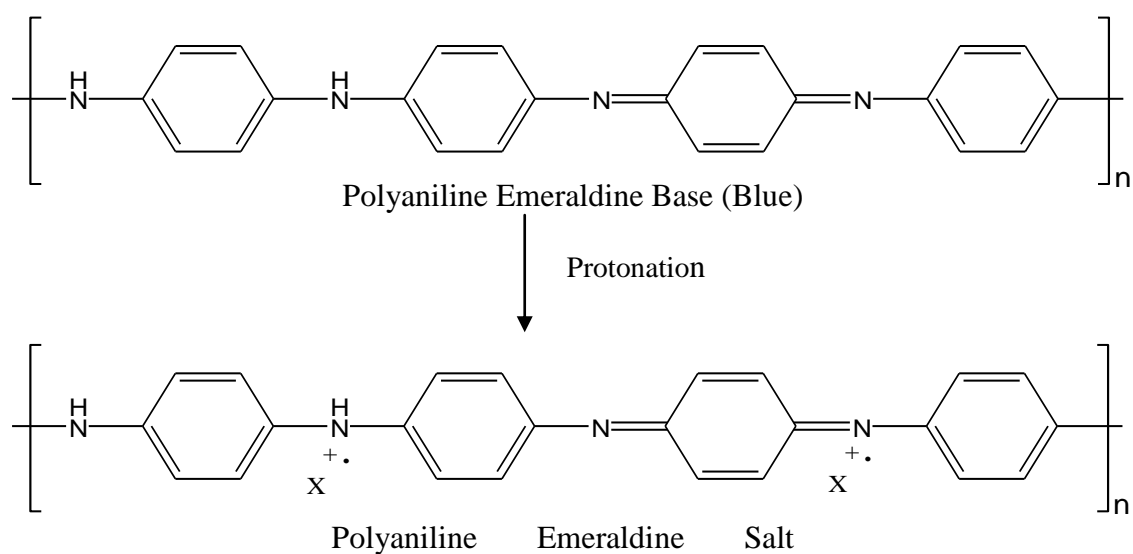


Figure 3.52 Chemical Structures of Emeraldine base and salt of PANI (X is dopant anion)

Characteristics peaks of the benzoid and the quinoid rings of polyaniline were observed at 1497 cm^{-1} and 1582 cm^{-1} . The peak at 1300 cm^{-1} was assigned to the angular deformation of CN group of polyaniline. (Figure 3.53)

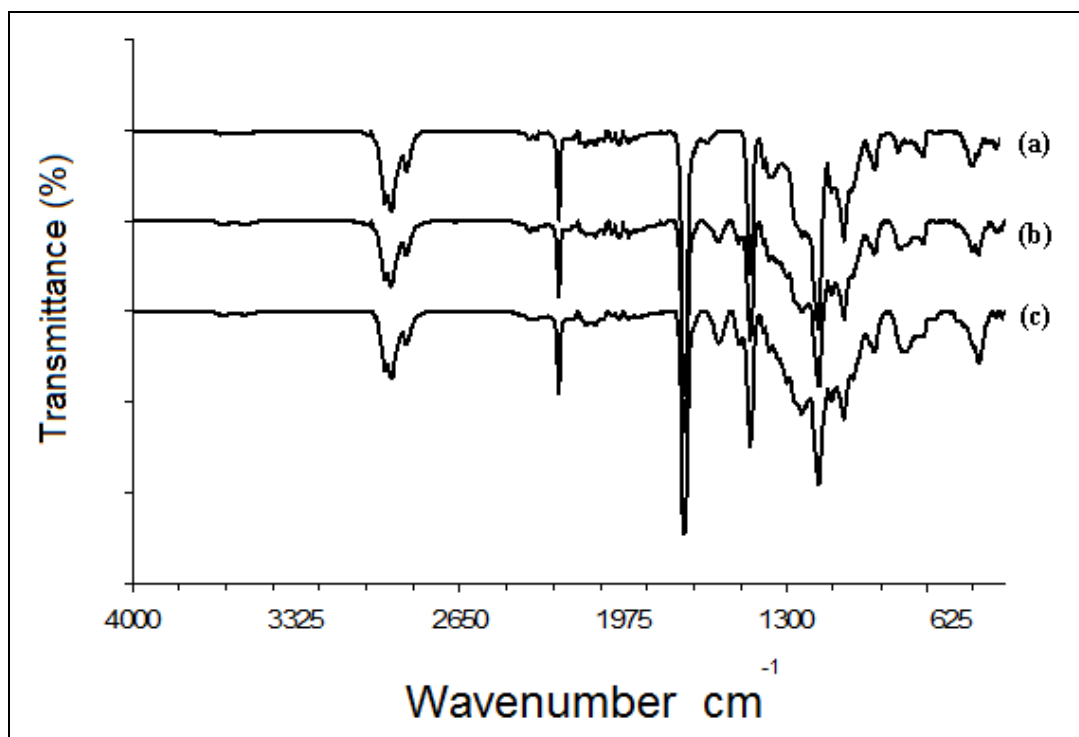


Figure 3.53 FTIR spectroscopy of a. PAN(88)-co-PMA(12) copolymer, b. PAN(88)-co-PMA(12)-PANI(5) c. PAN(88)-co-PMA(12)-PANI(10)

3.6.2 Fracture Morphology of the Nanocomposites Nanoporous Membranes

Fracture morphologies of PAN(88)-PMA(12) copolymer, PAN(88)-PMA(12)-PANI(5) and PAN(88)-PMA(12)-PANI(10) nanocomposite membranes can be seen in Figure 3.54. No phase separation was observed in the cross sectional morphology which was an indication of a nanocomposite formation. As seen in Figure 3.54, porosity size slightly decreases with the addition of PANI. This decrease in the porosity becomes a little bit more pronounced at 10 percent PANI loading. However, it is crucial to point out that porosity size changes in the range of 100-140 nm for all compositions. Therefore, we can conclude that SEM fracture morphologies of copolymer membranes and nanocomposite membranes were comparable.

3.6.3 Swelling and Electrical Properties of the Nanocomposites Membranes

Since fracture morphologies of these copolymers were very comparable, the swelling characteristics were mainly attributed to the addition of PANI. As can be seen in Table 3.19, the swelling ratio of the membranes increased with the addition of PANI. Since PANI influences the membrane hydrophilicity due to charges (Protonation, Figure 3.52) produced by doping process. These charges, especially on the surface of the membrane, adsorb more water compared to the bare copolymer membrane. As PANI content increased further, the swelling ratio was also increased and the absorbed water was almost three times enhanced with respect to the swelling ratio of the PAN(88)-co-PMA(12) copolymer. Similarly, electrical conductivities of nanocomposites membranes were increased (about 5.5 times) when PANI content was increased from 5 to 10 percent. This showed that number of protonation was enhanced with increasing PANI content.

Table 3.19 Swelling Ratios and Sheet Resistivities of Copolymer and Nanocomposite Membranes

Copolymer and Nanocomposite Membranes	AN Content (molar percent)	Methylacrylate Content (molar percent)	Polyaniline Content (weight percent)	Swelling Ratio (weight percent)	Sheet Resistivity (ohm/square)
PAN(88)-co-PMA(12)	88	12	-	3	-
PAN(88)-co-PMA(12) PANI(5)	88	12	5	5	2.3×10^5
PAN(88)-co-PMA(12) PANI(10)	88	12	10	8	4.2×10^4

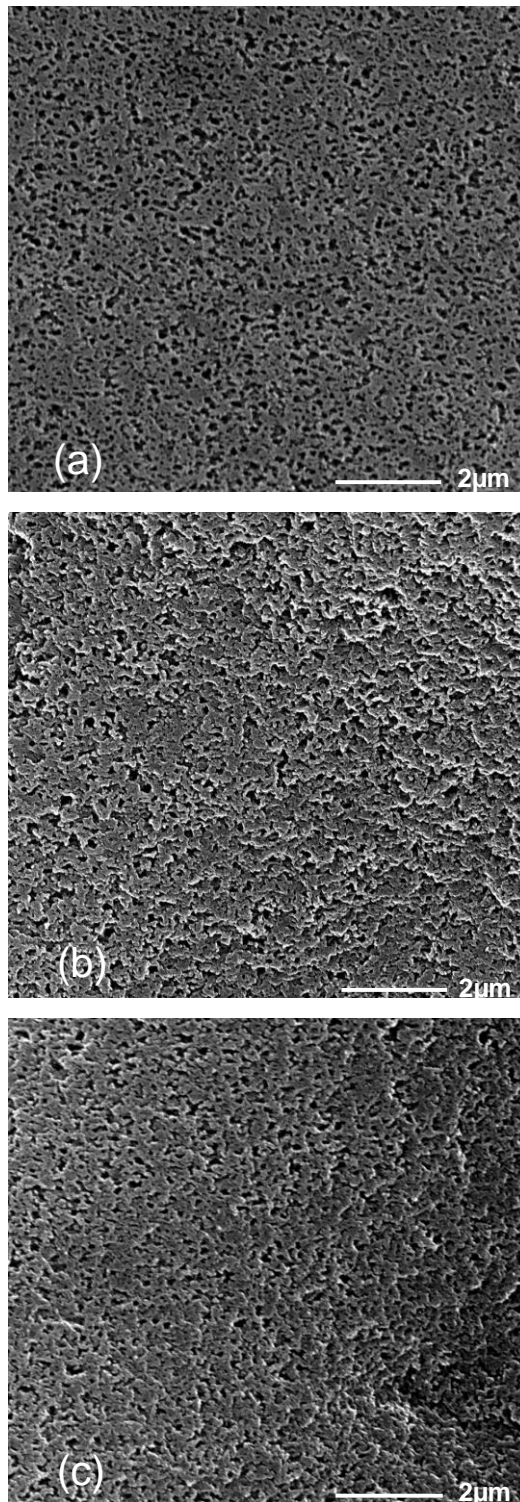


Figure 3.54 Fracture morphology of a. PAN(88)-co-PMA(12) membrane, b. PAN(88)-co-PMA(12)PANI(5) c. PAN(88)-co-PMA(12)PANI(10)

3.6.4 Performances of Nanocomposite Membranes

The pure water fluxes of the PAN(88)-PMA(12)-PANI(5) and the PAN(88)-PMA(12)-PANI(10) nanocomposites membranes were measured as 1679 L/m²h and 1735 L/m²h, respectively (Table 3.20). Since both nanocomposite membranes had similar cross sectional morphology, the observed 3.2 percent increase in pure water flux was attributed to the increase in PANI content. Similarly, swelling of these nanocomposite membranes were also increased when the PANI content varied from 5 to 10 percent. It can be concluded that doped PANI content (protonated) had an influence on water transport due to its created additional hydrophilicity. This is well known transport behaviour; as water uptake increases, water transport become much easier [99,100]. Table 3.20 shows the permeate flux of PAN(88)coPMA(12)-PANI(5) nanocomposite membranes at various concentrations and pH ranges.

Interestingly, although high chromium (VI) removal was achieved at 50 and 100 ppm concentrations, there were almost no chromium (VI) rejection observed for solutions containing 250 ppm Cr (VI). That is, the chromium (VI) solution was directly passed through a membrane with almost no rejection (maximum 1 %). This was almost equal to pure copolymer matrix performance without PANI loading. At lower concentrations, permeate flux were ranged between 1000 and 1200 L/m²h for PAN88coPMA12-PANI(5) nanocomposite membranes. One can easily understand from these results that PANI influenced flux and rejection of the chromium (VI) solution during filtration. This is why PANI content increased from 5 to 10 percent to explore the influence of PANI on membrane performances. Permeate fluxes were increased significantly when PANI content were increased from 5 to 10 percent (Table 3.20). Chromium (VI) removal was successfully achieved at 250 ppm for 10 weight percent PANI containing nanocomposite membranes (labeled as PAN(88)coPMA(12)-PANI(10)).

Table 3.20 Pure Water and Permeate Fluxes of Nanocomposite Membranes at Various Chromium (VI) concentrations and pHs

Membrane	Pure Water Flux (L/m ² h)	pH	Cr(VI) (ppm)	Permeate Flux (L/m ² h)	Membrane	Pure Water Flux (L/m ² h)	pH	Cr(VI) (ppm)	Permeate Flux (L/m ² h)
PAN(88)coPMA(12)-PANI(5)	1679	2	50	1024	PAN(88)coPMA(12)-PANI(10)	1735	2	50	1485
		2	100	1011			2	100	1323
		2	250	1353			2	250	1073
		3	50	1187			3	50	1265
		3	100	1171			3	100	1059
		3	250	1349			3	250	1197
		5	50	1097			5	50	1392
		5	100	1164			5	100	1190
		5	250	1288			5	250	1520
		7	50	1209			7	50	1188
		7	100	1188			7	100	1254
		7	250	1210			7	250	1698

Permeate fluxes were in between about 1050 and 1500 L/m²h at lower concentrations where rejection was always very successful. It can be concluded that PANI addition increases the flux. Since, doped polyaniline is intrinsically positive charged, it adsorbed chromate on the surface as well as protons from chromate solution at lower pHs. Also, doped PANI increases the hydrophilicity of membranes. This will help chromate adsorption on the surface and water transport through the membrane.

It is well known that chromium (VI) removal from water is highly pH dependent. Since the hydrogen ion itself has an adsorbent capacity and it changes the chemical nature of the metal ions. Also, the chemical nature of the chromium (VI) ion depends on pH and its concentration. Hence, hexavalent chromium species can be found in various forms as chromic acid (H₂CrO₄), hydrogen chromate (HCrO₄⁻) and chromate (CrO₄²⁻) at different pHs and chromium concentrations [78]. On the other hand, dichromate is dimer of HCrO₄⁻ and it appears when chromium concentration exceeds 1000 ppm (Figure 3.55). Since experiments were carried out by varying the pH of solutions from pH=2 to pH=7 at three different concentrations (5, 100, 250 ppm) dichromate species is out of the focus of this study.

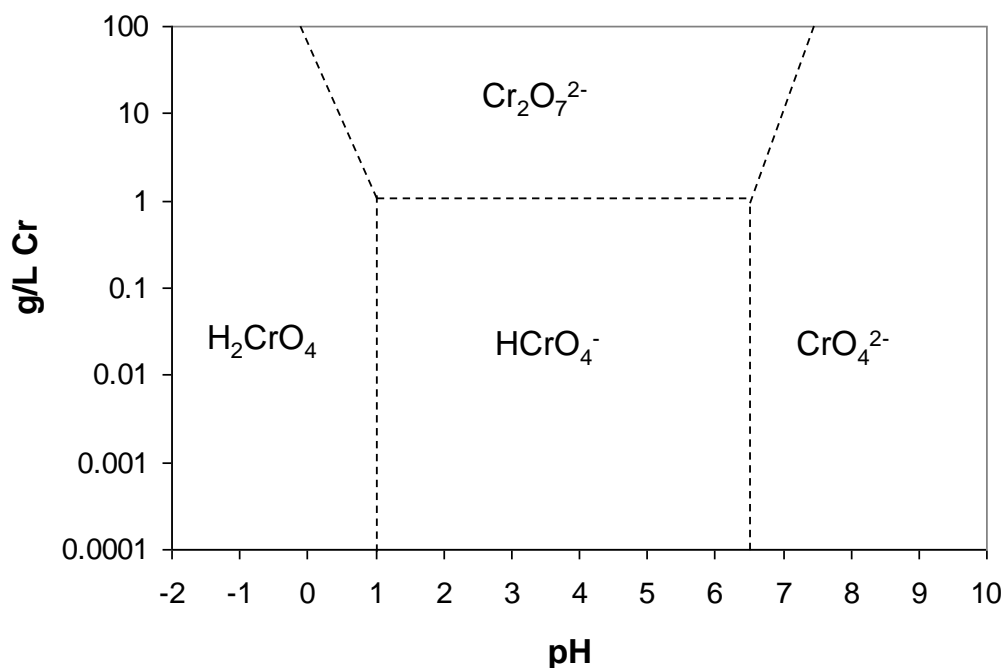


Figure 3.55 Influence of pH and hexavalent chromium concentration on formation of hexavalent chromium species

As it is mentioned earlier, all cross sectional morphologies of the copolymer and the nanocomposites membranes were comparable and copolymer membranes showed the poorest chromium (VI) removal (less than 0.7 percent). It is obvious that prepared nanocomposites membranes are positively charged due to its amine protonation after acid treatment. Also, it was understood that amine salt functionalized nanocomposites successfully bound the Cr(VI) as monovalent and divalent chromates. This explains the successful rejection performances observed for nanocomposites membranes. Figure 3.56 shows the percent chromium (VI) removal capability of PAN(88)-co-PMA(12)-PANI(5) copolymer nanocomposite membranes at three different chromium (VI) compositions and various pH values. Maximum rejection of 99.3 % was observed at pH=2 for 50 ppm chromium (VI) solution. At 50 ppm, concentration rejection was decreased approximately 82 % with increasing pH from pH=2 to pH=7. Similar behavior was also observed for

100 ppm solutions. Rejection was as high as 98 percent at pH=2, but it was reduced to about 47 % at pH=7. It can be concluded that the hydronium ion concentration on the membrane surface decreases with increasing pH causing decrease in removal of chromium (VI). When polyaniline weight content was increased from 5 to 10 percent, better performances were observed at all concentrations (Figure 3.57). Very high chromium (VI) removals (99.5 %) were observed for the PAN(88)-PMA(12)-PANI(10) copolymer nanocomposite membranes having 10 percent PANI loadings at 50 and 100 ppm chromium (VI) concentrations. Additionally, the chromium (VI) removal by PAN(88)-PMA(12)-PANI(10) nanocomposite membranes was about 97 percent at 250 ppm and pH=2. The worst rejection was observed as 61 % for the solutions having 250 ppm chromium (VI) at pH= 7. This was possibly due to increase in number of positive charge provided from doped polyaniline adsorbed more mono and divalent anion on the membrane surface.

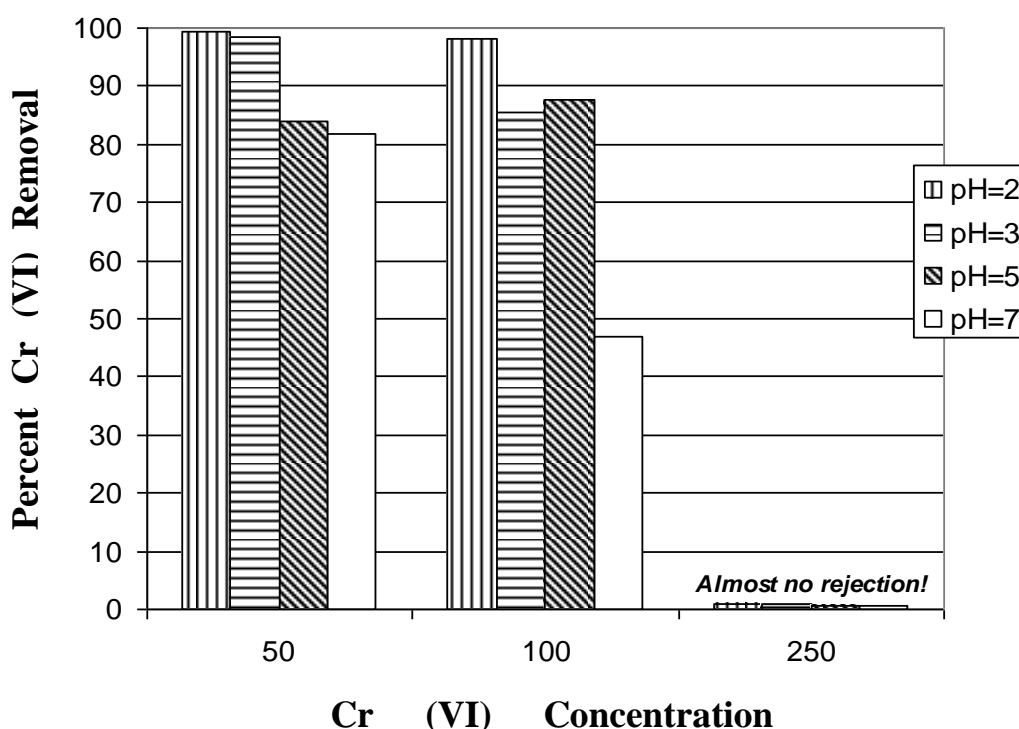


Figure 3.56 Percent chromium removal of PAN(88)-co-PMA(12)-PANI(5) nanocomposites membranes at various pHs

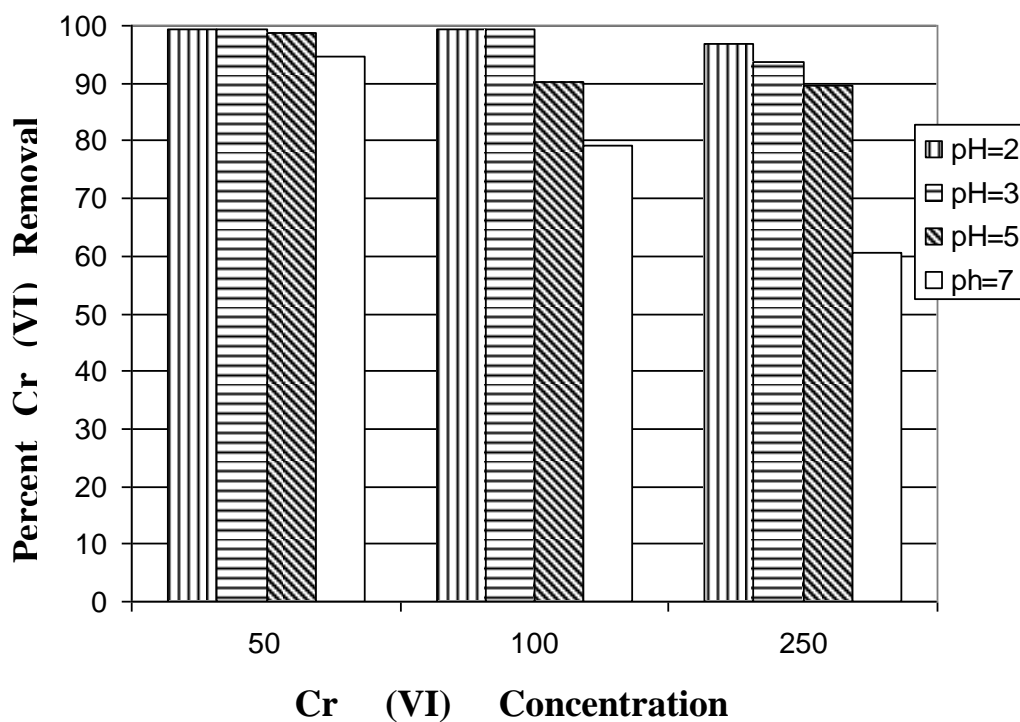


Figure 3.57 Percent chromium removal of PAN(88)-co-PMA(12)-PANI(10) nanocomposites membranes at various pHs

Since better chromium (VI) removal performances were observed for 10 percent PANI loading nanocomposites, fouling analysis were performed for the 10 percent PANI loading nanocomposites membranes at 689.5 kPa for 2h continuous permeation. The data from fouling analysis were used to calculate percent flux recovery, total flux loss, reversible and irreversible flux losses [101-102]. It was observed that all nanocomposite membranes showed higher flux recovery (greater than 90 percent) promising better long term performances (Table 3.21). Total flux loss caused by total fouling was also investigated. Lower total flux numbers of nanocomposites membranes were indicating the smaller number of adsorption on membrane surface. As expected, it was observed that the total flux loss was always higher at 100 ppm concentration compared to 50 ppm concentration for corresponding pHs. Total flux loss includes reversible and irreversible flux losses. Reversible flux loss can easily be removed by water washing of the membranes.

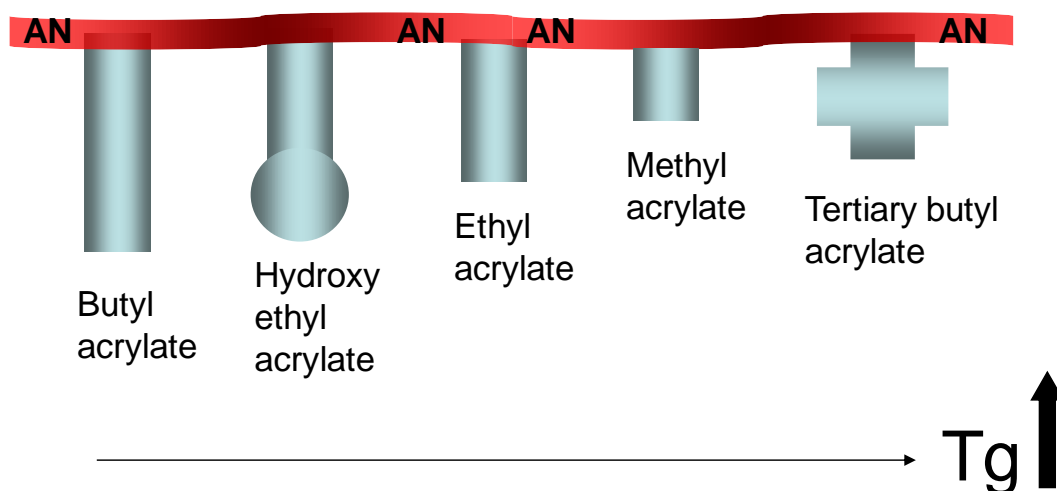
However, irreversible flux loss is permanent and caused by irreversible deposition of permeate on the membrane active surface. Table 3.21 shows that the total flux can easily be attributed to reversible flux which can be eliminated by washing or cross flushing of the membranes. Similarly, reversible flux losses were always higher for 100 ppm solutions for corresponding pHs. However, irreversible flux losses were comparable for all samples. In other words, permanent deposition characteristics of chromium on nanocomposite membranes for all pHs and concentrations were similar, however temporary adsorption on the surface was more varied on concentration of chromium. This also justifies that nanocomposite membranes were fouling resistant.

Table 3.21 Fouling Analysis for 10 percent PANI Loading Nanocomposite Membranes PAN88coPMA12-PANI(10)

pH	Cr(VI) (ppm)	Percent Flux Recovery	Total Flux Loss	Reversible Flux Loss	Irreversible Flux Loss
2	50	95.5	0.47	0.43	0.040
2	100	94.0	0.65	0.61	0.040
3	50	95.2	0.64	0.59	0.050
3	100	93.0	0.69	0.64	0.050
5	50	93.5	0.45	0.41	0.040
5	100	92.0	0.55	0.51	0.040
7	50	93.0	0.58	0.53	0.050
7	100	94.0	0.63	0.59	0.040

3.7 Structure Property Relationship

3.7.1 Composition-Comonomer-Glass Transition Temperature



Polymer properties are related not only to the chemical nature of the polymer but also to such factors as extent and distribution of crystallinity, distribution of polymer chain lengths, and nature and amount of additives, such as fillers, plasticizers. These factors influence essentially all the polymeric properties to some extent, such as hardness, flammability, weatherability, chemical resistance, stiffness and glass transition temperature etc. [103]. Glass transition temperature of the copolymers and the homopolymer were determined by DSC analysis.

Table 3.22 shows the glass transition temperature of homo and copolymers with different compositions. In this table, there are mainly five types of copolymers. Giving this order; PAN-PBA, PAN-PHEA, PAN-PEA, PAN-PMA and PAN-PtBA should help to understand the T_g and the composition relationship between them. It is clearly seen that the T_g values of copolymers increases in the given order. The thermal motion is dependent on the freedom of the chain to undergo changes in conformation. When this freedom is higher, the chain is subjected to a stronger thermal motion than a chain which is more rigid.

Table 3.22 Glass Transition Temperatures and intrinsic viscosities of homo and copolymers at three different compositions

Polymer	Glass Transition Temperature	Intrinsic Viscosity
PAN	103.5	-
PBA	-48.6	-
PHEA	3.46	-
PEA	-21.4	-
PMA	8.0 ^[104]	-
PtBA	37.6	-
PAN(92)-co-PBA(8)	75.8	1.04
PAN(88)-co-PBA(12)	67.5	1.36
PAN(84)-co-PBA(16)	56.4	0.90
PAN(92)-co-PHEA(8)	80.9	1.25
PAN(88)-co-PHEA(12)	74.0	0.72
PAN(84)-co-PHEA(16)	69.3	0.92
PAN(92)-co-PEA(8)	85.6	1.79
PAN(88)-co-PEA(12)	76.9	1.07
PAN(84)-co-PEA(16)	72.4	1.09
PAN(92)-co-PMA(8)	88.94	1.61
PAN(88)-co-PMA(12)	85.47	1.47
PAN(84)-co-PMA(16)	82.29	1.48
PAN(92)-co-PtBA(8)	91.7	1.21
PAN(88)-co-PtBA(12)	85.3	1.03
PAN(84)-co-PtBA(16)	83.7	0.70

Ethyl acrylate copolymers and butyl acrylate copolymers which are in the same composition can be compared for a clear explanation. Butyl acrylate copolymers can move more easily than ethyl acrylate ones because they are further from each other. For another explanation, tert-butyl acrylate and butyl acrylate copolymers were compared. tBA copolymers has an anchor like side groups which makes the polymer chain move much more slowly causing an increase in Tg. Butyl, HEA and EA copolymers have a higher free volume than the methyl acrylate ones, therefore they have a lower Tg than the methyl acrylate copolymers. When we compare methyl and t-butyl acrylate copolymers, methyl acrylate copolymers have a little higher chain ability than t-BA ones due to this methyl acrylate copolymer Tg's was lower than tBA ones. For a final explanation; HEA copolymers and EA copolymers were chosen. HEA copolymers have a large free volumes however, they have a capacity to produce intermolecular forces and this is why it's Tg is comparable to ethyl acrylate copolymers.

When the butyl acrylate comonomer is incorporated into the copolymer, the glass transition decreases in a much bigger step than the others types of comonomers. BA is a bulkier molecule than the other acrylates and the disruption in the long-range order is expected to be greater in the PAN copolymer for the same amount of comonomer addition, and thus the decrease in Tg would be greater.

In conclusion, it can be understood that the incorporation of the acrylate comonomers in the PAN chain leads to a drop in the Tg values. This is indicative of the disrupting of the order in the PAN homopolymer attributed to the random inclusion of the comonomer, leading to an increase in the free volume of the chains and thereby lowering the Tg.

3.7.2 Composition-Comonomer-Mechanical Properties

The mechanical properties of the polyacrylonitrile copolymers were characterized by their average values of elastic modulus, ultimate tensile strength and elongation

at break. The results were obtained at room temperature and are presented in Table 3.23.

Mechanical properties of these copolymers are dependent on the molecular weight of copolymers however, they are also dependent on copolymer composition and comonomer type. Generally, all the UTS values are showed the same tendency with respect to comonomer composition. It is probably due to interrupting the AN ordered chain. All the copolymers have different IV values meaning that they have different molecular weights. However, elastic modulus of different molecular weight copolymers are showed the same inclination as copolymer composition. It is clear evidence for affect of comonomer type and composition on mechanical properties. All synthesized acrylonitrile based copolymers are ductile with high modulus.

Table 3.23 Mechanical Properties of Acrylonitrile based copolymers

	UTS (MPa)	E (MPa)	EAB (%)	IV
PAN(92)-PHEA(8)	29.65 ±0.50	785 ± 87.5	52.89 ±1.40	1.25
PAN(88)-PHEA(12)	22.03 ± 1.41	194 ± 13.4	428.45 ± 45.65	0.72
PAN(84)-PHEA(16)	12.84 ±0.21	161 ± 25.1	337.17 ± 26.45	0.92
PAN(92)-PBA(8)	36.62 ±0.58	1165 ±51.2	342.81 ±35.97	1.04
PAN(88)-PBA(12)	32.16 ±2.55	1103 ±50.8	273.58 ±71.26	1.36
PAN(84)-PBA(16)	30.57 ±0.62	1060 ±35.6	119.45 ±11.97	0.90
PAN(92)-PtBA(8)	38.86 ±2.87	287 ±18.4	258.13 ±49.41	1.21
PAN(88)-PtBA(12)	29.41 ±0.69	228 ±30.7	1324.92 ±267.25	1.03
PAN(84)-PtBA(16)	26.17 ±3.17	226 ±22.3	1538.44 ±331.51	0.70
PAN(92)-PEA(8)	37.65 ± 0.60	300 ± 14.1	838.08 ± 27.43	1.79
PAN(88)-PEA(12)	26.93 ± 5.40	233 ± 16.7	400.44 ± 45.28	1.07
PAN(84)-PEA(16)	19.10 ± 2.97	114 ± 26.5	1723.91 ± 212.97	1.09
PAN(92)-PMA(8)	127.80 ± 1.03	200 ± 8.2	455.62 ± 0.86	1.61
PAN(88)-PMA(12)	125.83 ± 2.77	181 ± 4.5	968.97 ± 273.85	1.47
PAN(84)-PMA(16)	135.25 ± 4.23	53 ± 8.7	2327.15 ± 185.92	1.48

CHAPTER 4

CONCLUSION

The work described in this thesis is a systematic study performed to identify the key parameters affecting PAN based random copolymers including: comonomer type, comonomer composition effect, hydrophilicity of comonomer and reduction of chromium. Also, several of these compositions were utilized in filtration technology for toxic chromium removal. Specific achievements of this research can be outlined as follows:

- The synthesis and the characterization of important acrylate comonomers were incorporated into copolymer backbone. The one-step process developed could be a very important starting point for commercialization efforts.
- Thermooxidatively and mechanically stable, novel PAN-PHEA, PAN-PBA, PAN-PEA, novel PAN-PtBA and PAN-PMA random copolymers and their homopolymers were successfully synthesized by one step emulsion polymerization. FTIR, ¹H-NMR and ¹³C-NMR were conformed the chemical structure of copolymers.
- The DSC study revealed that glass transition temperatures of copolymers varied between T_g of homopolymers of PAN and polyacrylates. Additionally, glass transition temperatures of PAN were lowered from 104 to 69 °C , 56 °C, 72 °C, 82 °C and 84 °C with the addition of comonomers HEA, BA, EA, MA and tBA, respectively.

- Thermal analysis of the homo and copolymers were carried out to determine the degradation temperature and also weight loss behavior during successive heating over a period of time. For all type of copolymers, the decomposition temperature increases with increase in the molar ratio of the acrylates.
- All PAN-polyacrylate copolymer compositions resulted in mechanically stable free standing films. Ultimate tensile strength and elastic modulus of the films decreased with increasing the acrylate content.
- Overshooting effect has been observed for the swelling behavior of the PAN-PHEA copolymers. The degree of swelling of all the copolymers presented here increased up to a critical time. After a certain time q values decreased and reached equilibrium due to the relaxation phenomenon of the polymer network. Moreover, it has been observed that, the degree of swelling increased with increasing the HEA content.
- For the first time, nanocomposites membranes from PAN(88)-co-PMA(12) and PANI were prepared and converted to filtration membrane for chromium (VI) removal. FTIR and SEM studies demonstrated the nanocomposite formation.
- Swelling of the nanocomposites membranes increased with PANI addition. One can easily conclude that sheet resistivity of nanocomposites membranes decreased with PANI addition.
- High performance nanocomposite membranes were achieved based on chromium removal. Chromium removal was achieved at lower concentrations at acidic pHs for 5 weight percent PANI content. However,

10 weight percent PANI containing nanocomposites produced almost complete removal (97 -99,5 %) acidic pHs. Fluxes of the nanocomposites membranes were as high as 1000-1700 L/m²h. Porosity size of the nanocomposites membranes and the copolymers were comparable (in the range of 100-140 nm). This was revealed that doped PANI has a great effect on chromium removal possibly due to the adsorption of mono and divalent chromium on the membrane surface causing better filtration of chromium (VI) and ease of water transport.

- Fouling analysis showed that nanocomposite membranes had higher percent flux recovery with lower total flux loss dominated with reversible flux loss which can be easily eliminated with water washing.
- An investigation of the relationships between the chemical structures, the copolymer composition and the glass transition temperatures of PAN based copolymers has been conducted. The incorporation of acrylate units systematically reduces Tg.
- Mechanical properties of copolymers clearly showed that they are directly related to the comonomer type and composition.
- All the copolymers synthesized in this thesis can be used as carbon fiber precursors and filtration membranes.

CHAPTER 5

SUGGESTED FUTURE RESEARCH

1. Investigate the kinetics of the polymerization process including effect of initiator concentration, effect of temperature, effect of surfactant concentration and effect of chain transfer agent concentration.
2. Expand on previous efforts via production of random copolymers with larger molar percent of acrylates.
3. Examine monomer reactivity ratios for the PAN/Polyacrylate systems.
4. Examine the thermal degradation behaviour of copolymer using TGA-FTIR and mass spectroscopy.
5. For comparison, replace the acrylate units in PAN/Polyacrylate systems with methacrylate ones.
6. Investigate copolymer compositions using DMA, melt and solution rheology.
7. Investigate the permeation of gases (like CO₂ and CH₄) through the copolymer membranes.
8. For improving the surface biocompatibility, immobilization of biomacromolecules onto membrane surface can be done.
9. Prepare the microporous gel polymer electrolyte membrane from PAN/Polyacrylate copolymers for lithium-ion batteries.

REFERENCES

1. Dar, Y. D.; Farwaha, R.; Caneba G. T. *Free Radical Polymerization, Encyclopedia of Chemical Processing*, Taylor&Francis, 2005.
2. Kricheldorf, H. R.; Nuyken, O.; Swift, G. *Handbook of Polymer Chemistry*, 240-245, Marcel Dekker, NewYork, 2005.
3. Asua, J. M. *Emulsion Polymerization: From Fundamental Mechanism to Process Developments*, J. Polymer Science: Part A: Polymer Chemistry, 42, 1025-1041, 2004.
4. Odian, G. *Principles of Polymerization*, 335-353, NewYork, John Wiley&Sons, Inc., 1991.
5. Gomes, V. G. *Emulsion Polymerization, Encyclopedia of Chemical Processing*, Taylor&Francis, 2005.
6. Schork, F. J.; Luo, Y.; Smulders, W.; Russum, J. P.; Butté A.; Fontenot, K. *Advanced Polymer Science*, 175, 129-255, 2005.
7. El-Aasser, M. S.; Lovell, P. A. (Eds.). *Emulsion Polymerization and Emulsion Polymers*, New York: John Wiley & Sons, 1997
8. Vorsina, I. A.; Mikhailov, I. Y. *Russion Chemical Bulletin*, 3, 539-542, 1996.
9. Van Herk, A. M. *Chemistry and Technology of Emulsion Polymerization*, Blackwell Publishing Ltd., 2005.
10. Smith, W. V.; Ewart, R. H. *Kinetics of Emulsion Polymerization*, *J. Chem. Phys.* 16, 592, 1948.

11. Gardon, J. L. *Emulsion Polymerization. J. Polym. Sci., Polym. Chem.*, 6 (3), 623, 1968.
12. Harada, M.; Nomura, M.; Kojima, H.; Eguchi, W.; Nagata, S. *Rate of Emulsion Polymerization of Styrene J. Appl. Polym. Sci*, 16, 811, 140, 1972.
13. Ugelstad, J.; Mork, P. C.; Aasen, J. O. *Kinetics of Emulsion Polymerization J. Polym. Sci., Polym. Chem.*, 5 (9), 2281, 1967.
14. Harkins, W. D. *Theory of the Mechanism of Emulsion Polymerization J. Am. Chem. Soc.* 69, 1428, 1947
15. Capek, I. *Sterically and Electrosterically Stabilized Emulsion Polymerization. Kinetics and Preparation, Advances in Colloid and Interface Science*, 99, 77-162, 2002.
16. Howard; R. N. *Polymerization in a System of Discrete Particles. J. Polym. Sci.*, 4, 273, 1949.
17. Ugelstad, J.; Mork, P. C.; Dahl, P.; Ranges, P. *Kinetic Investigation of the Emulsion Polymerization of Vinyl Chloride J. Polym. Sci. Polym. Sym.* 27, 49, 1969.
18. Litt, M. H.; Patsiga, R.; Stannett, V. T. *Emulsion Polymerization of Vinyl Acetate II. J. Polym. Sci. Polym Chem.*, 8 (12), 3607, 1970.
19. Suresh, K. I.; Sitaramam, B. S.; Raju, K. V. S. N. *Effect of Copolymer Composition on the Dynamic Mechanical and Thermal Behaviour of Butyl Acrylate-Acrylonitrile Copolymers, Macromolecular Materials and Engineering*, 288, 980-988, 2003.
20. Wiles, K. B.; Bhanu, V. A. ; Pasquale, A. J.; Long, T. E.; McGrath, J. E. *Monomer Reactivity Ratios for Acrylonitrile FreeRadical Copolymerization, Journal of Polymer Science: Part A: Polymer Chemistry*, 42, 2994-3001, 2004.

21. McManus, N.T.; Kim, J. D.; Pendilis, A. *Observations on styrene-hydroxyethyl acrylate and styrene-hydroxyethyl acrylate-ethyl acrylate polymerizations*, *Polymer Bulletin* 41, 661-668, 1998.
22. Tejedor, J. A. G.; Acosta, T. R.; Ribelles, J. L. G.; Polizos, G.; Pissis, P. *Poly(ethyl methacrylate-co-hydroxyethyl acrylate) random co-polymers: Dielectric and dynamic-mechanical characterization*, *J Non-Cryst Solids* 353, 276-285, 2007.
23. Mun, G. A.; Nurkeeva, Z. S.; Beissegul, A. B.; Dubolazov, A. V.; Urkimbaeva, P. I.; Park, K.; Khutoryanskiy, V. V. *Temperature-Responsive Water-Soluble Copolymers Based on 2-Hydroxyethyl Acrylate and Butyl Acrylate Macromolecular Chemistry and Physics*, 208, 979-987, 2007.
24. Capek, I.; Potisk, P. *Polymer Journal (Tokyo)*, 24, 1037, 1992.
25. Capek, I.; Mlynarova, M.; Barton, J. *Chem. Pap.*, 42, 763, 1988.
26. Capek, I.; Mlynarova, M.; Barton, J. *Makromol. Chem.*, 189, 341, 1988.
27. Pokhriyal, N. K.; Sanghvi, P. G.; Hassan P. A.; Devi S. *Transparent nanolatexes by polymerization of precursor emulsions*, *European Polymer Journal*, 37, 1695-1704, 2001.
28. Brar, A. S.; Sunita *Sequence determination of acrylonitrile-(ethyl acrylate) copolymers by ¹³C-NMR spectroscopy and correlation with glass transition temperature* *European Polymer Journal*, 28 (7), 803-808, 1992.
29. Braun, D.; Meyer, M. I. *Macromol. Chem. Phys.*, 199, 735-744, 1998.
30. Martinez, G.; Sanchez-Chaves, M.; Madruga, E. L.; Monreal C. F. *Monomer reactivity ratios and microstructural analysis of 2-hydroxyethyl methacrylate-*t*-butyl acrylate copolymers*, *Polymer*, 41(15), 6021-6026, 2000.

31. Rangarajan, P.; Yang, J.; Bhanu, V.; Godshall, D.; McGrath, J.; Wilkes, G.; Baird, D. *J Appl Polym Sci* 85, 69-83, 2002.
32. Rangarajan, P.; Yang, J.; Bhanu, V.; Godshall, D.; Wilkes, G.; McGrath, J.; Baird, D. *Polymer* 43, 2699-2709, 2002.
33. Godshall, D.; Rangarajan, P.; Baird, D. G.; Wilkes, G. L.; Bhanu, V. A.; McGrath, J. E. *Polymer* 44, 4221-4228, 2003.
34. Bortner, M. J.; Bhanu, V.; McGrath, J. E.; Baird, D. G. *J Appl Polym Sci* 93, 2856-2865, 2004.
35. Joseph, R.; Devi, S.; Rakshit, A. K. *Synthesis and characterization of homopolymers and copolymers of various acrylates and acrylonitrile, Journal of Applied Polymer Science*, 50 (1), 173-180, 1993.
36. Penzel, E.; Rieger, J.; Schneider, H. A. *The glass transition temperature of random copolymers: 1. Experimental data and the Gordon-Taylor equation, Polymer* 1997, 38 (2), 325-337
37. Donescu, D.; Fusulan, L.; Petcu, C.; Vasilescu, M.; Smarandache, C.; Capek, I. *Ternary microemulsions of vinylic and acrylic monomers, European Polymer Journal*, 38 (8), 1691-1701, 2002.
38. Baker, R. W. *Membrane Technology and applications*, 2nd Edition, John Wiley&Sons Ltd., 2004
39. Cheryan, M. *Ultrafiltration and Microfiltration Handbook*, Technomic Publishing Company Inc., 1998
40. Mohd Idham Bin Mustaffar, *Development of Asymmetric Polyethersulfone Hollow Fiber Ultrafiltration Membrane For Cyclodextrin Separation*, Ph.D Thesis, 2004.
41. Mahanim Sarif@Mohd Ali, *Development of Integrally Skinned Polysulfone Ultrafiltration Membrane: Effect of Casting Parameters*, Ms. Thesis, 2005

42. Chandavas, Chaiya *Microporous polymeric membranes via melt processing*, Ph.D. Thesis, 2001.
43. Çapar, Goksen *Development Of A Membrane Based Treatment Scheme For Water Recovery From Textile Effluents*, Ph.D. Thesis, 2005.
44. Noble, R. D.; Stern, S. A. *Membrane Separations Technology: Principles and Applications*, Elsevier Science Publishing Company, 1995.
45. Tien, Chi *Introduction to Cake Filtration: Analyses, Experiments and Applications*, Elsevier Science Publishing Company, 2006.
46. Fried, J. R. *Polymer Science and Technology*, Prentice Hall PTR., 1995
47. Burggraff, A. J.; Cot, L. *Fundamentals of Inorganic Membrane Science and Technology*, Elsevier Science Publishing Company, 1996.
48. Khulbe, K. C.; Feng, C. Y.; Matsuura, T. *Synthetic Polymeric Membranes*, Springer-Verlag Berlin Heidelberg, 2008.
49. Matsuura, Takashi *Synthetic Membranes and Membrane Separation Processes*, CRC Press, Inc. , 1994.
50. Li, N. N.; Fane, A. G.; Winston Ho, W. S.; Matsuura, T. *Advanced Membrane Technology and Applications*, John Wiley & Sons, Inc. , 2008.
51. Peinemman, K. V.; Ebet, K.; Hicke, H. G.; Schanagl, N. *Polymeric composite ultrafiltration membranes for non-aqueous applications*, Environ. Prog. 20, 17, 2001.
52. Hicke, H. G.; Lehmann, I.; Malsch, G.; Ulbricht, M.; Becker, M. *Preparation and characterization of a novel solvent-resistant and autoclavable polymer membrane*, J. Membr. Sci. 198, 187, 2002.

53. Pasternak, M. *Membrane process for treating a charge containing dewaxing solvent and dewaxed oil*, U.S. Patent 5,234,579, 1993.
54. Linder, C.; Perry, M.; Nemas, M.; Katrarro, R. *Solvent stable membranes*, U.S. Patent 5,039,421, 1991.
55. Katz, S.A.; Salem, H. *J.Appl.Toxicol.*, 13, 217-224, 1993.
56. Yusof, A.M.; Malek, N.A.N.N. *J. Hazard. Mater.* 162, 1019-1024, 2009.
57. World Health Organization, *Guidelines for Drinking Water Quality* vol.1: Recommendation, World Health Organization(WHO), Geneva, 1993.
58. Acar, F.N.; Malkoc, E.; *Bioresource Technol.* 94, 13-15, 2004.
59. Arslan, G.; Pehlivan, E.; *Bioresource Technol.* 98, 2836-2845, 2007.
60. Kroschwitz, J.L.; Kirk-Othmer; *Encyclopedia of Chemical Technology*, Wiley, New York,1991.
61. Frenzel, I.; Stamatialis, D.F.; Wessling, M.; *Sep. Purif. Technol.* 49, 76-83, 2006.
62. Pradhan, J.; Nath, S.; Thakur, R.S. *J. Colloid Interf. Sci.* 217, 137, 1999.
63. Patterson, J.W. *Water Treatment Technology*, 3rd ed., Ann Arbor Science, Ann Arbor Michigan, MI, 1978.
64. Petruzzelli, D.; Passino, R.; Tiravanti, G. *Ind. Eng. Chem. Res.* 34, 2612-2617, 1995.
65. Kongsricharoern, N.; Polprasert, C. *Water. Sci. Technol.*, 34, 109-116, 1996.

66. Gupta, V.K.; Shrivastava, A.K.; Jain, N. *Water Res.*, 35, 4079-4085, 2001.
67. Aksu, Z.; Kutsal, T. *Environ. Technol.*, 11, 979-987, 1990.
68. Dragan, S.; Dinu, M.V.; Vlad, C.D. *J. Appl. Polym. Sci.*, 89, 2701-2707, 2003.
69. Kadirvelu, K.; Thamaraiselvi, K.; Namasivayam, C. *Bioresour. Technol.*, 76, 63, 2001.
70. Gzara, L.; Dhabbi, M. *Desalination*, 137, 241-250, 2001.
71. Hafiane, A.; Lemordant, D.; Dhabbi, M. *Desalination*, 130, 305-312, 2000.
72. Chen, S.S.; Hsu, B.C.; Ko, C.H.; Chuang, P.C. *Desalination*, 229, 147-155, 2008.
73. Shaalan, H.F.; Sorour, M.H.; Tewfik, S.R. *Desalination*, 141, 315, 2001.
74. Danis, U.; Aydiner, C. *J. Hazard. Mater.*, 162, 577-587, 2009.
75. Neelakandan, C.; Pugazhenti, G.; Kumar, A. *Eur. Polym. J.*, 39, 2383-2391, 2003.
76. Sachdeva, S.; Kumar, A. *J. Membrane. Sci.*, 307, 37-52, 2008.
77. Kumar, P.A.; Chakraborty, S. *J. Hazard. Mater.*, 162, 1086-1098, 2009.
78. Tasselli, F.; Donato, L.; Drioli, E. *J. Membrane. Sci.*, 320, 167-172, 2008.

79. Sankir, N.D.; Claus, R.O; Mecham, J.B; Harrison, W.L *Applied Physics Letters*, 87-24, 241910/1-241910/2, 2005.
80. Cleseri, L.S.; Greenberg, A.E.; Trusells, R.R.; (Eds.), *Standard Methods for the Examination of Water and Wastewater*, 17th ed., American Public Health Association, Washington, 1989.
81. Ray, S.; Ray, S. K. *Synthesis of Highly Selective Copolymer Membranes and Their Application for the Dehydration of Tetrahydrofuran by Pervaporation*, *Journal of Applied Polymer Science*, 103, 728–737, 2007.
82. Tonelli, A. E. *Glass Transition Temperatures of Regularly Alternating Acrylonitrile-Vinyl Acetate Copolymers*, *Macromolecules*, 10(3), 716-717, 1977.
83. Bunia, I.; Neagu, V.; Luca, C. *Reactive&Functional Polymers*, 66, 871-883, 2006.
84. Reddy, G.V.R.; Ranganathan, R.; Sivakumar, S.; Sriram, R. *Designed Monomers and Polymers*, 5(1), 97-114, 2002.
85. Xue, T. J.; McKinney, M. A.; Wilkie C. A. *Polym. Degradation and Stability*, 58, 193-202, 1997.
86. Rahaman, M. S. A.; Ismail, A. F.; Mustafa, A. *Polym. Degradation and Stability*, 92, 1421-1432, 2007.
87. Vargün, E.; Usanmaz, A. Polymerization of 2-hydroxyethyl acrylate in bulk and solution by chemical initiator and by ATRP method, *Jour. of Polym. Sci.: Part A, Polym. Chem.*, 43, 3957-3965, 2005.
88. Thomson, T. *Polyurethanes as specialty chemicals: principles and applications*, CRC Press LLC, Florida, 2005.
89. Lee, Wen-Fu; Lin, Yu-Hung *J Appl Polym Sci* ,81, 1360, 2001.

90. Krusic, M. K.; Filipovic, J. *Polymer*, 47, 148, 2006.
91. Young, L. J. *Polymer Handbook*, 2nd Edi., Jonh Wiley&Sons, Newyork, 1969.
92. Tian, Z.; He, X.; Pu, W.; Wan, C., Jiang, C. *Preparation of poly(acrylonitrile-butyl acrylate) gel electrolyte for lithium-ion batteries, Electrochimica Acta*, 52, 688-693, 2006.
93. Silverstein, R. M.; Webster, F. X. *Spectrometric Identification of Organic Compounds*, 6th Edi., John Wiley&Sons, Inc., 1998.
94. Schaefgen, J. R.; Sarasohn, J. M. *Journal of Polymer Science, Polym. Chem. Ed.*, 58, 1049, 1962.
95. Eisenberg, A.; Yokoyama, T. *Journal of Polymer Science, Polym. Chem. Ed.*, 7, 1717, 1969.
96. Fyfe, C.A.; McKinnon, M. S. *Macromolecules*, 19, 1909, 1986.
97. Martinez, G.; Sanchez-Chavez, M.; Marco Rocha C.; Ellis, G. *Thermal Degradation behavior of 2-hydroxyethyl methacrylate-tert-butyl acrylate copolymers, Polymer Degradation and Stability*, 76, 205-210, 2002.
98. Mukundan, T.; Bhanu, V. A.; Wiles, K. B.; Johnson, H.; Bortner, M.; Baird, D. G.; Naskar, A. K.; Ogale, A. A.; Edie, D. D.; McGrath, J. E. *Polymer*, 47, 4163-4171, 2006.
99. Amado, F.D.R.; Rodrigues, M.A.S.; Bertuol, D.A.; Bernardes, A.M.; Ferreira, J.Z.; Ferreira, C.A. *J. Membrane. Sci.*, 330, 227-232, 2009.

100. Sankir, M.; Kim, Y.S.; Pivovar, B.S.; McGrath, J.E. *J. Membrane. Sci.*, 299, 8–18, 2007.
101. Arthanareeswaran, G.; Sriyamuna, T.K.; Mohan, D.D. *Sep. Purif. Technol.* , 67, 271-281, 2009.
102. Rahimpour, A.; Madaeni, S.S.; Amirinejad, M.; Mansourpanah, Y.; Zereshki, S.; *J.Membrane Science*, doi;10.1016/j.memsci.2008.12.059.
103. Carraher, C. E.; Seymour, R. B. *Polymer Chemistry*, 6th Edi., Marcel Dekker Inc., 2003.
104. Mark, J.E. *Physical Properties of Polymer Handbook*, Springer, 2007.

CURRICULUM VITAE

PERSONAL INFORMATION

Surname, Name: Aran, Bengi

Nationality: Turkish (T.C.)

Date and Place of Birth: 14 February 1979, Ankara

Marital Status: Single

Phone: +90 532 4155329

E-mail: bengiaran@yahoo.com

EDUCATION

Degree	Institution	Year of Graduation
MS	METU Polymer Science&Tech.	2004
BS	METU Department of Chemistry	2001
High School	Bahçelievler Deneme	1996

WORK EXPERIENCE

Year	Place	Enrollment
Oct 04 - Present	TOBB, Economy and Technology University	Instructor
Sep 03 - Oct 04	Turkish Standards Institute	Analytical Chemist
June 02 - May 03	The Union Of Chambers And Commodity Exchanges Of Turkey (UCCET)	Assistant Director
June 00 - Aug 00	Hoffmann-La Roche Inc.	Intern

FOREIGN LANGUAGES: Advanced English

PUBLICATIONS

1. Aran, B.; Usanmaz, A. *Stereoregular Polymerization of Methylmethacrylate by Atom Transfer Radical Polymerization*, *Journal of Macromolecular Science, Part A: Pure and Applied Chemistry*, 43(2), 233-245, 2006.
2. Aran, B.; Sankir, M.; Vargun, E.; Sankir, N.D.; Usanmaz, A. *Tailoring the swelling and glass transition temperature of the Acrylonitrile/Hydroxyethyl Acrylate copolymers* *Journal of Applied Polymer Science* DOI: 10.1002/app.30854 , 2010 (article in press).
3. Vargun, E.; Sankir, M.; Aran, B.; Sankir, N. D.; Usanmaz, A. *Synthesis and Characterization of 2-Hydroxyethyl methacrylate (HEMA) and Methyl methacrylate (MMA) Copolymer Used as Biomaterial*, *Journal of Macromolecular Science, PAC*, A-47(3), 2010 (article in press).
4. Sankir, M.; Bozkir, S.; Aran, B. *Preparation and Performance Analysis of Novel Nanocomposite Copolymer Membranes for Cr(VI) Removal from Aqueous Solution*, *Desalination* DOI:10.1016/j.desal.2009.09.134, 2010 (article in press).